NASA Technical Memorandum 106915
AIAA–95–1754

The Method of Space-Time Conservation Element and Solution Element-Applications to One-Dimensional and Two-Dimensional Time-Marching Flow Problems

Sin-Chung Chang
Lewis Research Center
Cleveland, Ohio

Xiao-Yen Wang and Chuen-Yen Chow
University of Colorado
Boulder, Colorado

Prepared for the
12th Computational Fluid Dynamics Conference
sponsored by the American Institute of Aeronautics and Astronautics
San Diego, California, June 19–22, 1995

National Aeronautics and
Space Administration

THE METHOD OF SPACE-TIME CONSERVATION ELEMENT AND SOLUTION ELEMENT –APPLICATIONS TO ONE-DIMENSIONAL AND TWO-DIMENSIONAL TIME-MARCHING FLOW PROBLEMS

Sin-Chung Chang
NASA Lewis Research Center
Cleveland, Ohio

and

Xiao-Yen Wang* and Chuen-Yen Chow†
University of Colorado
Boulder, Colorado

Abstract

A nontraditional numerical method for solving conservation laws is being developed. The new method is designed from a physicist's perspective, i.e., its development is based more on physics than numerics. Even though it uses only the simplest approximation techniques, a 2D time-marching Euler solver developed recently using the new method is capable of generating nearly perfect solutions for a 2D shock reflection problem used by Helen Yee and others. Moreover, a recent application of this solver to computational aeroacoustics (CAA) problems reveals that: (i) accuracy of its results is comparable to that of a 6th order compact difference scheme even though nominally the current solver is only of 2nd-order accuracy; (ii) generally, the non-reflecting boundary condition can be implemented in a simple way without involving characteristic variables; and (iii) most importantly, the current solver is capable of handling *both* continuous and discontinuous flows very well and thus provides a unique numerical tool for solving those flow problems where the interactions between sound waves and shocks are important, such as the noise field around a supersonic over- or under-expansion jet.

*Graduate student, Student member AIAA.
†Professor, Associate Fellow AIAA.

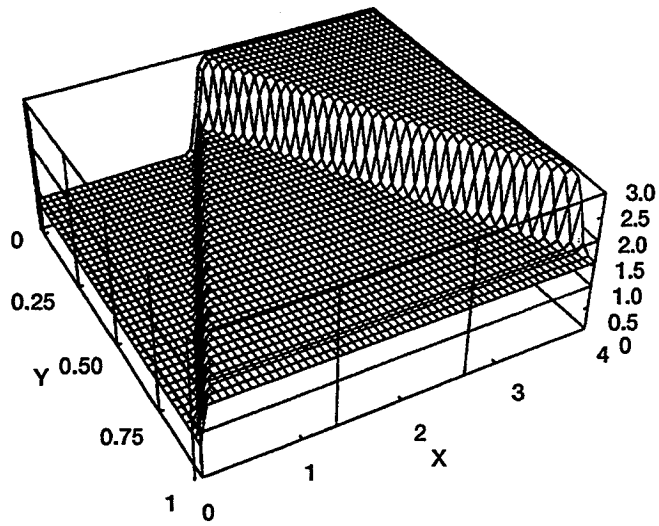

Figure 1.—Pressure distribution for a shock reflection problem (a flow of Mach number 2.9 enters from the left; the shock is reflected by a wall on the back).

1. Introduction

The method of space-time conservation element and solution element is a new numerical discretization method for solving conservation laws [1-13]. The new method differs substantially in both concept and methodology from the well-established methods–i.e., finite difference, finite volume, finite element, and spectral methods. It is designed to overcome several key limitations of the above traditional methods. In addition, its development is driven by an emphasis on simplicity, generality, and accuracy. In this paper, we shall describe a 2D time-marching Euler solver developed recently using the new method [2]. Even though it does not use (i) any approximation

techniques more complicated than Taylor's expansion or weighted averaging, (ii) any mesh-refinement techniques, (iii) any monotonicity constraints, (iv) any characteristics-based techniques, or (v) any ad hoc techniques that are used only in the neighborhood of a discontinuity, this solver is capable of generating highly accurate solutions for a 2D shock reflection problem used by Helen Yee and others [14]. As shown in Fig. 1, *both the incident and the reflected shocks can be resolved by a single data point without the presence of numerical oscillations near the discontinuity.*

Recently, Loh and others [13] have successfully simulated some benchmark aeroacoustics problems using the new Euler solver. The non-reflecting boundary condition is nearly perfect with almost no modification of the original code. In several free shear layer calculations, the smallest eddies are consistently resolved in 3-4 grid cells. Some interesting vortex/shock (or Mach waves) interactions, which have never been reported before, were also observed. A further discussion of these results is given near the end of Sec. 5.

The Introduction section of [1] begins with a lengthy discussion that includes (i) an examination of the traditional methods and their limitations, and (ii) a study of the general requirements for an accurate solver of conservation laws. The current method is built on a set of design principles that emerge from the above discussion. In this section, an overall view of the current method will be given from a historical perspective. Particularily, it will be explained how the current method was shaped by fundamental physics considerations.

The first physical problem considered in the current development is an initial-value problem involving the PDE

$$\frac{\partial u}{\partial t} + a\frac{\partial u}{\partial x} = 0 \qquad (1.1)$$

where the convection speed a is a constant. The exact solution to any such problem has three fundamental properties: (i) it does not dissipate with time, (ii) its value at a spatial point at a later time has a finite domain of dependence (a point) at an earlier time, and (iii) it is completely determined by the initial data at a given time. Ideally, a numerical solution for Eq. (1.1) should also possess the same three properties. Because (i) a solution of a *dissipative* numerical scheme will dissipate with time; (ii) the value of a solution of an *implicit* scheme at any point (x,t) is dependent on all initial data, and all the boundary data up to the time t; and (iii) the unique determination of a solution of a *multi-level* scheme requires the specification of the initial data at two or more time levels, an ideal solver must be a *two-level, explicit, and neutrally stable (i.e., non-dissipative) scheme.* In 1991, such a solver was reported in [5]. Because this new solver models Eq. (1.1) which is characterized by the parameter a, hereafter it will be referred to as the a scheme. The a scheme is neutrally stable if the Courant number < 1. It is the only two-level explicit solver of Eq. (1.1) known to the authors to be neutrally stable.

Development of the a scheme is aided by recasting Eq. (1.1) into an integral form that represents a law of flux conservation [1,5,9]. The a scheme is derived by using both Eq. (1.1) and its integral form. Note that the conservation law appears in a form in which space and time are unified and treated on the the same footing. *This unity of space and time, and the requirement that flux-conservation be enforced locally (i.e., down to a computational cell) and globally (i.e., over the entire computational domain) are two tenets of the current numerical method. They are also the key characteristics that distinguish the current method from most of the traditional methods.*

Note that *the enforcement of both local and global flux conservation may also prevent inconsistency among initial/boundary conditions.*

The a scheme has many nontraditional features. At each mesh point (j,n), it has two *independent* marching variables u_j^n and $(u_x)_j^n$ with the latter being the analogue of $\partial u/\partial x$ at the mesh point. It also has the simplest stencil, i.e., a triangle with one vertex at the given time level and the other two vertices at the previous time level. In contrast to a typical finite-volume scheme, extrapolation and interpolation are not used in the a scheme for the evaluation of the flux at an interface separating two neighboring conservation elements. Moreover, the a scheme is a two-way marching scheme, i.e., *the forward marching scheme can be inverted to become the backward marching scheme. In other words, the marching variables at the $(n-1)$th time level can be determined in terms of those at the nth time level.* These and other nontraditional features of the a scheme are discussed in depth in [1,9].

Because there are two independent marching variables at each mesh point (j,n), two amplification factors appear in the von Neumann stability analysis of the a scheme [1,5,9]. It happens that these two factors are identical to those of the Leapfrog scheme [15] if the latter factors arise from a "proper" von Neumann analysis. Note that a solution to the main Leapfrog scheme (excluding the starting scheme which relates the mesh variables at the first two time levels) is formed by two decoupled solutions. Traditionally the von Neumann analysis for the Leapfrog scheme is performed without

taking into account this decoupled nature. In [1,9], it is performed separately for each decoupled solution. The amplification factors thus obtained are identical to those of the a scheme. This coincidence was unexpected because the Leapfrog and the a schemes are structually different.

The fact that the amplification factors of the a scheme are related to those of a celebrated classical scheme is only one among a string of similar unexpected coincidences encountered during the development of the current method. As will be explained in this paper, the amplification factors of the Lax-Wendroff, the Lax, the Crank-Nicolson, and the DuFort-Frankel schemes [15] also are identical to those of some of the extensions of the a scheme.

Because the solutions of the a scheme were required to share with those of Eq. (1.1) the same fundamental properties referred to earlier, during the early day of its development Chang realized that such a scheme must share with Eq. (1.1) certain basic invariant properties in space-time. He studied the invariant properties of Eq. (1.1) with respect to spatial reflection, time reversal, and space-time inversion. He then defined *rigorously* what it means for a *two-level constant-coefficient finite-difference analogue* of Eq. (1.1) to have similar invariant properties. In this study, it is assumed that there is only one marching variable u_j^n at a mesh point for a *finite-difference* analogue of Eq. (1.1). With the above assumptions, it was shown that the von Neumann amplification factor of a numerical analogue satisfies a special relation for each invariant property that this analogue possesses. Particularly, an analogue is *unconditionally* neutrally stable if it is invariant under space-time inversion. As an example, the implicit Wendroff scheme [16] is invariant under space-time inversion. Its amplification factor is

$$G = \frac{\cos(\theta/2) - i\nu\sin(\theta/2)}{\cos(\theta/2) + i\nu\sin(\theta/2)} \quad (i = \sqrt{-1}) \qquad (1.2)$$

Here θ is the phase angle variation per mesh interval and ν is the Courant number. Note that $|G| = 1$ for any ν.

The results of the above study were presented in a conference that took place in 1992 [6]. Because a two-level explicit *finite-difference* scheme is not invariant under space-time inversion, one can infer from the arguments made in [6] that such a scheme cannot be an ideal scheme, i.e., neutrally stable.

The two-level finite-difference scheme has only one amplification factor. For a numerical analogue of Eq. (1.1) with two amplification factors G_+ and G_-, generally one cannot conclude that the scheme is unconditionally neutrally stable if it is invariant under space-time inversion. For the Leapfrog scheme or the a scheme, we have $G_+G_- = -1$. In general it does not imply neutral stability, i.e., $|G_+| = |G_-| = 1$. However, it does imply that *such a scheme must be neutrally stable if it is stable, i.e., if* $|G_+| \leq 1$ *and* $|G_-| \leq 1$. For both the a and the Leapfrog schemes, this implies that they are neutrally stable if the Courant number < 1.

In the 11th AIAA CFD conference (July, 1993), Thomas and Roe* presented a paper [17] in which the concept of the invariance under space-time inversion is also used to construct non-dissipative numerical schemes. Note that the concept of "rotational symmetry" in space-time (i.e., "invariance under space-time inversion") was discussed briefly in [17]. Unfortunately, this discussion is faulty in two aspects. It considers only one amplification factor G in spite of the fact that the scheme under consideration, i.e., the "Upwind Leapfrog scheme" has two amplification factors. Furthermore, it leads to the conclusion that $G = 1$ for a scheme that is invariant under space-time inversion. Even for a scheme that has only one amplification factor, this conclusion is obviously false. As an example, consider the Wendroff scheme. It is invariant under space-time inversion and yet $G \neq 1$, except for the case $\nu\sin(\theta/2) = 0$ (see Eq. (1.2)).

In a 1994 ICASE report [18], the concept of invariance under space-time inversion is again used by Roe to construct non-dissipative linear Bicharacteristic schemes.

The a scheme is only a special case of a more general two-level explicit scheme described in [5]. It is a solver for

$$\frac{\partial u}{\partial t} + a\frac{\partial u}{\partial x} - \mu\frac{\partial^2 u}{\partial x^2} = 0 \qquad (1.3)$$

where the viscosity coefficient $\mu(\geq 0)$ is a constant. Because this solver models Eq. (1.3) which is characterized by the parameters a and μ, hereafter it is referred to as the a-μ scheme. The a-μ scheme reduces to the a scheme if $\mu = 0$. Because the a scheme is neutrally stable, the a-μ scheme has the property that *the numerical dissipation of its solution approaches zero as the physical dissipation approaches zero.*

*A participant of the 23rd Conference on Modeling and Simulation, April 30-May 1, 1992, Pittsburgh, PA. He was in the audience when the paper [6] was presented by Chang, and participated in the discussion afterward.

The above property is important because of the following observation: With a few exceptions, numerical dissipation generally appears in a numerical solution of a time-marching problem. In other words, the numerical solution dissipates faster than the corresponding physical solution. For a nearly inviscid problem, e.g., flow at a large Reynolds number, this could be a serious difficulty because numerical dissipation may overwhelm physical dissipation and cause a complete distortion of solutions. To avoid such a difficulty, at the minimum, a model solver for Eq. (1.3) should be required to have the special property mentioned above.

In [5], it is shown that the a-μ scheme, which is explicit, has the unusual property that its stability is limited only by the CFL condition, i.e., it is independent of μ. Furthermore, *the amplification factors of the a-μ scheme reduce to those of the DuFort-Frankel scheme if $a = 0$* [1,9]. Note that a solution of the latter scheme is also formed by two decoupled solutions. As a result, the von Neumann analysis should be performed separately for each decoupled solution.

In order to "explore the concept of a dynamic space-time mesh and the need for a unified treatment of physical variables and mesh parameters" [5, p.24], a moving mesh with a uniform speed b was introduced in [5] (see Fig. 2(a)). With the aid of a Galilean transformation, it is shown that the a-μ scheme or a typical finite-difference solver of Eq. (1.1) or (1.3) can be converted to its moving-mesh form by simply replacing the parameter a with $a - b$. As an example, the moving-mesh form of the Leapfrog scheme is

$$\frac{u_j^{n+1} - u_j^{n-1}}{2\Delta t} + (a - b)\frac{u_{j+1}^n - u_{j-1}^n}{2\Delta x} = 0 \qquad (1.4)$$

Note that: (i) Eq. (1.4) reduces to the regular form of the Leapfrog mesh if $b = 0$, i.e., if the mesh becomes stationary, and (ii) a moving-mesh form and its stationary-mesh counterpart actually represent two different schemes (read Sec. 3, "The Dynamic Space-Time Mesh" in [5]).

Let $b = a$. Then (i) a mesh line with j being a constant along this line points in the characteristic direction of Eq. (1.1), and (ii) Eq. (1.4) is reduced to $u_j^{n+1} = u_j^{n-1}$, i.e., the numerical value of u is constant along such a mesh line. Because u is constant along a characteristic line if it is an exact solution of Eq. (1.1), aside from round-off errors, a numerical solution matches perfectly with its analytical counterpart.

As a result of the above observation, and other considerations given in [5], one arrives at the important conclusion [5, p.3]: "$\cdots$ *(i) stability and accuracy can be improved, and (ii) dissipation and dispersion can be reduced, if the space-time mesh is allowed to evolve with the physical variables such that the local convective motion of physical variables relative to the moving mesh is kept to a minimum.*"

Because of the complexity involved, the dynamic space-time mesh has not yet been used in the current development beyond the applications reported in [5].

Note that the "Upwind Leapfrog scheme" referred to in [17,18] can be considered as a special case of Eq. (1.4). Let $b = \Delta x/\Delta t$. Then, as depicted in Figs. 2(a) and 2(b), the mesh points $(j, n+1)$ and $(j+1, n)$ line up at one spatial location, while the mesh points $(j-1, n)$ and $(j, n-1)$ line up at another spatial position. Also Eq. (1.4) becomes

$$\frac{(u_j^{n+1} - u_{j+1}^n) + (u_{j-1}^n - u_j^{n-1})}{2\Delta t} + a\frac{u_{j+1}^n - u_{j-1}^n}{2\Delta x} = 0 \qquad (1.5)$$

The stencil of Eq. (1.5) is shown in Fig. 2(b). The stencil of the "Upwind Leapfrog scheme" is depicted in Fig. 4 in [17] and reproduced in Fig. 2(c) here.

A comparison between Figs. 2(b) and 2(c) reveals that (i) the mesh points $(j, n+1)$, $(j+1, n)$, $(j-1, n)$, and $(j, n-1)$ in Fig. 2(b) correspond, respectively, to the mesh points $(j, n+1)$, (j, n), $(j-1, n)$, and $(j-1, n-1)$ in Fig. 2(c); (ii) the mesh interval $2\Delta x$ in Fig. 2(b) corresponds to the mesh interval Δx in Fig. 2(c); and (iii) the time-step size Δt in Fig. 2(b) corresponds to the time-step size Δt in Fig. 2(c). Note that the moving-mesh indices are used here, while the stationary-mesh indices are used in [17]. By replacing (i) the moving-mesh indices with the corresponding stationary-mesh indices, and (ii) $2\Delta x$ with Δx, Eq. (1.5) becomes

$$\frac{(u_j^{n+1} - u_j^n) + (u_{j-1}^n - u_{j-1}^{n-1})}{2\Delta t} + a\frac{u_j^n - u_{j-1}^n}{\Delta x} = 0 \qquad (1.6)$$

i.e., the defining equation for the "Upwind Leapfrog scheme" (see Eq. (4) in [17]).

The a scheme is neutrally stable and reversible in time [1,5,9]. It is well known that a neutrally stable numerical analogue of Eq. (1.1) generally becomes unstable or highly dispersive when it is extended to model the Euler equations. It is also obvious that a scheme that is reversible in time cannot model a physical problem that is irreversible in time, e.g., an inviscid flow problem involving shocks. Hence, the a scheme is extended to become the a-ϵ scheme [1,9]. Stability of this scheme is limited by the CFL condition and $0 \le \epsilon \le 1$ where ϵ is a special parameter that controls numerical dissipation. Moreover, if $\epsilon = 0$, the a-ϵ scheme reduces to the a scheme which has no numerical dissipation. On the other hand, if $\epsilon = 1$, the

two amplification factors of the a-ϵ scheme become the same function of the Courant number and the phase angle. Unexpectedly, *this function also is the amplification factor of the highly diffusive Lax scheme.*

The a-ϵ scheme was extended [1,9] to solve the 1D time-dependent Euler equations of a perfect gas. The Euler extension has stability conditions similar to those of the a-ϵ scheme itself. It has the unusual property that numerical dissipation at all mesh points can be controlled by a set of local parameters. Moreover, it is capable of generating accurate shock tube solutions with the CFL number ranging from 1.0, to 0.022.

The a-μ scheme was also extended [1,9] to solve the 1D time-dependent Navier-Stokes equations of a perfect gas. Stability of this *explicit* solver also is limited only by the CFL condition. In spite of the fact that it does not use (i) *any* techniques related to the high-resolution upwind methods, and (ii) *any* ad hoc parameter, the *Navier-Stokes* extension is capable of generating highly accurate shock tube solutions. Particularly, for high-Reynolds-number flows, shock discontinuities can be resolved within one mesh interval.

This concludes the review of the development of the current method up to 1993. In the rest of this paper, we shall describe several 2D extensions of the 1D schemes discussed earlier. The first scheme to be discussed is the 2D version of the a scheme. Again, it is a two-level, explicit, and neutrally stable scheme.

2. The 2D a Scheme

In this section, we consider a dimensionless form of the 2D convection equation, i.e.,

$$\frac{\partial u}{\partial t} + a_x \frac{\partial u}{\partial x} + a_y \frac{\partial u}{\partial y} = 0 \tag{2.1}$$

where a_x, and a_y are constants. Let $x_1 = x$, $x_2 = y$, and $x_3 = t$ be the coordinates of a three-dimensional Euclidean space E_3. By using Gauss' divergence theorem in the space-time E_3, it can be shown that Eq. (2.1) is the differential form of the integral conservation law

$$\oint_{S(V)} \vec{h} \cdot d\vec{s} = 0 \tag{2.2}$$

Here (i) $S(V)$ is the boundary of an arbitrary space-time region V in E_3, (ii)

$$\vec{h} \stackrel{\text{def}}{=} (a_x u,\ a_y u,\ u) \tag{2.3}$$

is a current density vector in E_3, and (iii) $d\vec{s} = d\sigma\, \vec{n}$ with $d\sigma$ and $\vec{n}$, respectively, being the area and the outward unit normal of a surface element on $S(V)$. Note that (i) $\vec{h} \cdot d\vec{s}$ is the *space-time* flux of $\vec{h}$ leaving the region V through the surface element $d\vec{s}$, and (ii) all mathematical operations can be carried out as though E_3 were an ordinary three-dimensional Euclidean space. As will be shown shortly, E_3 will be divided into nonoverlapping space-time regions referred to as conservation elements (CEs).

In the following, we shall introduce a nontraditional space-time mesh. Its use will result in the simplest stencil possible for the current scheme, i.e., a tetrahedron in 3D space-time with one vertex at the upper time level and other three at the lower time level. Also this mesh is compatible with the requirement that the 2D a scheme be invariant under space-time inversion. Most importantly, three conservation elements per mesh point are embedded in this mesh such that each mesh point is associated with three flux-conservation conditions. This mesh structure matches perfectly with the fact that there are three unknowns (the numerical analogues of u, $\partial u/\partial x$ and $\partial u/\partial y$) at each mesh point.

Let n denote the time level and

$$t^n \stackrel{\text{def}}{=} n\Delta t, \qquad n = 0, \pm 1/2, \pm 1, \pm 3/2, \ldots \tag{2.4}$$

Let j and k be spatial mesh indices with $j, k = 0, \pm 1/3, \pm 2/3, \pm 1, \ldots$ (see Figs. 3–6). Let Ω_1 denote the set of mesh points (j, k, n) with $j, k = 0, \pm 1, \pm 2, \ldots$, and $n = \pm 1/2, \pm 3/2, \pm 5/2, \ldots$. These mesh points are marked by solid circles. Let Ω_2 denote the set of mesh points (j, k, n) with $j, k = 1/3, 1/3 \pm 1, 1/3 \pm 2, \ldots$, and $n = 0, \pm 1, \pm 2, \ldots$. These mesh points are marked by open circles. The union of Ω_1 and Ω_2 will be denoted by Ω.

Each mesh point $(j, k, n + 1/2)$ in Ω_1 (by definition, this implies that $n = 0, \pm 1, \pm 2, \ldots$) is associated with three CEs, denoted by $\text{CE}_\ell^{(1)}(j, k, n + 1/2)$, $\ell = 1, 2, 3$ (see Fig. 7(a)). It is also associated with a solution element (SE), denoted by $\text{SE}^{(1)}(j, k, n + 1/2)$ (see Fig. 7(b)). Similarly, each mesh point $(j, k, n + 1)$ in Ω_2 is associated with three conservation elements $\text{CE}_\ell^{(2)}(j, k, n + 1)$, $\ell = 1, 2, 3$ (see Fig. 8(a)), and a solution element $\text{SE}^{(2)}(j, k, n + 1)$ (see Fig. 8(b)). Each CE is a quadrilateral cylinder in space-time while each SE is the union of three vertical planes, a horizontal plane, and their immediate neighborhood. The geometry of the hexagon $ABCDEF$, which appears in both Figs. 7(a) and 8(a), is determined by three positive parameters w, b and h (see Fig. 9(a)). Without any loss of generality, we assume that the line segment joining points D and A in Fig. 9(a) is parallel to the x-axis. Note that the form of Eq. (2.1) will not change under an orthogonal transformation on the x-y plane.

Thus one always can introduce a set of Cartesian coordinates (x, y) such that the above line segment is parallel to the x-axis. However, the values of a_x and a_y may change as a result of such a transformation.

According to Fig. 3, E_3 can be filled with the CEs defined above. Moreover, it is seen from Figs. 7(a), 7(b), 8(a), and 8(b) that *the boundary of a CE is formed by the subsets of two neighboring SEs.*

Let the space-time mesh be uniform, i.e., the parameters Δt, w, b, and h are constants. Let $x_{j,k}$ and $y_{j,k}$ be the x- and y- coordinates of any mesh points $(j, k, n) \in \Omega$. Let $x_{0,0} = 0$ and $y_{0,0} = 0$. Then information provided by Figs. 9(a) and 9(b) implies that

$$x_{j,k} = (j+k)w + (k-j)b, \quad y_{j,k} = (k-j)h \tag{2.5}$$

Let $\vec{n}_1$, $\vec{n}_2$, $\vec{n}_3$, $\vec{n}_4$, $\vec{n}_5$, and $\vec{n}_6$ be the vectors depicted in Fig. 9(a). They lie on the x-y plane and are the outward unit normals to $\overline{AB}$, $\overline{BC}$, $\overline{CD}$, $\overline{DE}$, $\overline{EF}$, and $\overline{FA}$, respectively. It can be shown that

$$\vec{n}_1 = \frac{(h, -b + w/3, 0)}{\sqrt{h^2 + (b - w/3)^2}}, \qquad \vec{n}_4 = -\vec{n}_1 \tag{2.6a}$$

$$\vec{n}_2 = (0, 1, 0), \qquad \vec{n}_5 = -\vec{n}_2 \tag{2.6b}$$

and

$$\vec{n}_3 = \frac{(-h, b + w/3, 0)}{\sqrt{h^2 + (b + w/3)^2}}, \qquad \vec{n}_6 = -\vec{n}_3 \tag{2.6c}$$

For any $(j, k, n) \in \Omega$, let

$$\mathrm{SE}(j,k,n) \stackrel{\text{def}}{=} \begin{cases} \mathrm{SE}^{(1)}(j,k,n), & \text{if } (j,k,n) \in \Omega_1 \\ \mathrm{SE}^{(2)}(j,k,n), & \text{if } (j,k,n) \in \Omega_2. \end{cases} \tag{2.7}$$

For any $(x, y, t) \in \mathrm{SE}(j, k, n)$, $u(x, y, t)$ and $\vec{h}(x, y, t)$, respectively, are approximated by

$$\begin{aligned} u^*(x,y,t;j,k,n) \stackrel{\text{def}}{=} u^n_{j,k} + (u_x)^n_{j,k}(x - x_{j,k}) \\ + (u_y)^n_{j,k}(y - y_{j,k}) + (u_t)^n_{j,k}(t - t^n) \end{aligned} \tag{2.8}$$

and

$$\begin{aligned} \vec{h}^*(x,y,t;j,k,n) \stackrel{\text{def}}{=} [a_x u^*(x,y,t;j,k,n), \\ a_y u^*(x,y,t;j,k,n), u^*(x,y,t;j,k,n)] \end{aligned} \tag{2.9}$$

where $u^n_{j,k}$, $(u_x)^n_{j,k}$, $(u_y)^n_{j,k}$, and $(u_t)^n_{j,k}$ are constants within $\mathrm{SE}(j, k, n)$. The last four coefficients, respectively, can be considered as the numerical analogues of the values of u, $\partial u/\partial x$, $\partial u/\partial y$, and $\partial u/\partial t$ at (x_j, y_k, t^n). As a result, the expression on the right side of Eq. (2.8) can be considered as the first-order Taylor's expansion of $u(x, y, t)$ at (x_j, y_k, t^n). Also note that Eq. (2.9) is the numerical analogue of Eq. (2.3).

We shall require that $u = u^*(x, y, t; j, k, n)$ satisfies Eq. (2.1) within $\mathrm{SE}(j, k, n)$. As a result,

$$(u_t)^n_{j,k} = -\left[a_x (u_x)^n_{j,k} + a_y (u_y)^n_{j,k}\right] \tag{2.10}$$

Substituting Eq. (2.10) into Eq. (2.8), one has

$$\begin{aligned} u^*(x,y,t;j,k,n) &= u^n_{j,k} \\ &+ (u_x)^n_{j,k}\left[(x - x_{j,k}) - a_x(t - t^n)\right] \\ &+ (u_y)^n_{j,k}\left[(y - y_{j,k}) - a_y(t - t^n)\right] \end{aligned} \tag{2.11}$$

Thus there are three independent marching variables, i.e., $u^n_{j,k}$, $(u_x)^n_{j,k}$, and $(u_y)^n_{j,k}$ associated with a mesh point $(j, k, n) \in \Omega$. For any $(j, k, n + 1/2) \in \Omega_1$, these variables will be determined in terms of those associated with the mesh points $(j + 1/3, k + 1/3, n)$, $(j - 2/3, k + 1/3, n)$, and $(j + 1/3, k - 2/3, n)$ (see Fig. 10(a)) by using the flux conservation relations:

$$\oint_{S(CE^{(1)}_\ell(j,k,n+1/2))} \vec{h}^* \cdot d\vec{s} = 0, \qquad \ell = 1, 2, 3 \tag{2.12}$$

Similarly, the marching variables at any $(j, k, n + 1) \in \Omega_2$ are determined in terms of those associated with the mesh points $(j - 1/3, k - 1/3, n + 1/2)$, $(j+2/3, k-1/3, n+1/2)$, and $(j-1/3, k+2/3, n+1/2)$ (see Fig. 10(b)) by using the flux conservation relations:

$$\oint_{S(CE^{(2)}_\ell(j,k,n+1))} \vec{h}^* \cdot d\vec{s} = 0, \qquad \ell = 1, 2, 3 \tag{2.13}$$

Obviously, Eqs. (2.12) and (2.13) are the numerical analogues of Eq. (2.2).

As a result of Eqs. (2.12) and (2.13), the total flux leaving the boundary of any CE is zero. Because the flux at any interface separating two neighboring CEs is calculated using the information from a single SE, the flux entering one of these CEs is equal to that leaving another. It follows that the local conservation conditions Eqs. (2.12) and (2.13) will lead to a global conservation condition, i.e., *the total flux leaving the boundary of any space-time region that is the union of any combination of CEs will also vanish.*

In the following, several preliminaries will be given prior to the evaluation of Eqs. (2.12) and (2.13). To proceed, note that a mesh line with j and n being constant or a mesh line with k and n being constant is not

aligned with the x-axis or the y-axis. We shall introduce a new spatial coordinate system (ζ, η) with its axes aligned with the above mesh lines (see Fig. 9(c)).

Let $\vec{e}_x$ and $\vec{e}_y$ be the unit vectors in the x- and the y- directions, respectively. Let $\vec{e}_\zeta$ and $\vec{e}_\eta$ be the unit vectors in the directions of $\overrightarrow{DF}$ and $\overrightarrow{DB}$ (i.e., the j- and the k- directions–see Figs. 9(a)-(c)), respectively. It can be shown that

$$\vec{e}_\zeta = [(w-b)\vec{e}_x - h\vec{e}_y]/\Delta\zeta \tag{2.14}$$

and

$$\vec{e}_\eta = [(w+b)\vec{e}_x + h\vec{e}_y]/\Delta\eta \tag{2.15}$$

where

$$\Delta\zeta \stackrel{\text{def}}{=} |\overrightarrow{DF}| = \sqrt{(w-b)^2 + h^2} \tag{2.16}$$

and

$$\Delta\eta \stackrel{\text{def}}{=} |\overrightarrow{DB}| = \sqrt{(w+b)^2 + h^2} \tag{2.17}$$

Let the origin of (x, y) also be that of (ζ, η). Then the spatial coordinates (x, y) and (ζ, η) of any point in E_3 are related by the condition

$$\zeta\,\vec{e}_\zeta + \eta\,\vec{e}_\eta = x\,\vec{e}_x + y\,\vec{e}_y \tag{2.18}$$

Substituting Eqs. (2.14) and (2.15) into Eq. (2.18), one has

$$\begin{pmatrix} x \\ y \end{pmatrix} = T \begin{pmatrix} \zeta \\ \eta \end{pmatrix} \tag{2.19}$$

and

$$\begin{pmatrix} \zeta \\ \eta \end{pmatrix} = T^{-1} \begin{pmatrix} x \\ y \end{pmatrix} \tag{2.20}$$

Here

$$T \stackrel{\text{def}}{=} \begin{pmatrix} \dfrac{w-b}{\Delta\zeta} & \dfrac{w+b}{\Delta\eta} \\ -\dfrac{h}{\Delta\zeta} & \dfrac{h}{\Delta\eta} \end{pmatrix} \tag{2.21}$$

and

$$T^{-1} \stackrel{\text{def}}{=} \begin{pmatrix} \dfrac{\Delta\zeta}{2w} & -\dfrac{(w+b)\Delta\zeta}{2wh} \\ \dfrac{\Delta\eta}{2w} & \dfrac{(w-b)\Delta\eta}{2wh} \end{pmatrix} \tag{2.22}$$

Note that the existence of T^{-1}, the inverse of T, is assured if $wh \neq 0$.

With the aid of Eqs. (2.5), (2.20), and (2.22), it can be shown that the coordinates (ζ, η) of any mesh point $(j, k, n) \in \Omega$ are given by

$$\zeta = j\,\Delta\zeta, \qquad \textit{and} \qquad \eta = k\,\Delta\eta \tag{2.23}$$

i.e., $\Delta\zeta$ and $\Delta\eta$ are the mesh intervals in the ζ- and the η- directions, respectively.

Next we shall introduce several coefficients that are tied to the coordinate system (ζ, η). Let

$$\begin{pmatrix} a_\zeta \\ a_\eta \end{pmatrix} \stackrel{\text{def}}{=} T^{-1} \begin{pmatrix} a_x \\ a_y \end{pmatrix} \tag{2.24}$$

Also, for any $(j, k, n) \in \Omega$, let

$$\begin{pmatrix} (u_\zeta)^n_{j,k} \\ (u_\eta)^n_{j,k} \end{pmatrix} \stackrel{\text{def}}{=} T^t \begin{pmatrix} (u_x)^n_{j,k} \\ (u_y)^n_{j,k} \end{pmatrix} \tag{2.25}$$

where T^t is the transpose of T. For those who are familiar with tensor analysis, the following comments will clarify the meaning of the above definitions:

(a) (a_ζ, a_η) are the *contravariant* components with respect to the coordinates (ζ, η) for the spatial vector whose x- and y- components are a_x and a_y, respectively.

(b) $((u_\zeta)^n_{j,k}, (u_\eta)^n_{j,k})$ are the *covariant* components with respect to the coordinates (ζ, η) for the spatial vector whose x- and y- components are $(u_x)^n_{j,k}$ and $(u_y)^n_{j,k}$, respectively.

(c) Because the contraction of the contravariant components of a vector and the covariant components of another is a scalar, Eq. (2.10) can be rewritten as

$$(u_t)^n_{j,k} = -\left[a_\zeta (u_\zeta)^n_{j,k} + a_\eta (u_\eta)^n_{j,k}\right] \tag{2.26}$$

(d) Under the *linear* coordinate transformation defined by Eqs. (2.19) and (2.20), $(\zeta - j\Delta\zeta, \eta - k\Delta\eta)$ are the contravariant components with respect to the coordinates (ζ, η) for the spatial vector whose x- and y- components are $x - x_{j,k}$ and $y - y_{j,k}$, respectively. Using the same reason given in (c), Eq. (2.11) implies that

$$u^*(x, y, t; j, k, n) = u^\star(\zeta, \eta, t; j, k, n) \tag{2.27}$$

where

$$\begin{aligned} u^\star(\zeta, \eta, t; j, k, n) &\stackrel{\text{def}}{=} u^n_{j,k} \\ &+ (u_\zeta)^n_{j,k}\left[(\zeta - j\Delta\zeta) - a_\zeta(t - t^n)\right] \\ &+ (u_\eta)^n_{j,k}\left[(\eta - k\Delta\eta) - a_\eta(t - t^n)\right] \end{aligned} \tag{2.28}$$

Note that Eqs. (2.26) and (2.27) can also be verified directly using Eqs. (2.20), (2.22), (2.24), and (2.25).

Next, let (i)

$$a_\zeta^+ \stackrel{\text{def}}{=} \frac{6}{\Delta\zeta} a_\zeta, \qquad a_\eta^+ \stackrel{\text{def}}{=} \frac{6}{\Delta\eta} a_\eta \tag{2.29}$$

(ii)

$$(u_\zeta^+)_{j,k}^n \stackrel{\text{def}}{=} \frac{\Delta\zeta}{6}(u_\zeta)_{j,k}^n, \quad (u_\eta^+)_{j,k}^n \stackrel{\text{def}}{=} \frac{\Delta\eta}{6}(u_\eta)_{j,k}^n \tag{2.30}$$

and (iii)

$$\nu_\zeta \stackrel{\text{def}}{=} \frac{\Delta t}{4} a_\zeta^+, \qquad \nu_\eta \stackrel{\text{def}}{=} \frac{\Delta t}{4} a_\eta^+ \tag{2.31}$$

The coefficients defined in Eqs. (2.29) and (2.30) can be considered as the *normalized* counterparts of those defined in Eqs. (2.24) and (2.25). Also note that $\Delta\zeta$, and $\Delta\eta$, respectively, are the lengths of the sides $\overline{DF}$, and $\overline{BD}$ of ΔBDF depicted in Figs. 9(a)–(c). Moreover, by substituting Eq. (2.29) into Eq. (2.31), one has

$$\frac{a_\zeta \Delta t}{\Delta\zeta} = \frac{2}{3}\nu_\zeta, \qquad \frac{a_\eta \Delta t}{\Delta\eta} = \frac{2}{3}\nu_\eta \tag{2.32}$$

In other words, $(2/3)\nu_\zeta$ and $(2/3)\nu_\eta$ are the Courant numbers in the ζ- and η- directions, respectively.

Furthermore, let $\sigma_{11}^{(1)+}$, $\sigma_{11}^{(1)-}$,..., be defined by

$$\sigma_{11}^{(1)\pm} \stackrel{\text{def}}{=} 1 - \nu_\zeta - \nu_\eta \tag{2.33}$$

$$\sigma_{12}^{(1)\pm} \stackrel{\text{def}}{=} \pm(1 - \nu_\zeta - \nu_\eta)(1 + \nu_\zeta) \tag{2.34}$$

$$\sigma_{13}^{(1)\pm} \stackrel{\text{def}}{=} \pm(1 - \nu_\zeta - \nu_\eta)(1 + \nu_\eta) \tag{2.35}$$

$$\sigma_{21}^{(1)\pm} \stackrel{\text{def}}{=} 1 + \nu_\zeta \tag{2.36}$$

$$\sigma_{22}^{(1)\pm} \stackrel{\text{def}}{=} \mp(1 + \nu_\zeta)(2 - \nu_\zeta) \tag{2.37}$$

$$\sigma_{23}^{(1)\pm} \stackrel{\text{def}}{=} \pm(1 + \nu_\zeta)(1 + \nu_\eta) \tag{2.38}$$

$$\sigma_{31}^{(1)\pm} \stackrel{\text{def}}{=} 1 + \nu_\eta \tag{2.39}$$

$$\sigma_{32}^{(1)\pm} \stackrel{\text{def}}{=} \pm(1 + \nu_\eta)(1 + \nu_\zeta) \tag{2.40}$$

$$\sigma_{33}^{(1)\pm} \stackrel{\text{def}}{=} \mp(1 + \nu_\eta)(2 - \nu_\eta) \tag{2.41}$$

$$\sigma_{11}^{(2)\pm} \stackrel{\text{def}}{=} 1 + \nu_\zeta + \nu_\eta \tag{2.42}$$

$$\sigma_{12}^{(2)\pm} \stackrel{\text{def}}{=} \mp(1 + \nu_\zeta + \nu_\eta)(1 - \nu_\zeta) \tag{2.43}$$

$$\sigma_{13}^{(2)\pm} \stackrel{\text{def}}{=} \mp(1 + \nu_\zeta + \nu_\eta)(1 - \nu_\eta) \tag{2.44}$$

$$\sigma_{21}^{(2)\pm} \stackrel{\text{def}}{=} 1 - \nu_\zeta \tag{2.45}$$

$$\sigma_{22}^{(2)\pm} \stackrel{\text{def}}{=} \pm(1 - \nu_\zeta)(2 + \nu_\zeta) \tag{2.46}$$

$$\sigma_{23}^{(2)\pm} \stackrel{\text{def}}{=} \mp(1 - \nu_\zeta)(1 - \nu_\eta) \tag{2.47}$$

$$\sigma_{31}^{(2)\pm} \stackrel{\text{def}}{=} 1 - \nu_\eta \tag{2.48}$$

$$\sigma_{32}^{(2)\pm} \stackrel{\text{def}}{=} \mp(1 - \nu_\eta)(1 - \nu_\zeta) \tag{2.49}$$

and

$$\sigma_{33}^{(2)\pm} \stackrel{\text{def}}{=} \pm(1 - \nu_\eta)(2 + \nu_\eta) \tag{2.50}$$

Note that:

(a) Each of Eqs. (2.33)–(2.50) represents two equations. One corresponds to the upper signs while the other, to the lower signs.

(b) The definitions given in Eqs. (2.33)–(2.41) will be used in the first marching step of the 2D a scheme; while those given in Eqs. (2.42)–(2.50) will be used in the second marching step. It is seen that the expressions on the right sides of the former can be converted to those of the latter, respectively, by reversing the "+" and "–" signs. Moreover, for every pair of m and ℓ, $\sigma_{m\ell}^{(1)-}$ and $\sigma_{m\ell}^{(2)-}$ are converted to $\sigma_{m\ell}^{(2)+}$ and $\sigma_{m\ell}^{(1)+}$, respectively, if ν_ζ, and ν_η are replaced by $-\nu_\zeta$, and $-\nu_\eta$, respectively.

To simplify the following development, let

$$(j,k;1,1) \stackrel{\text{def}}{=} j + 1/3, k + 1/3 \tag{2.51a}$$

$$(j,k;1,2) \stackrel{\text{def}}{=} j - 2/3, k + 1/3 \tag{2.51b}$$

$$(j,k;1,3) \stackrel{\text{def}}{=} j + 1/3, k - 2/3 \tag{2.51c}$$

$$(j,k;2,1) \stackrel{\text{def}}{=} j - 1/3, k - 1/3 \tag{2.52a}$$

$$(j,k;2,2) \stackrel{\text{def}}{=} j + 2/3, k - 1/3 \tag{2.52b}$$

$$(j,k;2,3) \stackrel{\text{def}}{=} j - 1/3, k + 2/3 \tag{2.52c}$$

Note that (i) $(j,k;1,\ell)$, $\ell = 1,2,3$, are the spatial mesh indices of points A, C, and E depicted in Fig. 7(a), respectively, (ii) $(j,k;2,\ell)$, $\ell = 1,2,3$, are the spatial mesh indices of points D, F, and B depicted in Fig. 8(a), respectively, and (iii) the mesh indices on the right sides of Eqs. (2.51a,b,c) can be converted to those in Eqs. (2.52a,b,c) by reversing the "+" and "–" signs.

Equations (2.12) and (2.13) are evaluated in [2]. With the aid of the above definitions, the results are summarized as follows:

(a) Eq. (2.12) with $\ell = 1$:

$$\left[\sigma_{11}^{(1)+}u + \sigma_{12}^{(1)+}u_\zeta^+ + \sigma_{13}^{(1)+}u_\eta^+\right]_{j,k}^{n+1/2} = \left[\sigma_{11}^{(1)-}u + \sigma_{12}^{(1)-}u_\zeta^+ + \sigma_{13}^{(1)-}u_\eta^+\right]_{(j,k;1,1)}^{n} \tag{2.53}$$

(b) Eq. (2.12) with $\ell = 2$:

$$\left[\sigma_{21}^{(1)+}u + \sigma_{22}^{(1)+}u_\zeta^+ + \sigma_{23}^{(1)+}u_\eta^+\right]_{j,k}^{n+1/2} = \left[\sigma_{21}^{(1)-}u + \sigma_{22}^{(1)-}u_\zeta^+ + \sigma_{23}^{(1)-}u_\eta^+\right]_{(j,k;1,2)}^{n} \tag{2.54}$$

(c) Eq. (2.12) with $\ell = 3$:

$$\left[\sigma_{31}^{(1)+}u + \sigma_{32}^{(1)+}u_\zeta^+ + \sigma_{33}^{(1)+}u_\eta^+\right]_{j,k}^{n+1/2} = \left[\sigma_{31}^{(1)-}u + \sigma_{32}^{(1)-}u_\zeta^+ + \sigma_{33}^{(1)-}u_\eta^+\right]_{(j,k;1,3)}^{n} \tag{2.55}$$

(d) Eq. (2.13) with $\ell = 1$:

$$\left[\sigma_{11}^{(2)+}u + \sigma_{12}^{(2)+}u_\zeta^+ + \sigma_{13}^{(2)+}u_\eta^+\right]_{j,k}^{n+1} = \left[\sigma_{11}^{(2)-}u + \sigma_{12}^{(2)-}u_\zeta^+ + \sigma_{13}^{(2)-}u_\eta^+\right]_{(j,k;2,1)}^{n+1/2} \tag{2.56}$$

(e) Eq. (2.13) with $\ell = 2$:

$$\left[\sigma_{21}^{(2)+}u + \sigma_{22}^{(2)+}u_\zeta^+ + \sigma_{23}^{(2)+}u_\eta^+\right]_{j,k}^{n+1} = \left[\sigma_{21}^{(2)-}u + \sigma_{22}^{(2)-}u_\zeta^+ + \sigma_{23}^{(2)-}u_\eta^+\right]_{(j,k;2,2)}^{n+1/2} \tag{2.57}$$

(f) Eq. (2.13) with $\ell = 3$:

$$\left[\sigma_{31}^{(2)+}u + \sigma_{32}^{(2)+}u_\zeta^+ + \sigma_{33}^{(2)+}u_\eta^+\right]_{j,k}^{n+1} = \left[\sigma_{31}^{(2)-}u + \sigma_{32}^{(2)-}u_\zeta^+ + \sigma_{33}^{(2)-}u_\eta^+\right]_{(j,k;2,3)}^{n+1/2} \tag{2.58}$$

Here $(j,k,n+1/2) \in \Omega_1$ is assumed in Eqs. (2.53)–(2.55); while $(j,k,n+1) \in \Omega_2$ is assumed in Eqs. (2.56)–(2.58). Also, to simplify notation, in the above and hereafter we adopt a convention that can be explained using the expression on the left side of Eq. (2.56) as an example, i.e.,

$$\left[\sigma_{11}^{(2)+}u + \sigma_{12}^{(2)+}u_\zeta^+ + \sigma_{13}^{(2)+}u_\eta^+\right]_{j,k}^{n+1} = \left[\sigma_{11}^{(2)+}u_{j,k}^{n+1} + \sigma_{12}^{(2)+}(u_\zeta^+)_{j,k}^{n+1} + \sigma_{13}^{(2)+}(u_\eta^+)_{j,k}^{n+1}\right]$$

According to Eqs. (2.33)–(2.35), $\sigma_{11}^{(1)\pm}$, $\sigma_{12}^{(1)\pm}$, and $\sigma_{13}^{(1)\pm}$ contain a common factor $(1-\nu_\zeta-\nu_\eta)$. Similarly, each of three consecutive pairs of coefficients defined in Eqs. (2.36)–(2.50) also contain a common factor. As a result, one concludes that:

(a) Eq. (2.53) is satisfied by either $1-\nu_\zeta-\nu_\eta = 0$ or

$$\left[u + (1+\nu_\zeta)u_\zeta^+ + (1+\nu_\eta)u_\eta^+\right]_{j,k}^{n+1/2} = \left[u - (1+\nu_\zeta)u_\zeta^+ - (1+\nu_\eta)u_\eta^+\right]_{(j,k;1,1)}^{n} \tag{2.59}$$

(b) Eq. (2.54) is satisfied by either $1+\nu_\zeta = 0$ or

$$\left[u - (2-\nu_\zeta)u_\zeta^+ + (1+\nu_\eta)u_\eta^+\right]_{j,k}^{n+1/2} = \left[u + (2-\nu_\zeta)u_\zeta^+ - (1+\nu_\eta)u_\eta^+\right]_{(j,k;1,2)}^{n} \tag{2.60}$$

(c) Eq. (2.55) is satisfied by either $1+\nu_\eta = 0$ or

$$\left[u + (1+\nu_\zeta)u_\zeta^+ - (2-\nu_\eta)u_\eta^+\right]_{j,k}^{n+1/2} = \left[u - (1+\nu_\zeta)u_\zeta^+ + (2-\nu_\eta)u_\eta^+\right]_{(j,k;1,3)}^{n} \tag{2.61}$$

(d) Eq. (2.56) is satisfied by either $1+\nu_\zeta+\nu_\eta = 0$ or

$$\left[u - (1-\nu_\zeta)u_\zeta^+ - (1-\nu_\eta)u_\eta^+\right]_{j,k}^{n+1} = \left[u + (1-\nu_\zeta)u_\zeta^+ + (1-\nu_\eta)u_\eta^+\right]_{(j,k;2,1)}^{n+1/2} \tag{2.62}$$

(e) Eq. (2.57) is satisfied by either $1-\nu_\zeta = 0$ or

$$\left[u + (2+\nu_\zeta)u_\zeta^+ - (1-\nu_\eta)u_\eta^+\right]_{j,k}^{n+1} = \left[u - (2+\nu_\zeta)u_\zeta^+ + (1-\nu_\eta)u_\eta^+\right]_{(j,k;2,2)}^{n+1/2} \tag{2.63}$$

(f) Eq. (2.58) is satisfied by either $1-\nu_\eta = 0$ or

$$\left[u - (1-\nu_\zeta)u_\zeta^+ + (2+\nu_\eta)u_\eta^+\right]_{j,k}^{n+1} = \left[u + (1-\nu_\zeta)u_\zeta^+ - (2+\nu_\eta)u_\eta^+\right]_{(j,k;2,3)}^{n+1/2} \tag{2.64}$$

Here $(j,k,n+1/2) \in \Omega_1$ is assumed in Eqs. (2.59)–(2.61); while $(j,k,n+1) \in \Omega_2$ is assumed in Eqs. (2.62)–(2.64). *The current 2D a scheme will be constructed using Eqs. (2.59)–(2.64) instead of*

Eqs. (2.53)–(2.58). Note that Eqs. (2.59)–(2.64) imply Eqs. (2.53)–(2.58). However, the reverse is false unless one assumes that

$$[1-(\nu_\zeta+\nu_\eta)^2]\,(1-\nu_\zeta^2)\,(1-\nu_\eta^2)\neq 0 \qquad (2.65)$$

Note that the expressions within the brackets in the first three equations in Eqs. (2.59)–(2.64), respectively, can be converted to those in the last three by reversing the "+" and "−" signs.

Let $s_1^{(1)}$, $s_2^{(1)}$, $s_3^{(1)}$, $s_1^{(2)}$, $s_2^{(2)}$, and $s_3^{(2)}$ denote the expressions on the right sides of Eqs. (2.59)–(2.64), respectively. Then it can be shown that Eqs. (2.59)–(2.61) are equivalent to

$$u_{j,k}^{n+1/2} = \frac{1}{3}\left[(1-\nu_\zeta-\nu_\eta)s_1^{(1)}+(1+\nu_\zeta)s_2^{(1)}+(1+\nu_\eta)s_3^{(1)}\right] \qquad (2.66)$$

$$(u_\zeta^+)_{j,k}^{n+1/2} = \frac{1}{3}\left(s_1^{(1)}-s_2^{(1)}\right) \qquad (2.67)$$

and

$$(u_\eta^+)_{j,k}^{n+1/2} = \frac{1}{3}\left(s_1^{(1)}-s_3^{(1)}\right) \qquad (2.68)$$

where $(j,k,n+1/2)\in\Omega_1$. Also Eqs. (2.62)–(2.64) are equivalent to

$$u_{j,k}^{n+1} = \frac{1}{3}\left[(1+\nu_\zeta+\nu_\eta)s_1^{(2)}+(1-\nu_\zeta)s_2^{(2)}+(1-\nu_\eta)s_3^{(2)}\right] \qquad (2.69)$$

$$(u_\zeta^+)_{j,k}^{n+1} = \frac{1}{3}\left(s_2^{(2)}-s_1^{(2)}\right) \qquad (2.70)$$

and

$$(u_\eta^+)_{j,k}^{n+1} = \frac{1}{3}\left(s_3^{(2)}-s_1^{(2)}\right) \qquad (2.71)$$

where $(j,k,n+1)\in\Omega_2$.

For any $(j,k,n)\in\Omega$, let

$$\vec{q}(j,k,n) \stackrel{\text{def}}{=} \begin{pmatrix} u \\ u_\zeta^+ \\ u_\eta^+ \end{pmatrix}_{j,k}^{n} \qquad (2.72)$$

Let the 3×3 matrices $Q_\ell^{(k)}$, $k=1,2$, and $\ell=1,2,3$, be the special cases ($\epsilon=0$) of the more general $Q_\ell^{(k)}$ defined in Sec. 3. Then Eqs. (2.66)–(2.68) can be expressed as [2]

$$\begin{aligned}\vec{q}(j,k,n+1/2) = {} & Q_1^{(1)}\vec{q}((j,k;1,1),n) \\ & + Q_2^{(1)}\vec{q}((j,k;1,2),n) \\ & + Q_3^{(1)}\vec{q}((j,k;1,3),n)\end{aligned} \qquad (2.73)$$

where $(j,k,n+1/2)\in\Omega_1$. Also, Eqs. (2.69)–(2.71) can be expressed as [2]

$$\begin{aligned}\vec{q}(j,k,n+1) = {} & Q_1^{(2)}\vec{q}((j,k;2,1),n+1/2) \\ & + Q_2^{(2)}\vec{q}((j,k;2,2),n+1/2) \\ & + Q_3^{(2)}\vec{q}((j,k;2,3),n+1/2)\end{aligned} \qquad (2.74)$$

where $(j,k,n+1)\in\Omega_2$. The marching procedure in the 2D *a* scheme is formed by applying the marching steps defined by Eqs. (2.73) and (2.74) successively.

The 2D *a* scheme has several nontraditional features. They are summarized in the following comments:

(a) The 2D *a* scheme has the simplest stencil in each of their two marching steps, i.e., a tetrahedron in 3D space-time with one vertex at the upper time level and the other three vertices at the lower time level.

(b) Each of the conservation conditions Eqs. (2.53)–(2.58) represents a relation among the marching variables associated with *only two neighboring SEs*. This is a fundamental difference between the current method and other traditional methods.

(c) It is shown in [2] that the 2D *a* scheme is *neutrally* stable if

$$|\nu_\zeta|<1.5, \quad |\nu_\eta|<1.5, \quad \text{and} \quad |\nu_\zeta+\nu_\eta|<1.5. \qquad (2.75)$$

As depicted in Fig. 11, the domain of stability defined by Eq. (2.73) is a hexagonal region in the ν_ζ-ν_η space. Moreover, it is also shown in [2] that Eq. (2.75) can be interpreted as the requirement that the physical domain of dependence of Eq. (2.1) should fall within the numerical domain of dependence.

(d) It is shown in [2] that the 2D *a* scheme has the following property, i.e., for any $(j,k,n)\in\Omega$,

$$\vec{q}(j,k,n+1)\to\vec{q}(j,k,n) \quad \text{as} \quad \Delta t\to 0 \qquad (2.76)$$

if a_x, a_y, w, b, and h are held constant. This property usually is not shared by other schemes that use a mesh that is staggered in time, e.g., the Lax scheme [15].

(e) The 2D *a* scheme is also a two-way marching scheme [2]. In other words, the same flux conservation relations Eqs. (2.12) and (2.13) can be used to construct the backward time-marching versions of the 2D *a* scheme [2].

This section is concluded with the following remarks:

(a) the 2D a scheme is only a special case of the 2D a-μ scheme described in [2]. It is a solver for the 2D convection-diffusion equation

$$\frac{\partial u}{\partial t}+a_x\frac{\partial u}{\partial x}+a_y\frac{\partial u}{\partial y}-\mu\left(\frac{\partial^2 u}{\partial x^2}+\frac{\partial^2 u}{\partial y^2}\right)=0 \quad (2.77)$$

where a_x, a_y, and μ (≥ 0) are constants. Note that this solver, as in the case of its 1D counterpart, is unconditionally stable if $a_x = a_y = 0$.

(b) It should be emphasized that, with the aid of Eqs. (2.19)–(2.22), (2.24), and (2.25), the 2D a scheme can also be expressed in terms of the marching variables and the coefficients tied to the coordinates (x, y). In other words, the coordinates (ζ, η) are introduced solely for the purpose of simplifying the current development. *The essence of the 2D a scheme, and the schemes to be introduced in the following sections, is not dependent on the choice of the coordinates in terms of which these schemes are expressed.*

3. The 2D a-ϵ Scheme

The 2D a scheme is neutrally stable and reversible in time. As explained in Sec. 1, such a scheme cannot be extended to become an Euler solver. As a result, it will be modified to become the 2D a-ϵ scheme. Here ϵ represents a special parameter that controls numerical dissipation.

To proceed, note that the CEs used in Sec. 2 will not be used in this section. As a result, Eqs. (2.12) and (2.13) will no longer be assumed. Instead, the CEs to be used are

$$CE^{(1)}(j,k,n+1/2) \stackrel{\text{def}}{=} \left[CE_1^{(1)}(j,k,n+1/2)\right] \cup \left[CE_2^{(1)}(j,k,n+1/2)\right] \cup \left[CE_3^{(1)}(j,k,n+1/2)\right] \quad (3.1)$$

where $(j,k,n+1/2) \in \Omega_1$, and

$$CE^{(2)}(j,k,n+1) \stackrel{\text{def}}{=} \left[CE_1^{(2)}(j,k,n+1)\right] \cup \left[CE_2^{(2)}(j,k,n+1)\right] \cup \left[CE_3^{(2)}(j,k,n+1)\right] \quad (3.2)$$

where $(j,k,n+1) \in \Omega_2$. We shall assume that the total flux leaving the boundary of any new CE vanishes, i.e.,

$$\oint_{S(CE^{(1)}(j,k,n+1/2))} \vec{h}^* \cdot d\vec{s} = 0, \quad (3.3)$$

and

$$\oint_{S(CE^{(2)}(j,k,n+1))} \vec{h}^* \cdot d\vec{s} = 0. \quad (3.4)$$

Obviously, (i) E_3 can be filled with the new CEs, and (ii) the total flux leaving the boundary of any space-time region that is the union of any new CEs will also vanish.

Moreover, it can be shown that Eqs. (3.3) and (3.4), respectively, are equivalent to Eqs. (2.66) and (2.69).

Proof: By subtracting the expressions on the right sides of Eqs. (2.53)–(2.55), respectively, from those on the left sides, and then multiplying the results by $2wh/3$, we obtain the fluxes leaving $\mathrm{CE}_1^{(1)}(j,k,n+1/2)$, $\mathrm{CE}_2^{(1)}(j,k,n+1/2)$, and $\mathrm{CE}_3^{(1)}(j,k,n+1/2)$, respectively (see Appendix A in [2]). Because the flux leaving an interface from the CE on one side is the negative of that leaving the same interface from the CE on the other side, it is easy to see that the flux leaving $\mathrm{CE}^{(1)}(j,k,n+1/2)$ (which is the union of $\mathrm{CE}_\ell^{(1)}(j,k,n+1/2)$, $\ell = 1,2,3$) is the sum of the fluxes leaving $\mathrm{CE}_\ell^{(1)}(j,k,n+1/2)$, $\ell = 1,2,3$. Thus, the flux leaving $\mathrm{CE}^{(1)}(j,k,n+1/2)$ can be obtained by subtracting the sum of the expressions on the right sides of Eqs. (2.53)–(2.55) from that on the left side, and then multiplying the result by $2wh/3$. Furthermore, we have

$$\sigma_{11}^{(k)\pm} + \sigma_{21}^{(k)\pm} + \sigma_{31}^{(k)\pm} = 3, \qquad k = 1,2 \quad (3.5)$$

and

$$\sigma_{12}^{(k)\pm} + \sigma_{22}^{(k)\pm} + \sigma_{32}^{(k)\pm} = \sigma_{13}^{(k)\pm} + \sigma_{23}^{(k)\pm} + \sigma_{33}^{(k)\pm} = 0, \qquad k = 1,2 \quad (3.6)$$

With the aid of the above considerations, and the fact that the expressions on the left sides of Eqs. (2.53)–(2.55) are all evaluated at the same mesh point $(j,k,n+1/2)$, it becomes obvious that Eq. (3.3) is equivalent to the statement that $u_{j,k}^{n+1/2}$ is 1/3 of the sum on the right sides of Eqs. (2.53)–(2.55). By using Eqs. (2.33)–(2.41), we arrive at the conclusion that Eq. (3.3) is equivalent to Eq. (2.66). By invoking a similar argument involving Eqs. (2.56)–(2.58), and (2.42)–(2.50), we also conclude that Eq. (3.4) is equivalent to Eq. (2.69). QED.

As a result, Eqs. (2.66) and (2.69) are shared by the 2D a scheme and 2D a-ϵ scheme. In this section we shall describe how the other equations in the 2D a scheme i.e., Eqs. (2.67), (2.68), (2.70), and (2.71), can be modified such that the numerical diffusion of the resulting new scheme can be controlled by an adjustable parameter ϵ.

To proceed, for any $(j,k,n+1/2) \in \Omega_1$, let

$$u'^{n+1/2}_{(j,k;1,\ell)} \stackrel{\text{def}}{=} \left(u + \frac{\Delta t}{2}u_t\right)^n_{(j,k;1,\ell)} \quad (3.7)$$

where $\ell = 1,2,3$. By their definitions, $u'^{n+1/2}_{(j,k;1,\ell)}$ can be considered as the finite-difference approximations of u at $((j,k;1,\ell), n+1/2)$, $\ell = 1,2,3$. With the aid of Eqs. (2.26), and (2.29)–(2.31), Eq. (3.7) implies that, for $\ell = 1,2,3$,

$$u'^{n+1/2}_{(j,k;1,\ell)} = \left[u - 2\left(\nu_\zeta u^+_\zeta + \nu_\eta u^+_\eta\right)\right]^n_{(j,k;1,\ell)} \tag{3.8}$$

In Fig. 12(a), P, Q, and R are three points in the ζ-η-u space. Using the coordinates given in the same figure and Eqs. (2.51a)–(2.51c), it can be shown that these points are on a plane represented by

$$u = (u'_\zeta)^{n+1/2}_{j,k}(\zeta - j\Delta\zeta) + (u'_\eta)^{n+1/2}_{j,k}(\eta - k\Delta\eta) + u'^{n+1/2}_{j,k} \tag{3.9}$$

where

$$u'^{n+1/2}_{j,k} = \frac{1}{3}\left(u'^{n+1/2}_{(j,k;1,1)} + u'^{n+1/2}_{(j,k;1,2)} + u'^{n+1/2}_{(j,k;1,3)}\right) \tag{3.10}$$

$$(u'_\zeta)^{n+1/2}_{j,k} = \left(u'^{n+1/2}_{(j,k;1,1)} - u'^{n+1/2}_{(j,k;1,2)}\right)/\Delta\zeta \tag{3.11}$$

and

$$(u'_\eta)^{n+1/2}_{j,k} = \left(u'^{n+1/2}_{(j,k;1,1)} - u'^{n+1/2}_{(j,k;1,3)}\right)/\Delta\eta \tag{3.12}$$

Equation (3.9) implies that point O depicted in Fig. 12(a) is also a point on the plane that contains P, Q, and R. Moreover, for every point on the plane represented by Eq. (3.9), including point O, we have

$$\left(\frac{\partial u}{\partial \zeta}\right)_\eta = (u'_\zeta)^{n+1/2}_{j,k}, \quad \text{and} \quad \left(\frac{\partial u}{\partial \eta}\right)_\zeta = (u'_\eta)^{n+1/2}_{j,k} \tag{3.13}$$

As a result of the above considerations, $u'^{n+1/2}_{j,k}$, $(u'_\zeta)^{n+1/2}_{j,k}$, and $(u'_\eta)^{n+1/2}_{j,k}$ can be considered as the finite-difference approximations of u, $\partial u/\partial\zeta$, and $\partial u/\partial\eta$ at the mesh point $(j,k,n+1/2)$, respectively. Note that $u'^{n+1/2}_{j,k}$ generally is different from $u^{n+1/2}_{j,k}$ which is defined by Eq. (2.66). Because Eq. (2.66) is equivalent to the conservation condition Eq. (3.3) and thus a fundamental part of the 2D a-ϵ scheme, $u'^{n+1/2}_{j,k}$ will not be used in the future development.

To proceed, let

$$(u'^+_\zeta)^{n+1/2}_{j,k} \stackrel{\text{def}}{=} \frac{\Delta\zeta}{6}(u'_\zeta)^{n+1/2}_{j,k} \tag{3.14a}$$

$$(u'^+_\eta)^{n+1/2}_{j,k} \stackrel{\text{def}}{=} \frac{\Delta\eta}{6}(u'_\eta)^{n+1/2}_{j,k} \tag{3.14b}$$

$$(u^{o+}_\zeta)^{n+1/2}_{j,k} \stackrel{\text{def}}{=} \frac{1}{3}\left(s^{(1)}_1 - s^{(1)}_2\right) \tag{3.15a}$$

and

$$(u^{o+}_\eta)^{n+1/2}_{j,k} \stackrel{\text{def}}{=} \frac{1}{3}\left(s^{(1)}_1 - s^{(1)}_3\right) \tag{3.15b}$$

where $s^{(1)}_1$, $s^{(1)}_2$, and $s^{(1)}_3$ are the expressions on the right sides of Eqs. (2.59)–(2.61), respectively. Several comments can be made about Eqs. (3.14a,b) and (3.15a,b):

(a) Eqs. (3.15a,b) simply say that the expressions on the right sides are *denoted* by the notations on the left sides, respectively. Contrarily, Eqs. (2.67) and (2.68) say that the marching variables on the left sides are *assigned* the values of the expressions on the right sides, respectively.

(b) Because the expressions on the right sides of Eqs. (3.15a,b) are functions of the marching variables at the nth time level, so are $(u^{o+}_\zeta)^{n+1/2}_{j,k}$ and $(u^{o+}_\eta)^{n+1/2}_{j,k}$.

(c) Eqs. (2.30), (2.67), (3.13), (3.14a), and (3.15a) imply that both $(u'^+_\zeta)^{n+1/2}_{j,k}$ and $(u^{o+}_\zeta)^{n+1/2}_{j,k}$ are numerical analogues of $\partial u/\partial\zeta$ at the mesh point $(j,k,n+1/2)$, normalized by $\Delta\zeta/6$. Similar interpretations can be given to $(u'^+_\eta)^{n+1/2}_{j,k}$ and $(u^{o+}_\eta)^{n+1/2}_{j,k}$.

(d) $(u'^+_\zeta)^{n+1/2}_{j,k}$ and $(u'^+_\eta)^{n+1/2}_{j,k}$ are defined as a result of a geometric construction involving *finite-difference approximations*. Generally, numerical dissipation will be introduced as a result of using such numerical analogues. On the other hand, $(u^{o+}_\zeta)^{n+1/2}_{j,k}$ and $(u^{o+}_\eta)^{n+1/2}_{j,k}$ emerge from the development of the 2D a scheme which is free from numerical dissipation. In the following, the 2D a-ϵ scheme will be constructed such that (i) $(u^+_\zeta)^{n+1/2}_{j,k}$ is a weighted average of $(u'^+_\zeta)^{n+1/2}_{j,k}$ and $(u^{o+}_\zeta)^{n+1/2}_{j,k}$ with the weight factors 2ϵ and $1-2\epsilon$, respectively; and (ii) $(u^+_\eta)^{n+1/2}_{j,k}$ is a weighted average of $(u'^+_\eta)^{n+1/2}_{j,k}$ and $(u^{o+}_\eta)^{n+1/2}_{j,k}$ with the weight factors 2ϵ and $1-2\epsilon$, respectively. As a result, numerical dissipation may be controlled by varying the value of ϵ.

To proceed, for any $(j,k,n+1/2) \in \Omega_1$, let

$$(du^+_\zeta)^{n+1/2}_{j,k} \stackrel{\text{def}}{=} 2\left[(u'^+_\zeta)^{n+1/2}_{j,k} - (u^{o+}_\zeta)^{n+1/2}_{j,k}\right] \tag{3.16}$$

and

$$(du^+_\eta)^{n+1/2}_{j,k} \stackrel{\text{def}}{=} 2\left[(u'^+_\eta)^{n+1/2}_{j,k} - (u^{o+}_\eta)^{n+1/2}_{j,k}\right] \tag{3.17}$$

Then, with the aid of Eqs. (3.8), (3.11), (3.12),

(3.14a,b), and (3.15a,b), one has

$$(du_\zeta^+)_{j,k}^{n+1/2} = \frac{1}{3}\left[\left(u + 4u_\zeta^+ - 2u_\eta^+\right)_{(j,k;1,2)}^{n} - \left(u - 2u_\zeta^+ - 2u_\eta^+\right)_{(j,k;1,1)}^{n}\right] \tag{3.18}$$

and

$$(du_\eta^+)_{j,k}^{n+1/2} = \frac{1}{3}\left[\left(u - 2u_\zeta^+ + 4u_\eta^+\right)_{(j,k;1,3)}^{n} - \left(u - 2u_\zeta^+ - 2u_\eta^+\right)_{(j,k;1,1)}^{n}\right] \tag{3.19}$$

Thus *both* $(du_\zeta^+)_{j,k}^{n+1/2}$ *and* $(du_\eta^+)_{j,k}^{n+1/2}$ *are functions of the marching variables at the nth time level.* As will be shown shortly, they play a key role in the first marching step of the 2D a-ϵ scheme.

Next we consider Fig. 12(b). For any $(j,k,n+1) \in \Omega_2$, let

$$u'^{n+1}_{(j,k;2,\ell)} \stackrel{\text{def}}{=} \left(u + \frac{\Delta t}{2}u_t\right)_{(j,k;2,\ell)}^{n+1/2} \tag{3.20}$$

where $\ell = 1,2,3$. Then it can be shown that

$$u'^{n+1}_{(j,k;2,\ell)} = \left[u - 2\left(\nu_\zeta u_\zeta^+ + \nu_\eta u_\eta^+\right)\right]_{(j,k;2,\ell)}^{n+1/2} \tag{3.21}$$

In Fig. 12(b), the points P, Q, and R are on a plane represented by

$$u = (u'_\zeta)_{j,k}^{n+1}(\zeta - j\Delta\zeta) + (u'_\eta)_{j,k}^{n+1}(\eta - k\Delta\eta) + u'^{n+1}_{j,k} \tag{3.22}$$

where

$$u'^{n+1}_{j,k} \stackrel{\text{def}}{=} \frac{1}{3}\left(u'^{n+1}_{(j,k;2,1)} + u'^{n+1}_{(j,k;2,2)} + u'^{n+1}_{(j,k;2,3)}\right) \tag{3.23}$$

$$(u'_\zeta)_{j,k}^{n+1} \stackrel{\text{def}}{=} \left(u'^{n+1}_{(j,k;2,2)} - u'^{n+1}_{(j,k;2,1)}\right)/\Delta\zeta, \tag{3.24}$$

and

$$(u'_\eta)_{j,k}^{n+1} \stackrel{\text{def}}{=} \left(u'^{n+1}_{(j,k;2,3)} - u'^{n+1}_{(j,k;2,1)}\right)/\Delta\eta. \tag{3.25}$$

Moreover, the current counterparts to Eqs. (3.14a,b) and (3.15a,b) are

$$(u'^+_\zeta)_{j,k}^{n+1} \stackrel{\text{def}}{=} \frac{\Delta\zeta}{6}(u'_\zeta)_{j,k}^{n+1} \tag{3.26a}$$

$$(u'^+_\eta)_{j,k}^{n+1} \stackrel{\text{def}}{=} \frac{\Delta\eta}{6}(u'_\eta)_{j,k}^{n+1} \tag{3.26b}$$

$$(u_\zeta^{o+})_{j,k}^{n+1} \stackrel{\text{def}}{=} \frac{1}{3}\left(s_2^{(2)} - s_1^{(2)}\right) \tag{3.27a}$$

and

$$(u_\eta^{o+})_{j,k}^{n+1} \stackrel{\text{def}}{=} \frac{1}{3}\left(s_3^{(2)} - s_1^{(2)}\right) \tag{3.27b}$$

where $s_1^{(2)}$, $s_2^{(2)}$, and $s_3^{(2)}$ are the expressions on the right sides of Eqs. (2.62)–(2.64), respectively. *Because these expressions are functions of the marching variables at the* $(n+1/2)$*th time level, so are* $(u_\zeta^{o+})_{j,k}^{n+1}$ *and* $(u_\eta^{o+})_{j,k}^{n+1}$.

With the above preparations, the current counterparts to Eqs. (3.16) and (3.17) are

$$(du_\zeta^+)_{j,k}^{n+1} \stackrel{\text{def}}{=} 2\left[(u'^+_\zeta)_{j,k}^{n+1} - (u_\zeta^{o+})_{j,k}^{n+1}\right] \tag{3.28}$$

and

$$(du_\eta^+)_{j,k}^{n+1} \stackrel{\text{def}}{=} 2\left[(u'^+_\eta)_{j,k}^{n+1} - (u_\eta^{o+})_{j,k}^{n+1}\right] \tag{3.29}$$

respectively, where $(j,k,n+1) \in \Omega_2$. With the aid of Eqs. (3.21) and (3.24)–(3.27a,b), Eqs. (3.28) and (3.29) imply that

$$(du_\zeta^+)_{j,k}^{n+1} = \frac{1}{3}\left[\left(u + 2u_\zeta^+ + 2u_\eta^+\right)_{(j,k;2,1)}^{n+1/2} - \left(u - 4u_\zeta^+ + 2u_\eta^+\right)_{(j,k;2,2)}^{n+1/2}\right] \tag{3.30}$$

and

$$(du_\eta^+)_{j,k}^{n+1} = \frac{1}{3}\left[\left(u + 2u_\zeta^+ + 2u_\eta^+\right)_{(j,k;2,1)}^{n+1/2} - \left(u + 2u_\zeta^+ - 4u_\eta^+\right)_{(j,k;2,3)}^{n+1/2}\right] \tag{3.31}$$

Thus *both* $(du_\zeta^+)_{j,k}^{n+1}$ *and* $(du_\eta^+)_{j,k}^{n+1}$ *are functions of the marching variables at the* $(n+1/2)$*th time level.*

The 2D a-ϵ scheme can now be stated using the above definitions. It consists of two marching steps. The first is formed by Eq. (2.66),

$$(u_\zeta^+)_{j,k}^{n+1/2} = (u_\zeta^{o+})_{j,k}^{n+1/2} + \epsilon(du_\zeta^+)_{j,k}^{n+1/2} \tag{3.32}$$

and

$$(u_\eta^+)_{j,k}^{n+1/2} = (u_\eta^{o+})_{j,k}^{n+1/2} + \epsilon(du_\eta^+)_{j,k}^{n+1/2} \tag{3.33}$$

where $(j,k,n+1/2) \in \Omega_1$. It was explained earlier that the expressions on the right sides of Eqs. (3.32)

and (3.33) are functions of the marching variables at the nth time level. Moreover, according to Eqs. (3.16) and (3.17), Eqs. (3.32) and (3.33) can also be expressed as

$$(u_\zeta^+)_{j,k}^{n+1/2} = (u_\zeta'^+)_{j,k}^{n+1/2} + (\epsilon - 1/2)(du_\zeta^+)_{j,k}^{n+1/2} \quad (3.34)$$

and

$$(u_\eta^+)_{j,k}^{n+1/2} = (u_\eta'^+)_{j,k}^{n+1/2} + (\epsilon - 1/2)(du_\eta^+)_{j,k}^{n+1/2} \quad (3.35)$$

respectively.

The second marching step is formed by Eq. (2.69),

$$(u_\zeta^+)_{j,k}^{n+1} = (u_\zeta^{o+})_{j,k}^{n+1} + \epsilon(du_\zeta^+)_{j,k}^{n+1}, \quad (3.36)$$

and

$$(u_\eta^+)_{j,k}^{n+1} = (u_\eta^{o+})_{j,k}^{n+1} + \epsilon(du_\eta^+)_{j,k}^{n+1}, \quad (3.37)$$

where $(j,k,n+1) \in \Omega_2$. It was explained earlier that the expressions on the right sides of Eqs. (3.36) and (3.37) are functions of the marching variables at the $(n+1/2)$th time level. Furthermore, according to Eqs. (3.28) and (3.29), Eqs. (3.36) and (3.37) can also be expressed as

$$(u_\zeta^+)_{j,k}^{n+1} = (u_\zeta'^+)_{j,k}^{n+1} + (\epsilon - 1/2)(du_\zeta^+)_{j,k}^{n+1}, \quad (3.38)$$

and

$$(u_\eta^+)_{j,k}^{n+1} = (u_\eta'^+)_{j,k}^{n+1} + (\epsilon - 1/2)(du_\eta^+)_{j,k}^{n+1}, \quad (3.39)$$

respectively.

At this juncture, note that:

(a) With the aid of Eqs. (3.15a,b) and (3.27a,b), it is seen that Eqs. (3.32), (3.33), (3.36), and (3.37), respectively, are reduced to Eqs. (2.67), (2.68), (2.70), and (2.71) when $\epsilon = 0$. As a result, the 2D a-ϵ scheme becomes the 2D a scheme when $\epsilon = 0$.

(b) For the special case with $\epsilon = 1/2$, Eqs. (3.34), (3.35), (3.38), and (3.39) are reduced to the forms that represent the finite-difference approximations defined in Eqs. (3.11), (3.12), (3.14a,b), and (3.24)–(3.26a,b). However, Eqs. (2.66) and (2.69), which are independent of ϵ and therefore always part of the a-ϵ scheme, are the results of the flux conservation conditions Eqs. (3.3) and (3.4).

(c) With the aid of Eqs. (2.30) and (3.18), Eq. (3.32) can be rewritten as

$$(u_\zeta)_{j,k}^{n+1/2} = \frac{6}{\Delta\zeta}(u_\zeta^{o+})_{j,k}^{n+1/2} + \frac{\epsilon}{3}\left[\left(\frac{6u}{\Delta\zeta} + 4u_\zeta - \frac{2\Delta\eta}{\Delta\zeta}u_\eta\right)_{(j,k;1,2)}^{n} - \left(\frac{6u}{\Delta\zeta} - 2u_\zeta - \frac{2\Delta\eta}{\Delta\zeta}u_\eta\right)_{(j,k;1,1)}^{n}\right] \quad (3.40)$$

Let (i) $u_{(j,k;1,2)}^n$, $(u_\zeta)_{(j,k;1,2)}^n$ and $(u_\eta)_{(j,k;1,2)}^n$ be identified with the values of u, $\partial u/\partial\zeta$ and $\partial u/\partial\eta$ at the mesh point $((j,k;1,2),n)$, respectively; and (ii) $u_{(j,k;1,1)}^n$, $(u_\zeta)_{(j,k;1,1)}^n$ and $(u_\eta)_{(j,k;1,1)}^n$ be identified with the values of u, $\partial u/\partial\zeta$ and $\partial u/\partial\eta$ at the mesh point $((j,k;1,1),n)$, respectively. Then it can be shown that the expression within the brackets on the right side of Eq. (3.40) is $O(\Delta\zeta,\Delta\eta)$. Furthermore, because Eq. (2.28) is applicable within SE(j,k,n) only, the expression that is enclosed within the first bracket on the right side of Eq. (2.28) is $O(\Delta\zeta,\Delta t)$. From the above considerations, one concludes that the addition of the extra term involving ϵ on the right side of Eq. (3.40) may result in errors that are second order in $\Delta\zeta$, $\Delta\eta$, and Δt. In other words, the addition of the term involving ϵ does not result in a scheme of lower order of accuracy. A similar conclusion is also applicable to Eqs. (3.33), (3.36), and (3.37).

(d) Equations (3.11), (3.13) and (3.14a) imply that $(u_\zeta'^+)_{j,k}^{n+1/2}$ is proportional to the directional derivative along the ζ-direction on the plane that contains points P, Q, and R which are depicted in Fig. 12(a). According to Eq. (3.16), $(du_\zeta^+)_{j,k}^{n+1/2}$ is twice the difference between $(u_\zeta'^+)_{j,k}^{n+1/2}$ and its counterpart in the 2D a scheme. Note that the variable $(du_x)_j^n$, that appears in Eqs. (3.2) and (3.10) of [1,9], plays a role in the 1D a-ϵ scheme [1,9] similar to that of $(du_\zeta^+)_{j,k}^{n+1/2}$ in the present 2D a-ϵ scheme. It can be shown that $(du_x)_j^n$ is equal to the difference between two slopes. The first slope is the central difference given on the right side of Eq. (3.10) in [1,9]. The second slope is the counterpart of the first in the 1D a scheme. Thus the 2D a-ϵ scheme is a natural extension of the 1D a-ϵ scheme.

The a-ϵ scheme will take the form of Eqs. (2.73) and (2.74) if the 3×3 matrices $Q_\ell^{(k)}$, $k = 1,2$, and $\ell = 1,2,3$ take the form to be specified immediately. Because of the limitation imposed by the current double-column format, their elements can only

be specified row by row, sequentially. Furthermore, for the sake of simplicity, the elements of the matrices $3Q_\ell^{(k)}$ will be listed:

$3Q_1^{(1)}$: $1-\nu_\zeta-\nu_\eta$, $-(1-\nu_\zeta-\nu_\eta)(1+\nu_\zeta)$, $-(1-\nu_\zeta-\nu_\eta)(1+\nu_\eta)$, $1-\epsilon$, $-(1+\nu_\zeta-2\epsilon)$, $-(1+\nu_\eta-2\epsilon)$, $1-\epsilon$, $-(1+\nu_\zeta-2\epsilon)$, $-(1+\nu_\eta-2\epsilon)$.

$3Q_2^{(1)}$: $1+\nu_\zeta$, $(1+\nu_\zeta)(2-\nu_\zeta)$, $-(1+\nu_\zeta)(1+\nu_\eta)$, $-(1-\epsilon)$, $-(2-\nu_\zeta-4\epsilon)$, $1+\nu_\eta-2\epsilon$, 0, 0, 0.

$3Q_3^{(1)}$: $1+\nu_\eta$, $-(1+\nu_\eta)(1+\nu_\zeta)$, $(1+\nu_\eta)(2-\nu_\eta)$, 0, 0, 0, $-(1-\epsilon)$, $1+\nu_\zeta-2\epsilon$, $-(2-\nu_\eta-4\epsilon)$.

$3Q_1^{(2)}$: $1+\nu_\zeta+\nu_\eta$, $(1+\nu_\zeta+\nu_\eta)(1-\nu_\zeta)$, $(1+\nu_\zeta+\nu_\eta)(1-\nu_\eta)$, $-(1-\epsilon)$, $-(1-\nu_\zeta-2\epsilon)$, $-(1-\nu_\eta-2\epsilon)$, $-(1-\epsilon)$, $-(1-\nu_\zeta-2\epsilon)$, $-(1-\nu_\eta-2\epsilon)$.

$3Q_2^{(2)}$: $1-\nu_\zeta$, $-(1-\nu_\zeta)(2+\nu_\zeta)$, $(1-\nu_\zeta)(1-\nu_\eta)$, $1-\epsilon$, $-(2+\nu_\zeta-4\epsilon)$, $1-\nu_\eta-2\epsilon$, 0, 0, 0.

$3Q_3^{(2)}$: $1-\nu_\eta$, $(1-\nu_\eta)(1-\nu_\zeta)$, $-(1-\nu_\eta)(2+\nu_\eta)$, 0, 0, 0, $1-\epsilon$, $1-\nu_\zeta-2\epsilon$, $-(2+\nu_\eta-4\epsilon)$.

It is shown in [2] that (i) the 2D a-ϵ scheme is unstable if $\epsilon<0$ or $\epsilon>1$, and (ii) numerical diffusion increases as ϵ increases, at least in the range of $0\le\epsilon\le 0.65$. In order to suppress numerical oscillations near a discontinuity, one may be forced to choose a large ϵ. However, with such a choice, the smooth part of a solution may become highly diffusive. To resolve this dilemma, in the following, we shall construct a generalization of the a-ϵ scheme.

To proceed, let $(j,k,n+1/2)\in\Omega_1$ and consider Fig. 13(a). This figure is essentially identical to Fig. 12(a) except that point O in the latter is replaced by point O^* in the former. The coordinates of point O^* are $(j\Delta\zeta, k\Delta\eta, u_{j,k}^{n+1/2})$ where $u_{j,k}^{n+1/2}$ is defined in Eq. (2.66). Thus point O^* generally is not on the plane that contains points P, Q, and R. Let planes #1, #2, and #3, respectively, be the planes containing the following trios of points: (i) points O^*, Q, and R; (ii) points O^*, R, and P; and (iii) points O^*, P, and Q. Then in general these planes differ from one another and from the plane that contains points P, Q, and R. In the following, first we shall study the former three planes.

As a preliminary, let

$$x_\ell \stackrel{\text{def}}{=} u'^{n+1/2}_{(j,k;1,\ell)} - u_{j,k}^{n+1/2}, \quad \ell=1,2,3 \tag{3.41}$$

$$(u_\zeta^{(1)})_{j,k}^{n+1/2} \stackrel{\text{def}}{=} -(2x_2+x_3)/\Delta\zeta \tag{3.42}$$

$$(u_\eta^{(1)})_{j,k}^{n+1/2} \stackrel{\text{def}}{=} -(x_2+2x_3)/\Delta\eta \tag{3.43}$$

$$(u_\zeta^{(2)})_{j,k}^{n+1/2} \stackrel{\text{def}}{=} (2x_1+x_3)/\Delta\zeta \tag{3.44}$$

$$(u_\eta^{(2)})_{j,k}^{n+1/2} \stackrel{\text{def}}{=} (x_1-x_3)/\Delta\eta \tag{3.45}$$

$$(u_\zeta^{(3)})_{j,k}^{n+1/2} \stackrel{\text{def}}{=} (x_1-x_2)/\Delta\zeta \tag{3.46}$$

and

$$(u_\eta^{(3)})_{j,k}^{n+1/2} \stackrel{\text{def}}{=} (2x_1+x_2)/\Delta\eta \tag{3.47}$$

Moreover, for $\ell=1,2,3$, let

$$(u_x^{(\ell)})_{j,k}^{n+1/2} \stackrel{\text{def}}{=} (u_\zeta^{(\ell)})_{j,k}^{n+1/2}\frac{\partial\zeta}{\partial x}+(u_\eta^{(\ell)})_{j,k}^{n+1/2}\frac{\partial\eta}{\partial x} \tag{3.48}$$

and

$$(u_y^{(\ell)})_{j,k}^{n+1/2} \stackrel{\text{def}}{=} (u_\zeta^{(\ell)})_{j,k}^{n+1/2}\frac{\partial\zeta}{\partial y}+(u_\eta^{(\ell)})_{j,k}^{n+1/2}\frac{\partial\eta}{\partial y} \tag{3.49}$$

With the aid of Eqs. (2.20) and (2.22), we have

$$(u_x^{(\ell)})_{j,k}^{n+1/2} = \frac{\Delta\zeta}{2w}(u_\zeta^{(\ell)})_{j,k}^{n+1/2}+\frac{\Delta\eta}{2w}(u_\eta^{(\ell)})_{j,k}^{n+1/2} \tag{3.50}$$

and

$$\begin{aligned}(u_y^{(\ell)})_{j,k}^{n+1/2} = &-\frac{(w+b)\Delta\zeta}{2wh}(u_\zeta^{(\ell)})_{j,k}^{n+1/2}\\ &+\frac{(w-b)\Delta\eta}{2wh}(u_\eta^{(\ell)})_{j,k}^{n+1/2}\end{aligned} \tag{3.51}$$

Combining Eqs. (3.42)–(3.47) with Eqs. (3.50) and (3.51), one has

$$(u_x^{(1)})_{j,k}^{n+1/2} = -\frac{3}{2w}(x_2+x_3) \tag{3.52}$$

$$(u_y^{(1)})_{j,k}^{n+1/2} = \frac{(3b+w)x_2+(3b-w)x_3}{2wh} \tag{3.53}$$

$$(u_x^{(2)})_{j,k}^{n+1/2} = \frac{3x_1}{2w} \tag{3.54}$$

$$(u_y^{(2)})_{j,k}^{n+1/2} = -\frac{(3b+w)x_1+2wx_3}{2wh} \tag{3.55}$$

$$(u_x^{(3)})_{j,k}^{n+1/2} = \frac{3x_1}{2w} \tag{3.56}$$

and

$$(u_y^{(3)})_{j,k}^{n+1/2} = \frac{(w-3b)x_1+2wx_2}{2wh} \tag{3.57}$$

With the above preparations, it can be shown that, for each $\ell = 1,2,3$, plane $\#\ell$ is represented by

$$u = (u_\zeta^{(\ell)})_{j,k}^{n+1/2}(\zeta - j\Delta\zeta) + (u_\eta^{(\ell)})_{j,k}^{n+1/2}(\eta - k\Delta\eta) + u_{j,k}^{n+1/2}, \tag{3.58}$$

if the coordinates (ζ,η) are used. Alternatively, it is represented by

$$u = (u_x^{(\ell)})_{j,k}^{n+1/2}(x - x_{j,k}) + (u_y^{(\ell)})_{j,k}^{n+1/2}(y - y_{j,k}) + u_{j,k}^{n+1/2}, \tag{3.59}$$

if the coordinates (x,y) are used. Using Eqs. (3.58) and (3.59), one concludes that, at any point on plane $\#\ell$, $\ell = 1,2,3$, we have

$$\left(\frac{\partial u}{\partial \zeta}\right)_\eta = (u_\zeta^{(\ell)})_{j,k}^{n+1/2}, \quad \text{and} \quad \left(\frac{\partial u}{\partial \eta}\right)_\zeta = (u_\eta^{(\ell)})_{j,k}^{n+1/2} \tag{3.60}$$

and

$$\left(\frac{\partial u}{\partial x}\right)_y = (u_x^{(\ell)})_{j,k}^{n+1/2}, \quad \text{and} \quad \left(\frac{\partial u}{\partial y}\right)_x = (u_y^{(\ell)})_{j,k}^{n+1/2} \tag{3.61}$$

Note that Eq. (3.60) is the current counterpart of Eq. (3.13) which is applicable to any point on the plane that contains points P, Q, and R. Let ∇u be the gradient of u. Then Eq. (3.61) implies that, at any point on plane $\#\ell$, $\ell = 1,2,3$, we have

$$|\nabla u| = (\theta_\ell)_{j,k}^{n+1/2} \stackrel{\text{def}}{=} \left[\sqrt{(u_x^{(\ell)})^2 + (u_y^{(\ell)})^2}\right]_{j,k}^{n+1/2} \tag{3.62}$$

To proceed further, we introduce the current counterpart of Eqs. (3.14a,b), i.e.,

$$(u_\zeta^{(\ell)+})_{j,k}^{n+1/2} \stackrel{\text{def}}{=} \frac{\Delta\zeta}{6}(u_\zeta^{(\ell)})_{j,k}^{n+1/2} \tag{3.63a}$$

and

$$(u_\eta^{(\ell)+})_{j,k}^{n+1/2} \stackrel{\text{def}}{=} \frac{\Delta\eta}{6}(u_\eta^{(\ell)})_{j,k}^{n+1/2} \tag{3.63b}$$

Then Eqs. (3.11), (3.12), (3.14a,b), and (3.41)–(3.47) imply that

$$(u_\zeta'^{+})_{j,k}^{n+1/2} = \frac{1}{3}\left[u_\zeta^{(1)+} + u_\zeta^{(2)+} + u_\zeta^{(3)+}\right]_{j,k}^{n+1/2} \tag{3.64}$$

and

$$(u_\eta'^{+})_{j,k}^{n+1/2} = \frac{1}{3}\left[u_\eta^{(1)+} + u_\eta^{(2)+} + u_\eta^{(3)+}\right]_{j,k}^{n+1/2} \tag{3.65}$$

i.e., (i) $u_\zeta'^{+}$ is the simple average of $u_\zeta^{(\ell)+}$, $\ell = 1,2,3$. and (ii) $u_\eta'^{+}$ is the simple average of $u_\eta^{(\ell)+}$, $\ell = 1,2,3$. Note that, for simplicity, hereafter we may suppress the space-time mesh indices if no confusion could occur.

The first marching step of the generalized a-ϵ scheme will be formed using Eqs. (2.66), (3.34), and (3.35) except that (i) $u_\zeta'^{+}$ in Eq. (3.34) is replaced by a *nonlinear* weighted average of $u_\zeta^{(\ell)+}$, $\ell = 1,2,3$, and (ii) $u_\eta'^{+}$ in Eq. (3.35) is replaced by a *nonlinear* weighted average of $u_\eta^{(\ell)+}$, $\ell = 1,2,3$. The design of these weighted averages will be guided by the requirement that the weight assigned to a quantity associated with plane $\#\ell$ is greater if θ_ℓ is smaller. This requirement is similar to that used in the construction of an 1D Euler solver described in [1,9].

To proceed, for any $\alpha \geq 0$, we shall define u_ζ^{w+} and u_η^{w+}, the weighted-average counterparts of $u_\zeta'^{+}$ and $u_\eta'^{+}$, respectively. Let

$$u_\zeta^{w+} = 0, \qquad \text{if} \quad \theta_1 = \theta_2 = \theta_3 = 0; \tag{3.66a}$$

and

$$u_\zeta^{w+} = \frac{(\theta_2\theta_3)^\alpha u_\zeta^{(1)+} + (\theta_3\theta_1)^\alpha u_\zeta^{(2)+} + (\theta_1\theta_2)^\alpha u_\zeta^{(3)+}}{(\theta_1\theta_2)^\alpha + (\theta_2\theta_3)^\alpha + (\theta_3\theta_1)^\alpha} \tag{3.66b}$$

otherwise. Also, let

$$u_\eta^{w+} = 0, \qquad \text{if} \quad \theta_1 = \theta_2 = \theta_3 = 0; \tag{3.67a}$$

and

$$u_\eta^{w+} = \frac{(\theta_2\theta_3)^\alpha u_\eta^{(1)+} + (\theta_3\theta_1)^\alpha u_\eta^{(2)+} + (\theta_1\theta_2)^\alpha u_\eta^{(3)+}}{(\theta_1\theta_2)^\alpha + (\theta_2\theta_3)^\alpha + (\theta_3\theta_1)^\alpha} \tag{3.67b}$$

otherwise. Note that the denominators of the fractions on the right sides of Eqs. (3.66b) and (3.67b) vanish if $\alpha > 0$, and any two of θ_1, θ_2, and θ_3 vanish. Thus, consistency of the above definitions requires the proof of the proposition: $\theta_1 = \theta_2 = \theta_3 = 0$, *if any two of* θ_1, θ_2, *and* θ_3 *vanish.*

Proof: As an example, let $\theta_1 = \theta_2 = 0$. Then Eq. (3.62) implies that $u_x^{(\ell)} = u_y^{(\ell)} = 0$, $\ell = 1,2$. In turn, Eqs. (3.52)–(3.55) imply that $x_1 = x_2 = x_3 = 0$. $\theta_3 = 0$ now follows from Eqs. (3.56), (3.57), and (3.62). QED.

As a result of Eq. (3.66b), we have

$$u_\zeta^{w+} = \begin{cases} u_\zeta^{(1)+}, & \text{if } \theta_1 = 0,\ \theta_2 > 0, \text{ and } \theta_3 > 0; \\ u_\zeta^{(2)+}, & \text{if } \theta_2 = 0,\ \theta_1 > 0, \text{ and } \theta_3 > 0; \\ u_\zeta^{(3)+}, & \text{if } \theta_3 = 0,\ \theta_1 > 0, \text{ and } \theta_2 > 0. \end{cases} \tag{3.68}$$

Assuming $\theta_\ell > 0$, $\ell = 1,2,3$, we have

$$u_\zeta^{w+} = \frac{(1/\theta_1)^\alpha u_\zeta^{(1)+} + (1/\theta_2)^\alpha u_\zeta^{(2)+} + (1/\theta_3)^\alpha u_\zeta^{(3)+}}{(1/\theta_1)^\alpha + (1/\theta_2)^\alpha + (1/\theta_3)^\alpha} \tag{3.69}$$

Thus the weight assigned to $u_\zeta^{(\ell)+}$ is proportional to $(1/\theta_\ell)^\alpha$. By using Eqs. (3.64), (3.66a), and (3.69), one arrives at the conclusion that

$$u_\zeta^{w+} = u_\zeta'^{+}, \qquad \text{if} \qquad \theta_1 = \theta_2 = \theta_3. \tag{3.70}$$

Obviously Eqs. (3.68)–(3.70) are still valid if each symbol ζ is replaced by the symbol η.

On the smooth part of a solution, θ_1, θ_2, and θ_3 are nearly equal. Thus the weighted averages u_ζ^{w+} and u_η^{w+} are nearly equal to the simple averages $u_\zeta'^{+}$, and $u_\eta'^{+}$, respectively (see Eqs. (3.64) and (3.65)). In other words, *the effect of weighted-averaging generally is not discernible on the smooth part of a solution.*

Next let $(j,k,n+1) \in \Omega_2$ and consider Fig. 13(b). The third coordinate $u_{j,k}^{n+1}$ of point O^* is that defined in Eq. (2.69). Let planes #1, #2, and #3, respectively, be the planes containing the following trios of points: (i) points O^*, Q, and R; (ii) points O^*, R, and P; and (iii) points O^*, P, and Q. In the following, we shall study these planes.

As a preliminary, let

$$y_\ell \stackrel{\text{def}}{=} u'^{n+1}_{(j,k;2,\ell)} - u_{j,k}^{n+1}, \quad \ell = 1,2,3 \tag{3.71}$$

$$(u_\zeta^{(1)})_{j,k}^{n+1} \stackrel{\text{def}}{=} (2y_2 + y_3)/\Delta\zeta \tag{3.72}$$

$$(u_\eta^{(1)})_{j,k}^{n+1} \stackrel{\text{def}}{=} (y_2 + 2y_3)/\Delta\eta \tag{3.73}$$

$$(u_\zeta^{(2)})_{j,k}^{n+1} \stackrel{\text{def}}{=} -(2y_1 + y_3)/\Delta\zeta \tag{3.74}$$

$$(u_\eta^{(2)})_{j,k}^{n+1} \stackrel{\text{def}}{=} (y_3 - y_1)/\Delta\eta \tag{3.75}$$

$$(u_\zeta^{(3)})_{j,k}^{n+1} \stackrel{\text{def}}{=} (y_2 - y_1)/\Delta\zeta \tag{3.76}$$

and

$$(u_\eta^{(3)})_{j,k}^{n+1} \stackrel{\text{def}}{=} -(2y_1 + y_2)/\Delta\eta \tag{3.77}$$

Moreover, for $\ell = 1,2,3$, let

$$(u_x^{(\ell)})_{j,k}^{n+1} \stackrel{\text{def}}{=} (u_\zeta^{(\ell)})_{j,k}^{n+1} \frac{\partial\zeta}{\partial x} + (u_\eta^{(\ell)})_{j,k}^{n+1} \frac{\partial\eta}{\partial x} \tag{3.78}$$

and

$$(u_y^{(\ell)})_{j,k}^{n+1} \stackrel{\text{def}}{=} (u_\zeta^{(\ell)})_{j,k}^{n+1} \frac{\partial\zeta}{\partial y} + (u_\eta^{(\ell)})_{j,k}^{n+1} \frac{\partial\eta}{\partial y} \tag{3.79}$$

With the above definitions, Eqs. (3.50) and (3.51) remain valid if each upper index $n+1/2$ is replaced by $n+1$. As a result, Eqs. (3.72)–(3.77) imply that

$$(u_x^{(1)})_{j,k}^{n+1} = \frac{3}{2w}(y_2 + y_3) \tag{3.80}$$

$$(u_y^{(1)})_{j,k}^{n+1} = -\frac{(3b+w)y_2 + (3b-w)y_3}{2wh} \tag{3.81}$$

$$(u_x^{(2)})_{j,k}^{n+1} = -\frac{3y_1}{2w} \tag{3.82}$$

$$(u_y^{(2)})_{j,k}^{n+1} = \frac{(3b+w)y_1 + 2wy_3}{2wh} \tag{3.83}$$

$$(u_x^{(3)})_{j,k}^{n+1} = -\frac{3y_1}{2w} \tag{3.84}$$

and

$$(u_y^{(3)})_{j,k}^{n+1} = -\frac{(w-3b)y_1 + 2wy_2}{2wh} \tag{3.85}$$

With the above preparations, the earlier developments that involve Eqs. (3.58)–(3.70) can be repeated for the current case with the only change being the replacement of each upper index $n+1/2$ by $n+1$. Particularly, $(u_\zeta^{w+})_{j,k}^{n+1}$ and $(u_\eta^{w+})_{j,k}^{n+1}$ can be defined using Eqs. (3.66a,b) and (3.67a,b) with the understanding that each symbol in these equations is associated with the mesh point $(j,k,n+1)$.

The generalized a-ϵ scheme, referred to as the weighted-average a-ϵ scheme, can now be stated. It consists of two marching steps. The first is formed by Eq. (2.66),

$$(u_\zeta^+)_{j,k}^{n+1/2} = (u_\zeta^{w+})_{j,k}^{n+1/2} + (\epsilon - 1/2)(du_\zeta^+)_{j,k}^{n+1/2} \tag{3.86}$$

and

$$(u_\eta^+)_{j,k}^{n+1/2} = (u_\eta^{w+})_{j,k}^{n+1/2} + (\epsilon - 1/2)(du_\eta^+)_{j,k}^{n+1/2} \tag{3.87}$$

where $(j,k,n+1/2) \in \Omega_1$. The second is formed by Eq. (2.69),

$$(u_\zeta^+)_{j,k}^{n+1} = (u_\zeta^{w+})_{j,k}^{n+1} + (\epsilon - 1/2)(du_\zeta^+)_{j,k}^{n+1} \tag{3.88}$$

and

$$(u_\eta^+)_{j,k}^{n+1} = (u_\eta^{w+})_{j,k}^{n+1} + (\epsilon - 1/2)(du_\eta^+)_{j,k}^{n+1} \quad (3.89)$$

where $(j,k,n+1) \in \Omega_2$.

Note that, according to Eq. (3.62), evaluation of $(\theta_\ell)^\alpha$ does not involve a fractional power if α is an even integer. Because a fractional power is costly to evaluate, use of the generalized a-ϵ scheme is less costly when α is an even integer.

4. The 2D Euler Solvers

We consider a dimensionless form of the 2D unsteady Euler equations of a perfect gas. Let ρ, u, v, p, and γ be the mass density, x-velocity component, y-velocity component, static pressure, and constant specific heat ratio, respectively. Let

$$u_1 = \rho, \quad u_2 = \rho u, \quad u_3 = \rho v \quad (4.1a)$$

$$u_4 = p/(\gamma - 1) + \rho(u^2 + v^2)/2 \quad (4.1b)$$

$$f_1^x = u_2, \quad (4.2)$$

$$f_2^x = (\gamma - 1)u_4 + (3 - \gamma)(u_2)^2/(2u_1) - (\gamma - 1)(u_3)^2/(2u_1) \quad (4.3)$$

$$f_3^x = u_2\, u_3/u_1, \quad (4.4)$$

$$f_4^x = \gamma u_2 u_4/u_1 - (1/2)(\gamma - 1)u_2\left[(u_2)^2 + (u_3)^2\right]/(u_1)^2 \quad (4.5)$$

$$f_1^y = u_3, \quad (4.6)$$

$$f_2^y = u_2\, u_3/u_1, \quad (4.7)$$

$$f_3^y = (\gamma - 1)u_4 + (3 - \gamma)(u_3)^2/(2u_1) - (\gamma - 1)(u_2)^2/(2u_1) \quad (4.8)$$

and

$$f_4^y = \gamma u_3 u_4/u_1 - (1/2)(\gamma - 1)u_3\left[(u_2)^2 + (u_3)^2\right]/(u_1)^2 \quad (4.9)$$

Then the Euler equations can be expressed as

$$\frac{\partial u_m}{\partial t} + \frac{\partial f_m^x}{\partial x} + \frac{\partial f_m^y}{\partial y} = 0, \quad m = 1,2,3,4 \quad (4.10)$$

The integral form of Eq. (4.10) in space-time E_3 is

$$\oint_{S(V)} \vec{h}_m \cdot d\vec{s} = 0, \qquad m = 1,2,3,4 \quad (4.11)$$

where

$$\vec{h}_m \stackrel{\text{def}}{=} (f_m^x, f_m^y, u_m), \qquad m = 1,2,3,4 \quad (4.12)$$

are the space-time mass, x-momemtum component, y-momemtum component, and energy current density vectors, respectively.

As a preliminary, let

$$f_{m,\ell}^x \stackrel{\text{def}}{=} \partial f_m^x/\partial u_\ell, \quad \text{and} \quad f_{m,\ell}^y \stackrel{\text{def}}{=} \partial f_m^y/\partial u_\ell \quad (4.13)$$

where $m,\ell = 1,2,3,4$. The matrices formed by $f_{m,\ell}^x$ and $f_{m,\ell}^y$, $m,\ell = 1,2,3,4$, respectively, are given in [2]. Because f_m^x and f_m^y, $m = 1,2,3,4$, are homogeneous functions of degree 1 [19] in u_1, u_2, u_3, and u_4, we have

$$f_m^x = \sum_{\ell=1}^4 f_{m,\ell}^x\, u_\ell, \quad \text{and} \quad f_m^y = \sum_{\ell=1}^4 f_{m,\ell}^y\, u_\ell. \quad (4.14)$$

For any $(x,y,t) \in \text{SE}(j,k,n)$, $u_m(x,y,t)$, $f_m^x(x,y,t)$, $f_m^y(x,y,t)$, and $\vec{h}_m(x,y,t)$, respectively, are approximated by $u_m^*(x,y,t\,;j,k,n)$, $f_m^{x*}(x,y,t\,;j,k,n)$, $f_m^{y*}(x,y,t\,;j,k,n)$, and $\vec{h}_m^*(x,y,t\,;j,k,n)$. They will be defined shortly. For $m = 1,2,3,4$, let

$$u_m^*(x,y,t\,;j,k,n) \stackrel{\text{def}}{=} (u_m)_{j,k}^n + (u_{mx})_{j,k}^n(x - x_{j,k}) + (u_{my})_{j,k}^n(y - y_{j,k}) + (u_{mt})_{j,k}^n(t - t^n) \quad (4.15)$$

where $(u_m)_{j,k}^n$, $(u_{mx})_{j,k}^n$, $(u_{my})_{j,k}^n$, and $(u_{mt})_{j,k}^n$ are constants in $\text{SE}(j,k,n)$. Obviously, they can be considered as the numerical analogues of the values of u_m, $\partial u_m/\partial x$, $\partial u_m/\partial y$, and $\partial u_m/\partial t$ at (x_j, y_k, t^n), respectively.

Let $(f_m^x)_{j,k}^n$, $(f_m^y)_{j,k}^n$, $(f_{m,\ell}^x)_{j,k}^n$, and $(f_{m,\ell}^y)_{j,k}^n$ denote the values of f_m^x, f_m^y, $f_{m,\ell}^x$, and $f_{m,\ell}^y$, respectively, when u_m, $m = 1,2,3,4$, respectively, assume the values of $(u_m)_{j,k}^n$, $m = 1,2,3,4$. Let

$$(f_{mx}^x)_{j,k}^n \stackrel{\text{def}}{=} \sum_{\ell=1}^4 (f_{m,\ell}^x)_{j,k}^n (u_{\ell x})_{j,k}^n \quad (4.16)$$

$$(f_{my}^x)_{j,k}^n \stackrel{\text{def}}{=} \sum_{\ell=1}^4 (f_{m,\ell}^x)_{j,k}^n (u_{\ell y})_{j,k}^n \quad (4.17)$$

$$(f_{mt}^x)_{j,k}^n \stackrel{\text{def}}{=} \sum_{\ell=1}^4 (f_{m,\ell}^x)_{j,k}^n (u_{\ell t})_{j,k}^n \quad (4.18)$$

$$(f_{mx}^y)_{j,k}^n \stackrel{\text{def}}{=} \sum_{\ell=1}^4 (f_{m,\ell}^y)_{j,k}^n (u_{\ell x})_{j,k}^n \quad (4.19)$$

$$(f_{my}^y)_{j,k}^n \stackrel{\text{def}}{=} \sum_{\ell=1}^4 (f_{m,\ell}^y)_{j,k}^n (u_{\ell y})_{j,k}^n \quad (4.20)$$

and

$$(f^y_{mt})^n_{j,k} \stackrel{\text{def}}{=} \sum_{\ell=1}^{4} (f^y_{m,\ell})^n_{j,k} (u_{\ell t})^n_{j,k} \tag{4.21}$$

Because (i)

$$\frac{\partial f^x_m}{\partial x} = \sum_{\ell=1}^{4} f^x_{m,\ell} \frac{\partial u_\ell}{\partial x}, \qquad m = 1,2,3,4 \tag{4.22}$$

and (ii) the expression on the right side of Eq. (4.16) is the numerical analogue of that on the right side of Eq. (4.22) at (x_j, y_k, t^n), $(f^x_{mx})^n_{j,k}$ can be considered as the numerical analogue of the value of $\partial f^x_m/\partial x$ at (x_j, y_k, t^n). Similarly, $(f^x_{my})^n_{j,k}$, $(f^x_{mt})^n_{j,k}$, $(f^y_{mx})^n_{j,k}$, $(f^y_{my})^n_{j,k}$, and $(f^y_{mt})^n_{j,k}$ can be considered as the numerical analogues of the values of $\partial f^x_m/\partial y$, $\partial f^x_m/\partial t$, $\partial f^y_m/\partial x$, $\partial f^y_m/\partial y$, and $\partial f^y_m/\partial t$ at(x_j, y_k, t^n), respectively. As a result, we assume that, for $m = 1,2,3,4$,

$$f^{x*}_m(x,y,t;j,k,n) \stackrel{\text{def}}{=} (f^x_m)^n_{j,k} + (f^x_{mx})^n_{j,k}(x - x_{j,k}) + (f^x_{my})^n_{j,k}(y - y_{j,k}) + (f^x_{mt})^n_{j,k}(t - t^n) \tag{4.23}$$

and

$$f^{y*}_m(x,y,t;j,k,n) \stackrel{\text{def}}{=} (f^y_m)^n_{j,k} + (f^y_{mx})^n_{j,k}(x - x_{j,k}) + (f^y_{my})^n_{j,k}(y - y_{j,k}) + (f^y_{mt})^n_{j,k}(t - t^n) \tag{4.24}$$

Also, as an analogue to Eq. (4.12), we assume that

$$\vec{h}^*_m(x,y,t;j,k,n) \stackrel{\text{def}}{=} \left(f^{x*}_m(x,y,t;j,k,n), f^{y*}_m(x,y,t;j,k,n), u^*_m(x,y,t;j,k,n)\right) \tag{4.25}$$

Note that, by their definitions: (i) f^x_m, f^y_m, $f^x_{m,\ell}$, and $f^y_{m,\ell}$, $m,\ell = 1,2,3,4$, are functions of $(u_m)^n_{j,k}$, $m = 1,2,3,4$; (ii) $(f^x_{mx})^n_{j,k}$ and $(f^y_{mx})^n_{j,k}$, $m = 1,2,3,4$, are functions of $(u_m)^n_{j,k}$ and $(u_{mx})^n_{j,k}$, $m = 1,2,3,4$; (iii) $(f^x_{my})^n_{j,k}$ and $(f^y_{my})^n_{j,k}$, $m = 1,2,3,4$, are functions of $(u_m)^n_{j,k}$ and $(u_{my})^n_{j,k}$, $m = 1,2,3,4$; and (iv) $(f^x_{mt})^n_{j,k}$ and $(f^y_{mt})^n_{j,k}$ are functions of $(u_m)^n_{j,k}$ and $(u_{mt})^n_{j,k}$, $m = 1,2,3,4$.

Moreover, we assume that, for any $(x,y,t) \in \text{SE}(j,k,n)$, and $m = 1,2,3,4$,

$$\frac{\partial u^*_m(x,y,t;j,k,n)}{\partial t} + \frac{\partial f^{x*}_m(x,y,t;j,k,n)}{\partial x} + \frac{\partial f^{y*}_m(x,y,t;j,k,n)}{\partial y} = 0 \tag{4.26}$$

Note that Eq. (4.26) is the numerical analogue of Eq. (4.10). With the aid of Eqs. (4.15), (4.16), (4.20), (4.23), and (4.24), Eq. (4.26) implies that, for $m = 1,2,3,4$,

$$(u_{mt})^n_{j,k} = -(f^x_{mx})^n_{j,k} - (f^y_{my})^n_{j,k} = -\sum_{\ell=1}^{4} \left[f^x_{m,\ell} u_{\ell x} + f^y_{m,\ell} u_{\ell y}\right]^n_{j,k} \tag{4.27}$$

Thus $(u_{mt})^n_{j,k}$ are functions of $(u_m)^n_{j,k}$, $(u_{mx})^n_{j,k}$, and $(u_{my})^n_{j,k}$. From this result and the facts stated following Eq. (4.25), one concludes that *the only independent discrete variables needed to be solved in the current marching scheme* are $(u_m)^n_{j,k}$, $(u_{mx})^n_{j,k}$, and $(u_{my})^n_{j,k}$.

Consider the conservation elements depicted in Figs. 7(a) and 8(a). The Euler counterparts to Eqs. (2.12) and (2.13), respectively, are (i)

$$\oint_{S(CE^{(1)}_\ell(j,k,n+1/2))} \vec{h}^*_m \cdot d\vec{s} = 0 \tag{4.28}$$

where $(j,k,n+1/2) \in \Omega_1$; and (ii)

$$\oint_{S(CE^{(2)}_\ell(j,k,n+1))} \vec{h}^*_m \cdot d\vec{s} = 0 \tag{4.29}$$

where $(j,k,n+1) \in \Omega_2$. Note that $\ell = 1,2,3$, and $m = 1,2,3,4$ in Eqs. (4.28) and (4.29).

Next we shall introduce the Euler counterparts of Eqs. (2.24), (2.25), (2.30), and (2.31). For any $(j,k,n) \in \Omega$, let

$$\begin{pmatrix} (f^\zeta_{m,\ell})^n_{j,k} \\ (f^\eta_{m,\ell})^n_{j,k} \end{pmatrix} \stackrel{\text{def}}{=} T^{-1} \begin{pmatrix} (f^x_{m,\ell})^n_{j,k} \\ (f^y_{m,\ell})^n_{j,k} \end{pmatrix} \tag{4.30}$$

and

$$\begin{pmatrix} (u_{m\zeta})^n_{j,k} \\ (u_{m\eta})^n_{j,k} \end{pmatrix} \stackrel{\text{def}}{=} T^t \begin{pmatrix} (u_{mx})^n_{j,k} \\ (u_{my})^n_{j,k} \end{pmatrix} \tag{4.31}$$

where $m,\ell = 1,2,3,4$. The *normalized* counterparts of those parameters defined in Eqs. (4.30) and (4.31) are

$$(u^+_{m\zeta})^n_{j,k} \stackrel{\text{def}}{=} \frac{\Delta\zeta}{6}(u_{m\zeta})^n_{j,k} \tag{4.32a}$$

$$(u^+_{m\eta})^n_{j,k} \stackrel{\text{def}}{=} \frac{\Delta\eta}{6}(u_{m\eta})^n_{j,k} \tag{4.32b}$$

$$(f^{\zeta+}_{m,\ell})^n_{j,k} \stackrel{\text{def}}{=} \frac{3\Delta t}{2\Delta\zeta}(f^\zeta_{m,\ell})^n_{j,k} \tag{4.33a}$$

and

$$(f^{\eta+}_{m,\ell})^n_{j,k} \stackrel{\text{def}}{=} \frac{3\Delta t}{2\Delta\eta}(f^\eta_{m,\ell})^n_{j,k} \tag{4.33b}$$

In the following development, for simplicity, we may strip from every variable in an equation its indices j, k, and n if all variables are associated with the same mesh point $(j,k,n) \in \Omega$. Let $F^{\zeta+}$ and $F^{\eta+}$, respectively, denote the 4×4 matrices formed by $f^{\zeta+}_{m,\ell}$ and $f^{\eta+}_{m,\ell}$, $m,\ell = 1,2,3,4$. Let I be the 4×4 identity matrix. Then the current counterparts to Eqs. (2.33)–(2.50) are

$$\Sigma^{(1)\pm}_{11} \stackrel{\text{def}}{=} I - F^{\zeta+} - F^{\eta+} \tag{4.34}$$

$$\Sigma^{(1)\pm}_{12} \stackrel{\text{def}}{=} \pm(I - F^{\zeta+} - F^{\eta+})(I + F^{\zeta+}) \tag{4.35}$$

$$\Sigma^{(1)\pm}_{13} \stackrel{\text{def}}{=} \pm(I - F^{\zeta+} - F^{\eta+})(I + F^{\eta+}) \tag{4.36}$$

$$\Sigma^{(1)\pm}_{21} \stackrel{\text{def}}{=} I + F^{\zeta+} \tag{4.37}$$

$$\Sigma^{(1)\pm}_{22} \stackrel{\text{def}}{=} \mp(I + F^{\zeta+})(2I - F^{\zeta+}) \tag{4.38}$$

$$\Sigma^{(1)\pm}_{23} \stackrel{\text{def}}{=} \pm(I + F^{\zeta+})(I + F^{\eta+}) \tag{4.39}$$

$$\Sigma^{(1)\pm}_{31} \stackrel{\text{def}}{=} I + F^{\eta+} \tag{4.40}$$

$$\Sigma^{(1)\pm}_{32} \stackrel{\text{def}}{=} \pm(I + F^{\eta+})(I + F^{\zeta+}) \tag{4.41}$$

$$\Sigma^{(1)\pm}_{33} \stackrel{\text{def}}{=} \mp(I + F^{\eta+})(2I - F^{\eta+}) \tag{4.42}$$

$$\Sigma^{(2)\pm}_{11} \stackrel{\text{def}}{=} I + F^{\zeta+} + F^{\eta+} \tag{4.43}$$

$$\Sigma^{(2)\pm}_{12} \stackrel{\text{def}}{=} \mp(I + F^{\zeta+} + F^{\eta+})(I - F^{\zeta+}) \tag{4.44}$$

$$\Sigma^{(2)\pm}_{13} \stackrel{\text{def}}{=} \mp(I + F^{\zeta+} + F^{\eta+})(I - F^{\eta+}) \tag{4.45}$$

$$\Sigma^{(2)\pm}_{21} \stackrel{\text{def}}{=} I - F^{\zeta+} \tag{4.46}$$

$$\Sigma^{(2)\pm}_{22} \stackrel{\text{def}}{=} \pm(I - F^{\zeta+})(2I + F^{\zeta+}) \tag{4.47}$$

$$\Sigma^{(2)\pm}_{23} \stackrel{\text{def}}{=} \mp(I - F^{\zeta+})(I - F^{\eta+}) \tag{4.48}$$

$$\Sigma^{(2)\pm}_{31} \stackrel{\text{def}}{=} I - F^{\eta+} \tag{4.49}$$

$$\Sigma^{(2)\pm}_{32} \stackrel{\text{def}}{=} \mp(I - F^{\eta+})(I - F^{\zeta+}) \tag{4.50}$$

and

$$\Sigma^{(2)\pm}_{33} \stackrel{\text{def}}{=} \pm(I - F^{\eta+})(2I + F^{\eta+}) \tag{4.51}$$

Note that Eqs. (2.33)–(2.50) become Eqs. (4.34)–(4.51), Eqs. (4.34)–(4.51), respectively, under the following rules of substitution:

Rule 1: 1, ν_ζ, and ν_η, be replaced by I, $F^{\zeta+}$, and $F^{\eta+}$, respectively.

Rule 2: $\sigma^{(1)\pm}_{m\ell}$ and $\sigma^{(2)\pm}_{m\ell}$ be replaced by $\Sigma^{(1)\pm}_{m\ell}$ and $\Sigma^{(2)\pm}_{m\ell}$, $m,\ell = 1,2,3$, respectively.

As will be shown, under the above and other rules of substitution, many other equations given in Secs. 2 and 3 can be converted to their counterparts in this section. The latter will be referred to as the Euler *images* of the former.

Equations (4.28) and (4.29) are evaluated in Appendix B of [2]. Let $\vec{u}$, $\vec{u}^+_\zeta$, and $\vec{u}^+_\eta$, respectively, be the 4×1 column matrices formed by u_m, $u^+_{m\zeta}$, and $u^+_{m\eta}$, $m = 1,2,3,4$. Then the results can be expressed as: (i)

$$\left[\Sigma^{(1)+}_{\ell 1}\vec{u} + \Sigma^{(1)+}_{\ell 2}\vec{u}^+_\zeta + \Sigma^{(1)+}_{\ell 3}\vec{u}^+_\eta\right]^{n+1/2}_{j,k} = \left[\Sigma^{(1)-}_{\ell 1}\vec{u} + \Sigma^{(1)-}_{\ell 2}\vec{u}^+_\zeta + \Sigma^{(1)-}_{\ell 3}\vec{u}^+_\eta\right]^{n}_{(j,k;1,\ell)} \tag{4.52}$$

where $(j,k,n+1/2) \in \Omega_1$ and $\ell = 1,2,3$, and (ii)

$$\left[\Sigma^{(2)+}_{\ell 1}\vec{u} + \Sigma^{(2)+}_{\ell 2}\vec{u}^+_\zeta + \Sigma^{(2)+}_{\ell 3}\vec{u}^+_\eta\right]^{n+1}_{j,k} = \left[\Sigma^{(2)-}_{\ell 1}\vec{u} + \Sigma^{(2)-}_{\ell 2}\vec{u}^+_\zeta + \Sigma^{(2)-}_{\ell 3}\vec{u}^+_\eta\right]^{n+1/2}_{(j,k;2,\ell)} \tag{4.53}$$

where $(j,k,n+1) \in \Omega_2$ and $\ell = 1,2,3$. Note that the six equations given in Eqs. (4.52) and (4.53) are the Euler images of Eqs. (2.53)–(2.58), respectively, under the substitution defined by Rule 2 given above and

Rule 3: u, u_t, u^+_ζ, and u^+_η be replaced by $\vec{u}$, $\vec{u}_t$, $\vec{u}^+_\zeta$, and $\vec{u}^+_\eta$, respectively.

Note that an Euler image is a matrix equation. Because (i) matrix multiplication is noncommutative, and (ii) the coefficient matrices of an Euler image are mesh-point dependent, an Euler image is more difficult to deal with than its counterpart in the 2D a or a-ϵ scheme.

Because the Euler images of Eqs. (3.5) and (3.6) are also true [2], by summing over the three equations given in Eq. (4.52), one concludes that, for any $(j,k,n+1/2) \in \Omega_1$,

$$\vec{u}^{n+1/2}_{j,k} = \frac{1}{3}\sum_{\ell=1}^{3}\left[\Sigma^{(1)-}_{\ell 1}\vec{u} + \Sigma^{(1)-}_{\ell 2}\vec{u}^+_\zeta + \Sigma^{(1)-}_{\ell 3}\vec{u}^+_\eta\right]^{n}_{(j,k;1,\ell)} \tag{4.54}$$

As a result, $\vec{u}^{n+1/2}_{j,k}$ can be evaluated in terms of the marching variables at the nth time level. Similarly, by using Eq. (4.53), one concludes that, for any $(j,k,n+1) \in \Omega_2$,

$$\vec{u}^{n+1}_{j,k} = \frac{1}{3}\sum_{\ell=1}^{3}\left[\Sigma^{(2)-}_{\ell 1}\vec{u} + \Sigma^{(2)-}_{\ell 2}\vec{u}^+_\zeta + \Sigma^{(2)-}_{\ell 3}\vec{u}^+_\eta\right]^{n+1/2}_{(j,k;2,\ell)} \tag{4.55}$$

As a result, $\vec{u}_{j,k}^{n+1}$ can be evaluated in terms of the marching variables at the $(n+1/2)$th time level.

For any $(j,k,n+1/2) \in \Omega_1$, the matrices $(\Sigma_{m\ell}^{(1)+})_{j,k}^{n+1/2}$, $m,\ell = 1,2,3$, are functions of $\vec{u}_{j,k}^{n+1/2}$. Thus they are also functions of the marching variables at the nth time level. Assuming the existence of the inverse of each of the matrices $(\Sigma_{m1}^{(1)+})_{j,k}^{n+1/2}$, $m = 1,2,3$, one can define

$$\vec{S}_\ell^{(1)} \stackrel{\text{def}}{=} \left[\left(\Sigma_{\ell 1}^{(1)+}\right)_{j,k}^{n+1/2}\right]^{-1} \times \left[\Sigma_{\ell 1}^{(1)-}\vec{u} + \Sigma_{\ell 2}^{(1)-}\vec{u}_\zeta^+ + \Sigma_{\ell 3}^{(1)-}\vec{u}_\eta^+\right]_{(j,k;1,\ell)}^{n} \tag{4.56}$$

where $\ell = 1,2,3$, and the inverse of a matrix A is denoted by $[A]^{-1}$. As a result of their definitions, $\vec{S}_\ell^{(1)}$, $\ell = 1,2,3$, can be evaluated using the marching variables at the nth time level.

For any $(j,k,n+1) \in \Omega_2$, the matrices $(\Sigma_{m\ell}^{(2)+})_{j,k}^{n+1}$, $m,\ell = 1,2,3$, are functions of $\vec{u}_{j,k}^{n+1}$. Thus they are also functions of the marching variables at the $(n+1/2)$th time level. Assuming the existence of the inverse of each of the matrices $(\Sigma_{m1}^{(2)+})_{j,k}^{n+1}$, $m = 1,2,3$, one can define

$$\vec{S}_\ell^{(2)} \stackrel{\text{def}}{=} \left[\left(\Sigma_{\ell 1}^{(2)+}\right)_{j,k}^{n+1}\right]^{-1} \times \left[\Sigma_{\ell 1}^{(2)-}\vec{u} + \Sigma_{\ell 2}^{(2)-}\vec{u}_\zeta^+ + \Sigma_{\ell 3}^{(2)-}\vec{u}_\eta^+\right]_{(j,k;2,\ell)}^{n+1/2} \tag{4.57}$$

As a result of their definitions, $\vec{S}_\ell^{(2)}$, $\ell = 1,2,3$, can be evaluated using the marching variables at the $(n+1/2)$th time level.

With the aid of Eqs. (4.34)–(4.51), (4.56), and (4.57), Eqs. (4.52) and (4.53) imply that [2]

$$\left[\vec{u} + \left(I + F^{\zeta+}\right)\vec{u}_\zeta^+ + \left(I + F^{\eta+}\right)\vec{u}_\eta^+\right]_{j,k}^{n+1/2} = \vec{S}_1^{(1)}, \tag{4.58}$$

$$\left[\vec{u} - \left(2I - F^{\zeta+}\right)\vec{u}_\zeta^+ + \left(I + F^{\eta+}\right)\vec{u}_\eta^+\right]_{j,k}^{n+1/2} = \vec{S}_2^{(1)}, \tag{4.59}$$

$$\left[\vec{u} + \left(I + F^{\zeta+}\right)\vec{u}_\zeta^+ - \left(2I - F^{\eta+}\right)\vec{u}_\eta^+\right]_{j,k}^{n+1/2} = \vec{S}_3^{(1)}, \tag{4.60}$$

$$\left[\vec{u} - \left(I - F^{\zeta+}\right)\vec{u}_\zeta^+ - \left(I - F^{\eta+}\right)\vec{u}_\eta^+\right]_{j,k}^{n+1} = \vec{S}_1^{(2)}, \tag{4.61}$$

$$\left[\vec{u} + \left(2I + F^{\zeta+}\right)\vec{u}_\zeta^+ - \left(I - F^{\eta+}\right)\vec{u}_\eta^+\right]_{j,k}^{n+1} = \vec{S}_2^{(2)}, \tag{4.62}$$

$$\left[\vec{u} - \left(I - F^{\zeta+}\right)\vec{u}_\zeta^+ + \left(2I + F^{\eta+}\right)\vec{u}_\eta^+\right]_{j,k}^{n+1} = \vec{S}_3^{(2)}, \tag{4.63}$$

where $(j,k,n+1/2) \in \Omega_1$ is assumed in Eqs. (4.58)–(4.60), while $(j,k,n+1) \in \Omega_2$ is assumed in Eqs. (4.61)–(4.63). Because $s_1^{(1)}$, $s_2^{(1)}$, $s_3^{(1)}$, $s_1^{(2)}$, $s_2^{(2)}$, and $s_3^{(2)}$, denote the expressions on the right sides of Eqs. (2.59)–(2.64), respectively, Eqs. (4.58)–(4.63) are the Euler images of the latter if one adds the following rule of substitution:

Rule 4: $s_\ell^{(k)}$ be replaced by $\vec{S}_\ell^{(k)}$, $k = 1,2$, and $\ell = 1,2,3$.

It follows from Eqs. (4.58)–(4.63) that (i)

$$\left(\vec{u}_\zeta^+\right)_{j,k}^{n+1/2} = \frac{1}{3}\left(\vec{S}_1^{(1)} - \vec{S}_2^{(1)}\right) \tag{4.64}$$

and

$$\left(\vec{u}_\eta^+\right)_{j,k}^{n+1/2} = \frac{1}{3}\left(\vec{S}_1^{(1)} - \vec{S}_3^{(1)}\right) \tag{4.65}$$

where $(j,k,n+1/2) \in \Omega_1$; and (ii)

$$\left(\vec{u}_\zeta^+\right)_{j,k}^{n+1} = \frac{1}{3}\left(\vec{S}_2^{(2)} - \vec{S}_1^{(2)}\right) \tag{4.66}$$

and

$$\left(\vec{u}_\eta^+\right)_{j,k}^{n+1} = \frac{1}{3}\left(\vec{S}_3^{(2)} - \vec{S}_1^{(2)}\right) \tag{4.67}$$

where $(j,k,n+1) \in \Omega_2$. Eqs. (4.64)–(4.67) are the Euler images of Eqs. (2.67), (2.68), (2.70), and (2.71), respectively. Note that the Euler images of Eqs. (2.66) and (2.69) are also true [2]. These images are equivalent to Eqs. (4.54) and (4.55). Because the latter are easier to use, they will be used exclusively in the following development.

With the above preparations, an Euler solver can now be defined. It consists of two marching steps. The first step is formed by Eqs. (4.54), (4.64), and (4.65); while the second is formed by Eqs. (4.55), (4.66), and (4.67). As explained earlier, $\vec{S}_\ell^{(k)}$, $k = 1,2$, and $\ell = 1,2,3$, become known after $\vec{u}_{j,k}^{n+1/2}$ and $\vec{u}_{j,k}^{n+1}$ are evaluated using Eqs. (4.54) and (4.55), respectively. This Euler solver has a two-way marching nature similar to that of the α scheme. As a result, it must be neutrally stable, (i.e., no numerical diffusion) if it is stable. Because it is reversible in time, this solver cannot model a physical problem that is irreversible in time, e.g., an inviscid flow problem involving shocks. Hereafter, this new Euler solver will be referred to as the 2D Euler α scheme.

At this juncture, note that the 2D Euler α scheme is greatly simplified by the fact that $\vec{u}_{j,k}^{n+1/2}$ and $\vec{u}_{j,k}^{n+1}$, respectively, can be directly evaluated in terms of the

marching variables at the nth and $(n+1/2)$th time levels (see Eqs. (4.54) and (4.55)). As a result, the matrices $(\Sigma^{(1)+}_{m\ell})^{n+1/2}_{j,k}$ and $(\Sigma^{(2)+}_{m\ell})^{n+1}_{j,k}$, which are *nonlinear* functions of $\vec{u}^{n+1/2}_{j,k}$ and $\vec{u}^{n+1}_{j,k}$, respectively, can be evaluated easily. In other words, nonlinearity of the above matrix functions does not cause a particular problem for the Euler a scheme.

To explain how Eqs. (4.54) and (4.55) arise, note that the conservation condtions (i)

$$\oint_{S(CE^{(1)}(j,k,n+1/2))} \vec{h}^*_m \cdot d\vec{s} = 0 \qquad (4.68)$$

for any $(j,k,n+1/2) \in \Omega_1$, and (ii)

$$\oint_{S(CE^{(2)}(j,k,n+1))} \vec{h}^*_m \cdot d\vec{s} = 0 \qquad (4.69)$$

for any $(j,k,n+1) \in \Omega_2$, are the direct results of Eqs. (4.28) and (4.29), the basic assumptions of the Euler a scheme. According to Eq. (3.1), $CE^{(1)}(j,k,n+1/2)$ is the cylinder $A'B'C'D'E'F'ABCDEF$ depicted in Fig. 7(a). Except for the top face $A'B'C'D'E'F'$, the other boundaries of this cylinder are the subsets of three solution elements at the nth time level. Thus, for any $m = 1,2,3,4$, the flux of $\vec{h}^*_m$ leaving $CE^{(1)}(j,k,n+1/2)$ through all the boundaries except the top face can be evaluated in terms of the marching variables at the nth time level. On the other hand, because the top face is a subset of $\mathrm{SE}(j,k,n+1/2)$, the flux leaving there is a function of the marching variables associated with $\mathrm{SE}(j,k,n+1/2)$. Furthermore, because the outward normal to the top face has no spatial component, Eq. (4.25) implies that the total flux of $\vec{h}^*_m$ leaving $CE^{(1)}(j,k,n+1/2)$ through the top face is the surface integration of u^*_m over the top face. *Because the center of* $SE(j,k,n+1/2)$ *coincides with the center of the top face*, it is easy to see that the first-order terms in Eqs. (4.15) do not contribute to the *total* flux leaving the top face. It follows that the total flux leaving the top face is a function of $(u_m)^{n+1/2}_{j,k}$ only. As a result of the above considerations, $\vec{u}^{n+1/2}_{j,k}$ can be determined in terms of the marching variables at the nth time level by using Eq. (4.68) only. Similarly, $\vec{u}^{n+1}_{j,k}$ can be determined in terms of the marching variables at the $(n+1/2)$th time level by using Eq. (4.69) only. Eqs. (4.54) and (4.55) are the direct results of Eqs. (4.68) and (4.69), respectively.

In an extension currently under development, the mesh used is not uniform in space. As a result, point G' depicted in Fig. 7(a) generally is not the center of the top face referred to earlier. To simplify the development, we have moved the center of $\mathrm{SE}(j,k,n+1/2)$ to the center of the top face, i.e., away from point G'.

Next we shall construct the 2D Euler a-ϵ scheme, i.e., the Euler version of the 2D a-ϵ scheme. For this scheme, we shall use the CEs defined in Eqs. (3.1) and (3.2), i.e., Eqs. (4.68) and (4.69) will be assumed. Thus Eqs. (4.54) and (4.55) will also be part of the Euler a-ϵ scheme. In the following, we shall describe the rest of the 2D Euler a-ϵ scheme.

As a preliminary, note that $\vec{S}^{(k)}_\ell$ can be evaluated by a direct application of Eqs. (4.56) and (4.57), if one does not mind inverting the 4×4 matrices $\left(\Sigma^{(1)+}_{\ell 1}\right)^{n+1/2}_{j,k}$, and $\left(\Sigma^{(2)+}_{\ell 1}\right)^{n+1}_{j,k}$. Alternatively, one may use the method of Gaussian elimination to obtain $\vec{S}^{(k)}_\ell$ as the solution to

$$\begin{aligned}&\left(\Sigma^{(1)+}_{\ell 1}\right)^{n+1/2}_{j,k} \vec{S}^{(1)}_\ell \\ &= \left[\Sigma^{(1)-}_{\ell 1}\vec{u} + \Sigma^{(1)-}_{\ell 2}\vec{u}^+_\zeta + \Sigma^{(1)-}_{\ell 3}\vec{u}^+_\eta\right]^n_{(j,k;1,\ell)}\end{aligned} \qquad (4.70)$$

and

$$\begin{aligned}&\left(\Sigma^{(2)+}_{\ell 1}\right)^{n+1}_{j,k} \vec{S}^{(2)}_\ell \\ &= \left[\Sigma^{(2)-}_{\ell 1}\vec{u} + \Sigma^{(2)-}_{\ell 2}\vec{u}^+_\zeta + \Sigma^{(2)-}_{\ell 3}\vec{u}^+_\eta\right]^{n+1/2}_{(j,k;2,\ell)}\end{aligned} \qquad (4.71)$$

To simplify computation further, in the following development of the Euler a-ϵ scheme, we shall assume that (i)

$$\left(\Sigma^{(1)+}_{\ell 1}\right)^{n+1/2}_{j,k} = \left(\Sigma^{(1)+}_{\ell 1}\right)^{n}_{(j,k;1,\ell)} \qquad (4.72)$$

where $\ell = 1,2,3$ and $(j,k,n+1/2) \in \Omega_1$, and (ii)

$$\left(\Sigma^{(2)+}_{\ell 1}\right)^{n+1}_{j,k} = \left(\Sigma^{(2)+}_{\ell 1}\right)^{n+1/2}_{(j,k;2,\ell)} \qquad (4.73)$$

where $\ell = 1,2,3$ and $(j,k,n+1) \in \Omega_2$.

To proceed, let (i)

$$\vec{s}^{(1)}_1 \stackrel{\text{def}}{=} \left[\vec{u} - \left(I + F^{\zeta+}\right)\vec{u}^+_\zeta - \left(I + F^{\eta+}\right)\vec{u}^+_\eta\right]^n_{(j,k;1,1)} \qquad (4.74)$$

$$\vec{s}^{(1)}_2 \stackrel{\text{def}}{=} \left[\vec{u} + \left(2I - F^{\zeta+}\right)\vec{u}^+_\zeta - \left(I + F^{\eta+}\right)\vec{u}^+_\eta\right]^n_{(j,k;1,2)} \qquad (4.75)$$

and

$$\vec{s}^{(1)}_3 \stackrel{\text{def}}{=} \left[\vec{u} - \left(I + F^{\zeta+}\right)\vec{u}^+_\zeta + \left(2I - F^{\eta+}\right)\vec{u}^+_\eta\right]^n_{(j,k;1,3)} \qquad (4.76)$$

where $(j,k,n+1/2) \in \Omega_1$; and (ii)

$$\vec{s}_1^{(2)} \stackrel{\text{def}}{=} \left[\vec{u} + \left(I - F^{\zeta+}\right)\vec{u}_\zeta^{+} + \left(I - F^{\eta+}\right)\vec{u}_\eta^{+}\right]_{(j,k;2,1)}^{n+1/2} \tag{4.77}$$

$$\vec{s}_2^{(2)} \stackrel{\text{def}}{=} \left[\vec{u} - \left(2I + F^{\zeta+}\right)\vec{u}_\zeta^{+} + \left(I - F^{\eta+}\right)\vec{u}_\eta^{+}\right]_{(j,k;2,2)}^{n+1/2} \tag{4.78}$$

and

$$\vec{s}_3^{(2)} \stackrel{\text{def}}{=} \left[\vec{u} + \left(I - F^{\zeta+}\right)\vec{u}_\zeta^{+} - \left(2I + F^{\eta+}\right)\vec{u}_\eta^{+}\right]_{(j,k;2,3)}^{n+1/2} \tag{4.79}$$

where $(j,k,n+1) \in \Omega_2$. Then, with the aid of Eqs. (4.34)–(4.51), (4.72), and (4.73), Eqs. (4.56) and (4.57) imply that

$$\vec{S}_\ell^{(k)} = \vec{s}_\ell^{(k)}, \qquad k = 1,2; \quad \ell = 1,2,3 \tag{4.80}$$

As a result, assuming Eqs. (4.72) and (4.73), Rule 4 given above should be replaced by

Rule 5: $s_\ell^{(k)}$ be replaced by $\vec{s}_\ell^{(k)}$, $k = 1,2$, and $\ell = 1,2,3$.

It follows that Eqs. (4.74)–(4.79) are the Euler images of the fact that $s_\ell^{(k)}$, $k = 1,2$, and $\ell = 1,2,3$, represent the expressions on the right sides of Eqs. (2.59)–(2.64).

Combining Eqs. (4.64), (4.65) and (4.80), for any $(j,k,n+1/2) \in \Omega_1$, one has

$$\left(\vec{u}_\zeta^{+}\right)_{j,k}^{n+1/2} = \left(\vec{u}_\zeta^{\circ+}\right)_{j,k}^{n+1/2} \tag{4.81a}$$

and

$$\left(\vec{u}_\eta^{+}\right)_{j,k}^{n+1/2} = \left(\vec{u}_\eta^{\circ+}\right)_{j,k}^{n+1/2} \tag{4.81b}$$

where

$$\left(\vec{u}_\zeta^{\circ+}\right)_{j,k}^{n+1/2} \stackrel{\text{def}}{=} \frac{1}{3}\left(\vec{s}_1^{(1)} - \vec{s}_2^{(1)}\right) \tag{4.82a}$$

and

$$\left(\vec{u}_\eta^{\circ+}\right)_{j,k}^{n+1/2} \stackrel{\text{def}}{=} \frac{1}{3}\left(\vec{s}_1^{(1)} - \vec{s}_3^{(1)}\right) \tag{4.82b}$$

Note that: (i) As a result of Eqs. (4.74)–(4.76), and (4.82a,b), $\left(\vec{u}_\zeta^{\circ+}\right)_{j,k}^{n+1/2}$ and $\left(\vec{u}_\eta^{\circ+}\right)_{j,k}^{n+1/2}$ can be evaluated in terms of the marching variables at the nth time level; and (ii) Eqs. (4.82a,b) are the Euler images of Eqs. (3.15a,b).

Similarly, Eqs. (4.66), (4.67), and (4.80) imply that, for any $(j,k,n+1) \in \Omega_2$,

$$\left(\vec{u}_\zeta^{+}\right)_{j,k}^{n+1} = \left(\vec{u}_\zeta^{\circ+}\right)_{j,k}^{n+1} \tag{4.83a}$$

and

$$\left(\vec{u}_\eta^{+}\right)_{j,k}^{n+1} = \left(\vec{u}_\eta^{\circ+}\right)_{j,k}^{n+1} \tag{4.83b}$$

where

$$\left(\vec{u}_\zeta^{\circ+}\right)_{j,k}^{n+1} \stackrel{\text{def}}{=} \frac{1}{3}\left(\vec{s}_2^{(2)} - \vec{s}_1^{(2)}\right) \tag{4.84a}$$

and

$$\left(\vec{u}_\eta^{\circ+}\right)_{j,k}^{n+1} \stackrel{\text{def}}{=} \frac{1}{3}\left(\vec{s}_3^{(2)} - \vec{s}_1^{(2)}\right) \tag{4.84b}$$

Note that: (i) As a result of Eqs. (4.77)–(4.79) and (4.84a,b), $\left(\vec{u}_\zeta^{\circ+}\right)_{j,k}^{n+1}$ and $\left(\vec{u}_\eta^{\circ+}\right)_{j,k}^{n+1}$ can be evaluated in terms of the marching variables at the $(n+1/2)$th time level; and (ii) Eq. (4.84a,b) are the Euler images of Eqs. (3.27a,b).

Furthermore, for any $(j,k,n) \in \Omega$, let $(\vec{u}_t)_{j,k}^{n}$ denote the column matrix formed by $(u_{mt})_{j,k}^{n}$, $m = 1,2,3,4$. Then Eqs. (4.27), (4.30), and (4.31) imply that

$$\vec{u}_t = -\frac{4}{\Delta t}\left(F^{\zeta+}\vec{u}_\zeta^{+} + F^{\eta+}\vec{u}_\eta^{+}\right). \tag{4.85}$$

With the above preliminaries, the Euler a-ϵ scheme and the Euler weighted-average a-ϵ scheme can be developed in a fashion parallel to the development of their non-Euler counterparts described in Sec. 3 [2]. Excluding a few exceptions to be discussed shortly, all other equations related to the Euler schemes are the trivial Euler images of its non-Euler counterparts under the substitution rules given in Rules 1-3, 5, and

Rule 6: Any scalar variables be replaced by its column-matrix counterpart.

In other words, one can obtain the Euler image from its non-Euler counterpart by adding an arrow over the symbols representing scalar variables. The complete set of equations that define the Euler a-ϵ scheme and the Euler weighted-average a-ϵ scheme is given in [2]. In the following, we shall only discuss those equations which cannot be obtained using the above substitution rules. One half of these special equations is formed by the Euler counterparts to Eqs. (3.62), (3.66a,b), and (3.67a,b). The other half is identical to the first half except that it is associated with $(j,k,n+1) \in \Omega_2$. As a result, we shall further restrict the discussion to those in the first half.

Let the mth components of the 4×1 column matrices $(\vec{u}_\zeta^{(\ell)+})_{j,k}^{n+1/2}$, $(\vec{u}_\eta^{(\ell)+})_{j,k}^{n+1/2}$, $(\vec{u}_x^{(\ell)})_{j,k}^{n+1/2}$, and $(\vec{u}_y^{(\ell)})_{j,k}^{n+1/2}$, be denoted by $(u_{m\zeta}^{(\ell)+})_{j,k}^{n+1/2}$, $(u_{m\eta}^{(\ell)+})_{j,k}^{n+1/2}$, $(u_{mx}^{(\ell)})_{j,k}^{n+1/2}$, and $(u_{my}^{(\ell)})_{j,k}^{n+1/2}$, respectively (these matrices can be defined by using the Euler images of

Eqs. (3.42)–(3.47), and (3.52)–(3.57)). Then, for $m = 1,2,3,4$, and $\ell = 1,2,3$, the Euler versions of Eqs. (3.62), (3.66a,b), and (3.67a,b) are (i)

$$\theta_{m\ell} \stackrel{\text{def}}{=} \sqrt{(u_{mx}^{(\ell)})^2 + (u_{my}^{(\ell)})^2}, \tag{4.86}$$

(ii)

$$u_{m\zeta}^{w+} = 0, \qquad \text{if } \theta_{m1}=\theta_{m2}=\theta_{m3}=0, \tag{4.87a}$$

and

$$u_{m\zeta}^{w+} = \frac{(\theta_{m2}\theta_{m3})^\alpha\, u_{m\zeta}^{(1)+} + (\theta_{m3}\theta_{m1})^\alpha\, u_{m\zeta}^{(2)+} + (\theta_{m1}\theta_{m2})^\alpha\, u_{m\zeta}^{(3)+}}{(\theta_{m1}\theta_{m2})^\alpha + (\theta_{m2}\theta_{m3})^\alpha + (\theta_{m3}\theta_{m1})^\alpha} \tag{4.87b}$$

otherwise; and (iii)

$$u_{m\eta}^{w+} = 0, \qquad \text{if } \theta_{m1}=\theta_{m2}=\theta_{m3}=0, \tag{4.88a}$$

and

$$u_{m\eta}^{w+} = \frac{(\theta_{m2}\theta_{m3})^\alpha\, u_{m\eta}^{(1)+} + (\theta_{m3}\theta_{m1})^\alpha\, u_{m\eta}^{(2)+} + (\theta_{m1}\theta_{m2})^\alpha\, u_{m\eta}^{(3)+}}{(\theta_{m1}\theta_{m2})^\alpha + (\theta_{m2}\theta_{m3})^\alpha + (\theta_{m3}\theta_{m1})^\alpha} \tag{4.88b}$$

otherwise. Here (i) $\alpha \geq 0$; (ii) the Euler counterpart to u_ζ^{w+} is the column matrix formed by $u_{m\zeta}^{w+}$, $m = 1,2,3,4$; and (iii) the Euler counterpart to u_η^{w+} is the column matrix formed by $u_{m\eta}^{w+}$, $m = 1,2,3,4$.

This section is concluded with the following comments:

(a) Because of the assumptions made in Eqs. (4.72) and (4.73), the Euler a scheme is not the special case of the Euler a-ϵ scheme with $\epsilon = 0$.

(b) Because (i) a fractional power is costly to evaluate, and (ii) evaluation of $(\theta_{m\ell})^\alpha$ does not involve a fractional power if α is an even integer, the Euler weighted-average a-ϵ scheme is more computationally efficient if α is an even integer.

5. Numerical Results

In [11], several numerical solutions of Eq. (2.1) generated using the a-ϵ schemes are compared with the exact solutions or the numerical solutions generated using traditional methods. These comparisons show that the a-ϵ scheme, which includes the a scheme as a special case with $\epsilon = 0$, is an accurate solver for Eq. (2.1).

The a-ϵ scheme was also generalized in [11] to solve the 2D inviscid Burgers' equation. In spite of its simplicity, particularly the fact that it does not use (i) any mesh refinement technique, or (ii) any moving meshes, this new solver is capable of generating highly accurate unsteady shock solutions. The shock discontinuities are resolved almost to within one mesh interval.

In this section, accuracy of the Euler weighted-average a-ϵ scheme defined in Sec. 4 will be evaluated using a steady-state shock reflection problem [14]. The computation domain and the shock locations ($\overline{AE}$ and $\overline{EF}$) are depicted in Fig. 14. The lower boundary is a solid wall. Assuming $\gamma = 1.4$, the exact Euler solution to this problem is:

(a) In the region ABE,

$$u = 2.9, \quad v = 0., \quad \rho = 1.0, \quad p = 1.0/1.4. \tag{5.1}$$

(b) In the region $AEFD$,

$$u = 2.6193, \quad v = -0.50632, \quad \rho = 1.7000, \quad p = 1.5282. \tag{5.2}$$

(c) In the region ECF,

$$u = 2.4015, \quad v = 0., \quad \rho = 2.6872, \quad p = 2.9340. \tag{5.3}$$

Note that the Mach number is equal to (i) 2.9 in the region ABE; (ii) 2.3781 in the region $AEFD$; and (iii) 1.9424 in the region ECF.

The mesh used in the current numerical calculations is depicted in Fig. 15. Again a mesh point $\in \Omega_1$ is marked by a solid circle; while a mesh point $\in \Omega_2$ is marked by an open circle. The mesh is a special case of that depicted in Figs. 3–6 with $b = 0$. Note that (i) only the mesh points $\in \Omega_2$ are present at the inflow boundary, and (ii) the mesh parameter w is so chosen that only the mesh points $\in \Omega_2$ are present at the outflow boundary. Moreover, for simplicity, a mesh point and the corresponding marching variable will be identified by the time-level number n, and two *new* mesh indices r and s which are given in Fig. 15 as a pair of integers enclosed in parentheses. Note that, for the mesh points $\in \Omega_1$, $r = 1,2,3,\ldots,R,R+1$, and $s = 1,2,3,\ldots,S$. On the other hand, for the mesh points $\in \Omega_2$, $r = 1,2,3,\ldots,R,R+1$, and $s = 1,2,3,\ldots,S,S+1$. Obviously two different mesh points *at the same time level* always have different pairs of r and s.

In the current numerical calculation, at the time level $n = 0$, u_m, $m = 1,2,3,4$, at all mesh points are calculated using Eq. (5.1). Also we assume that

$$u_{m\zeta}^{+} = u_{m\eta}^{+} = 0, \qquad m = 1,2,3,4. \tag{5.4}$$

The above initial conditions are also assumed at the inflow boundary for all $n = 1, 2, 3, \ldots$. At the upper boundary, for all $n = 1/2, 1, 3/2, 2, \ldots$, Eq. (5.4) is also assumed. Moreover, u_m, $m = 1, 2, 3, 4$, are calculated using Eq. (5.2).

To impose the proper boundary conditions at the lower boundary, note that the solid wall boundary conditions at $\overline{BC}$ (see Fig. 14) are equivalent to the condition that the flow field below $\overline{BC}$ is the mirror image of that above. By using Eq. (4.1) and the fact that $y = 0$ at any point on $\overline{BC}$, it can be shown that the last condition implies that

$$u_m(x, -y) = u_m(x, y), \qquad m = 1, 2, 4 \tag{5.5a}$$

$$u_3(x, -y) = -u_3(x, y) \tag{5.5b}$$

$$\frac{\partial u_m(x, -y)}{\partial x} = \frac{\partial u_m(x, y)}{\partial x}, \quad m = 1, 2, 4 \tag{5.6a}$$

$$\frac{\partial u_3(x, -y)}{\partial x} = -\frac{\partial u_3(x, y)}{\partial x} \tag{5.6b}$$

$$\frac{\partial u_m(x, -y)}{\partial y} = -\frac{\partial u_m(x, y)}{\partial y}, \quad m = 1, 2, 4 \tag{5.7a}$$

and

$$\frac{\partial u_3(x, -y)}{\partial y} = \frac{\partial u_3(x, y)}{\partial y} \tag{5.7b}$$

Consider the mesh depicted in Fig. 15. Then it becomes clear that the numerical analogues of Eqs. (5.5a) –(5.7b) are

$$(u_m)^n_{R+1,s} = (u_m)^n_{R,s}, \quad m = 1, 2, 4 \tag{5.8a}$$

$$(u_3)^n_{R+1,s} = -(u_3)^n_{R,s} \tag{5.8b}$$

$$(u_{mx})^n_{R+1,s} = (u_{mx})^n_{R,s}, \quad m = 1, 2, 4 \tag{5.9a}$$

$$(u_{3x})^n_{R+1,s} = -(u_{3x})^n_{R,s} \tag{5.9b}$$

$$(u_{my})^n_{R+1,s} = -(u_{my})^n_{R,s}, \quad m = 1, 2, 4 \tag{5.10a}$$

and

$$(u_{3y})^n_{R+1,s} = (u_{3y})^n_{R,s} \tag{5.10b}$$

respectively. According to Fig. 15, the range of s in Eqs. (5.8a)–(5.10b) is dependent on the time level n. Let (i) $S^+ \overset{\text{def}}{=} S + 1$, and $S^- \overset{\text{def}}{=} S$ if S is even; and (ii) $S^+ \overset{\text{def}}{=} S$, and $S^- \overset{\text{def}}{=} S - 1$ if S is odd. Then (i) $s = 2, 4, 6, \ldots, S^-$ if $n = 1/2, 3/2, \ldots$, and (ii) $s = 1, 3, 5, \ldots, S^+$ if $n = 1, 2, \ldots$. Furthermore, because $b = 0$, it can be shown that Eqs. (5.9a,b) and (5.10a,b) are eqivalent to

$$\left(u^+_{m\zeta}\right)^n_{R+1,s} = (u^+_{m\eta})^n_{R,s}, \quad m = 1, 2, 4 \tag{5.11a}$$

$$\left(u^+_{3\zeta}\right)^n_{R+1,s} = -(u^+_{3\eta})^n_{R,s} \tag{5.11b}$$

$$(u^+_{m\eta})^n_{R+1,s} = \left(u^+_{m\zeta}\right)^n_{R,s}, \quad m = 1, 2, 4 \tag{5.12a}$$

and

$$(u^+_{3\eta})^n_{R+1,s} = -\left(u^+_{3\zeta}\right)^n_{R,s} \tag{5.12b}$$

respectively. Equations (5.8a,b), (5.11a,b), and (5.12a,b) are the boundary conditions at the lower wall (a solid wall) in the current numerical calculations. In other words, the marching variables associated with the mesh points below the solid wall will be determined using these equations.

Next we discuss the outflow boundary conditions. For any $n = 1, 2, 3, \ldots$, and $r = 1, 2, 3, \ldots, R$, we assume that

$$(u_m)^n_{r,S+1} = (u_m)^{n-1/2}_{r,S}, \qquad m = 1, 2, 3, 4 \tag{5.13}$$

$$(u_{mx})^n_{r,S+1} = 0, \qquad m = 1, 2, 3, 4 \tag{5.14}$$

and

$$(u_{my})^n_{r,S+1} = (u_{my})^{n-1/2}_{r,S}, \qquad m = 1, 2, 3, 4 \tag{5.15}$$

When the time-marching solution reaches its steady-state limit, the above conditions can be considered as a result of the requirement that the partial derivatives of the flow variables with respect to x are zero at the outflow boundary. Because $b = 0$, it can be shown that Eqs. (5.14) and (5.15) are equivalent to

$$\left(u^+_{m\zeta}\right)^n_{r,S+1} = \frac{1}{2}\left(u^+_{m\zeta} - u^+_{m\eta}\right)^{n-1/2}_{r,S} \tag{5.16}$$

and

$$(u^+_{m\eta})^n_{r,S+1} = \frac{1}{2}\left(u^+_{m\eta} - u^+_{m\zeta}\right)^{n-1/2}_{r,S} \tag{5.17}$$

where $m = 1, 2, 3, 4$, $n = 1, 2, 3, \ldots$, and $r = 1, 2, 3, \ldots, R$. Equations (5.13), (5.16), and (5.17) are the outflow boundary conditions in the current numerical calculations. As a result, the marching variables at the outflow boundary will be determined using these equations.

With the aid of the above initial and boundary conditions, the marching variables at all time levels can be determined using the Euler weighted-averaged a-ϵ scheme. As an example, at any $n = 1/2, 3/2, \ldots$, the marching variables associated with the mesh point $(2, 1)$ (marked by a solid circle in Fig. 15) can be determined in terms of those associated with the mesh

points (1,1), (2,1), and (2,2) at the $(n-1/2)$th time level (marked by open circles). As another example, at any $n = 1,2,3,\ldots$, the marching variables associated with the mesh point (1,3) (marked by an open circle) can be determined in terms of those associated with the mesh points (1,2), (2,3), and (1,3) at the $(n-1/2)$th time level (marked by solid circles).

According to Fig. 14, the distance between the inflow and the outflow boundaries is 4., while the distance between the upper and the lower boundaries is 1.. On the other hand, according to Fig. 15, the above two distances are $w \cdot S$ and $2h \cdot R$, respectively. Thus

$$w = \frac{4}{S}, \qquad \text{and} \qquad h = \frac{1}{2R} \tag{5.18}$$

In addition to the initial conditions, the boundary conditions, and the integers R and S, the other input parameters for the current numerical calculations are ϵ, α, Δt, and a positive integer n_t. Here we assume that the time marching ends at the n_tth time level, i.e., at $t = T \stackrel{\text{def}}{=} n_t \cdot \Delta t$.

It is shown in [2] that, for any Euler solver constructed in Sec. 4, a local CFL number ν_e associated with any mesh point $(j,k,n) \in \Omega$ can be defined in terms of u, v, c, w, h, and Δt. Here u, v, and c are the x-velocity, the y-velocity, and the sonic speed at the mesh point, respectively. Two global CFL numbers are considered in the current calculations. The first, denoted by ν_{em_s}, is the maximum of ν_e with respect to the steady-state solution given in Eqs. (5.1)–(5.3). The second, denoted by ν_{em}, is the largest value of ν_e ever reached at any mesh point $(j,k,n) \in \Omega$, where $n = 0, 1/2, 2, 3/2, 2, \ldots, n_t$. Excluding the initial and the boundary conditions, ν_{em_s} is dependent on R, S, and Δt only. On the other hand, ν_{em} is a function of R, S, Δt, n_t, ϵ, and α. According to a series of numerical experiments, the value of α plays only a minor role on the stability of the Euler weighted-average α-ϵ scheme. Generally the scheme is stable if

$$0 \le \epsilon \le 1 \qquad \text{and} \qquad \nu_{em} \le 1. \tag{5.19}$$

To measure the convergence of a time-marching solution to the corresponding steady-state solution (note: this steady-state solution generally differs from the exact solution given in Eqs. (5.1)–(5.3)), for any $n = 1,2,3,\ldots,n_t$, and $m = 1,2,3,4$, let

$$E_m(n) \stackrel{\text{def}}{=} -\log_{10}\left\{\frac{1}{RSc_m}\left[\sum_{s=2}^{S+1}\sum_{r=r(s)}^{r(s)+R-1}\left|(u_m)_{r,s}^{n} - (u_m)_{r,s}^{n-1}\right|\right]\right\} \tag{5.20}$$

Here, for any $m = 1,2,3,4$, c_m is the maximal value of $|u_m|$ within the exact steady-state solution defined by Eqs. (5.1)–(5.3). It can be shown that $c_1 = 2.6872$, $c_2 = 6.4534$, $c_3 = 0.86073$, and $c_4 = 15.084$. Moreover,

$$r(s) \stackrel{\text{def}}{=} \begin{cases} 1, & \text{if } s \text{ is odd;} \\ 2, & \text{otherwise.} \end{cases} \tag{5.21}$$

According to Fig. 15, the summation that takes place in Eq. (5.20) involves all the mesh points at the nth time level excluding those located (i) at the inflow boundary, (ii) at the upper boundary, and (iii) below the lower boundary. Because $n = 1,2,3,\ldots,n_t$, the mesh points involved in the summation are all marked by open circles in Fig. 15. The values of u_m at the inflow and the upper boundaries do not change with time, while those at the mesh points in (iii) are dependent on the values of u_m at other interior mesh points. Note that the values of u_m at the outflow boundary change with time and are dependent on those at a lower time level. Because the summation involves a total of $R \times S$ mesh points, the result of this summation divided by $R \times S$ is the average value of the change of u_m at the same spatial mesh point (measured by the absolute value of this change) from the $(n-1)$th time level to the nth time level per mesh point. This average value is further normalized using the constant c_m. If we further assume that the time-marching solution converges to a steady-state solution that is similar to the exact steady-state solution (such that the normalization by c_m makes sense), then $E_m(n)$ can be interpreted as the average number of correct significant figures in u_m at the nth time level as compared with the converged value of u_m (which, of course, is not identical to that given in Eqs. (5.1)–(5.3)).

Because the time marching solution can not reach a steady-state solution before the boundary conditions are fully felt at all interior points, rapid convergence generally can not occur before the time has elapsed that allows a fluid particle to travel the full length of the computation domain. It can be shown that, for the solution given in Eqs. (5.1)–(5.3), the average value of u over the computational domain is 2.6261. Thus an average fluid particle requires $4.0/2.6261 = 1.5232$ time units to travel from the inflow boundary to the outflow boundary. The number of time steps corresponding to the above number of time uints is

$$n_c \stackrel{\text{def}}{=} \frac{1.5232}{\Delta t} \tag{5.22}$$

i.e., rapid convergence can not occur before $n > n_c$.

With the above preliminaries, the numerical results generated using the Euler weighted-average α-ϵ

scheme can now be presented. Six test problems, with different combinations of ϵ, α, R, S, Δt, and n_t, are defined in Table 1. For each problem, the values of T, ν_{ems}, ν_{em}, and n_c are also given in the same table. In Figs. 16–21, the numerical results (triangular symbols) of the pressure coefficient c_p at $n = n_t$ for Problems #1–#6 are compared with the exact solution (solid lines). Here

$$c_p \stackrel{\text{def}}{=} \frac{2}{\gamma M_\infty^2}\left(\frac{p}{p_\infty} - 1\right) \tag{5.23}$$

with $M_\infty = 2.9$ and $p_\infty = 1.0/1.4$ being the inflow Mach number and pressure, respectively. Note that: (i) at the mid-section of the computation domain ($y = 0.5$ in Fig. 14), two neighboring mesh points at the same time level are separated by a distance $= 2w$, and (ii) the mesh points at the n_tth time level are marked by open circles in Fig. 15 because n_t is a whole number. In Figs. 16–21, the values of $E_m(n)$, $m = 1, 2, 3, 4$, are also plotted against n for all six test problems. In Fig. 22, twenty-six pressure contour levels between the values of 0.6 and 3.1 with uniform increment 0.1 were used for the contour plots of Problem #3. Finally, for Problem #3, a 3D pressure-distribution plot is shown in Fig. 1. Note that, for easier visualization, only pressure values at the mesh points with $s = 2, 4, 6, \ldots$ are used in the last plot.

The significance of the results shown in Figs. 1 and 16–22 is discussed in the following remarks:

(a) From Table 1 and the results shown in Figs. 16-18, it appears that the convergence to steady-state is much faster with a smaller value of ν_{em} (or ν_{ems}). As a matter of fact, convergence to steady-state can reach a plateau representing some number of correct significant figures if ν_{em} is too close to 1. From Table 1 and a comparison among Figs. 16, 19, and 20, one also concludes that slower convergence generally occurs with a value of ϵ much smaller than 0.5. A comparison between Figs. 16 and 21 reveals that a change of the value of α from 2 to 1 also causes a slight decrease in convergence rate. Because numerical diffusion generally increases with (i) a smaller value of ν_{em}, (ii) a larger value of ϵ, and (iii) a larger value of α, one may conclude that faster convergence generally occurs with larger numerical diffusion. This trend is consistent with the fact that shocks cannot be formed without physical or numerical diffusion.

(b) The effectiveness of weighted-averaging as a tool to surpress numerical oscillations near discontinuities is clearly demonstrated by the results shown in Figs. 1 and 16-22. Moreover, the current weighted-averaging does not cause the smearing of shock discontinuities and has no discernible effect on the smooth part of the solution. From table 1 and a comparison between Fig. 16 and 21, one also concludes that the increase of the value of α from 1 to 2 has a marginal impact on the numerical results.

(c) Comparing the numerical results shown in Figs. 16–21 with the exact solution, one concludes that the Euler weighted-average α-ϵ scheme is capable of generating highly accurate solutions for the steady-state shock reflection problem under consideration. Also a comparison of the results shown in Figs. 16, 17, and 19-21 reveals that accuracy of the numerical results generally is not sensitive to the change of the values of ν_{em}, ϵ, and α. An exception is that numerical results may become more diffusive and thus shock resolution becomes less sharp if the value of ϵ is too large, e.g., $\epsilon = 0.8$ in Problem #5. Finally, a comparison of the results shown in Fig. 18 (Problem #3) with the results of other test problems reveals that accuracy increases sharply with a decrease of the mesh size.

This section is concluded with a brief discussion on recent applications of the current solver to computational aeroacoustics (CAA) problems. CAA is an area of current interest in CFD. It is of both theoretical interests and practical importance. For a scheme to be a useful research tool, it must be accurate enough to resolve sound wave details. Furthermore, its boundary conditions must be non-reflecting. There have been a large number of papers published on these two topics. In practice, CAA will help to reduce jet noise level for air-borne vehicles, and hence becomes an important topic in HSR (High Speed Research) and AST (Advanced Subsonic Technology) programs.

The most popular numerical schemes for CAA are the high order (4-6th) compact or non-compact difference schemes, marching forward by Runge-Kutta method. These schemes work quite well when incorporated with delicatedly designed non-reflecting boundary conditions. They are even capable of capturing Mach waves and weak shocks.

When conducting numerical experiments of the current solver for CAA problems, surprisingly we found the following attractive features:

- Accuracy of the current solver is comparable to that of a 6th-order compact difference scheme, even though nominally the current solver is only of 2nd-order accuracy. For example, the smallest

eddy can be resolved in 3-4 grid cells.

- Generally, the non-reflecting (radiation) boundary condition can be implemented in a simple way without involving characteristic variables.
- Most importantly, the current solver is capable of handling BOTH continuous and discontinuous flows very well and thus provides a unique numerical tool for solving those flow problems where the interactions between sound waves and shocks are important, such as the noise field around a supersonic over- or under expansion jet.

Details of our investigation will be reported elsewhere [13]. Here as an example, we present the numerical results of a calculation involving a free shear layer which is subjected to upstream time-dependent perturbation. The Mach number of the fast stream is 1.5 and the slow stream is subsonic. Fig. 23 illustrates the contours of pressure, v-velocity and vorticity in the near field. The computational mesh is formed by 240×150 uniform cells. From v-velocity contours, eddies created by the upstream perturbation are clearly visible. On the subsonic side, sound waves propagate freely to far field, while on the fast stream side (lower 1/3 domain) the sound waves are bounded by the Mach line, even smaller eddies are created around the Mach line due to their interactions. In summary, the current results reveals a lot of physical details of the perturbed shear layer and we believe that the current method will develop into a robust and unique numerical technique for aeroacoustics computation.

6. Conclusions and Discussions

A new numerical method is being developed for solving one-dimensional and multidimensional flow problems. This new method represents a clear break from the traditional methods in the basic concept of *numerical discretization*. It emphasizes *simplicity, generality, and accuracy*. The history of this new method and the considerations that motivate its development are described in Sec. 1.

In this paper, the same design principles that were used to construct several solvers for 1D time-marching problems [5] are used to construct their 2D counterparts. Because of the similarity in their designs, each of the present 2D solvers shares with its 1D counterpart virtually the same fundamental characteristics. Furthermore, it has been shown that the 2D solvers, as in the case of the 1D solvers, generally are more accurate than the traditional solvers despite the advantage the current solvers have over the latter in *simplicity and generality*. Accuracy of the current 2D Euler solver is most vividly demonstrated by the pressure-contour plot (Fig. 22) and the 3D pressure-distribution plot (Fig. 1) it generates for a famous shock reflection problem [14]. Both the incident and the reflected shocks are resolved by a single data point without the presence of numerical oscillations near the discontinuity.

Construction of the 1D solvers referred to above is simplified by the use of a mesh that is staggered in time [1,9]. Its use results in the simplest stencil possible, i.e., a triangle in 2D space-time with one vertex at the upper time level and other two at the lower time level. Similarly, construction of the current 2D solvers is simplified by the use of a nontraditional space-time mesh that is also staggered in time (Figs. 3–6). Its use results in the simplest stencil possible, i.e., a tetrahedron (Fig. 10) in 3D space-time with one vertex at the upper time level and the other three at the lower time levels.

The meshes used by the 1D and 2D solvers consist of whole-integer and half-integer time levels with a half-integer time level being sandwiched between two whole-integer time levels, and vice versa. The spatial positions of the mesh points at a whole-integer (half-integer) time level coincide with those at another whole-integer (half-integer) time level. However, the spatial positions of the mesh points at a whole-integer time level shift from those at a half-integer time level. For the mesh used by the 1D solvers, the spatial projection of a mesh point at a whole-integer time level is right at the center of those of two neighboring mesh points at a half-integer time level, and vice versa [1,5,9]. It follows that the stencil of the 1D solvers is always an isosceles triangle, i.e., one cannot distinguish a stencil with its upper vertex at a whole-integer time level from another with its upper vertex at a half-integer time level. As a result, each of the 1D solvers constructed in [1,5,9] is formed by two identical marching steps. Contrarily, for the present 2D solvers, a stencil (a tetrahedron) with its vertex at a whole-integer time level is different from another with its vertex at a half-integer time level (Fig. 10). Thus, each of the present 2D solvers is formed by two distinctly different marching steps. In spite of their structural differences, the last two marching steps *compensate* each other and their combination results in several important symmetric properties that are discussed in [2].

The Euler a scheme constructed in Sec. 4 is free from numerical diffusion when it is stable. This scheme is a limiting case of a Navier-Stokes solver currently under development, i.e., the former is a special case of

the latter when the viscosity vanishes. As a result, the new Navier-Stokes solver will have a special property that a classical solver lacks, i.e., as the physical diffusion (viscosity) approaches zero, so does the numerical diffusion. The significance of this property was discussed earlier. Because a Navier-Stokes problem fundamentally is an initial-value/boundary-value problem, i.e., information from any spatial point can be felt instantly by other spatial points, the new Navier-Stokes solver is implicit when viscosity is present. However, it becomes explicit when viscosity is absent.

Finally, note that a new implicit solver for Eq. (1.3) has been developed recently [4]. This new solver shares with the above Navier-Stokes solver essentially the same characteristics. In the inviscid limit, this new scheme becomes explicit and its amplification factors are identical to those of the Leapfrog schemes. *On the other hand, in the pure diffusion limit, its principal amplification factor becomes the amplification factor of the Crank-Nicolson scheme.* By using an approach similar to that described in [4], a new α-ϵ solver for Eq. (1.1) was also developed. Stability of this new α-ϵ scheme is again limited by the CFL condition and $0 \leq \epsilon \leq 1$. Moreover, if $\epsilon = 0$, its amplification factors are identical to those of the Leapfrog scheme. *On the other hand, if $\epsilon = 1$, its principal amplification factor becomes the amplification factor of the Lax-Wendroff scheme.* This new α-ϵ scheme will be reported in the near future.

References

[1] Chang, S.C., "The Method of Space-Time Conservation Element and Solution Element–A New Approach for Solving the Navier-Stokes and Euler Equations," accepted for publication in the Journal of Computational Physics.

[2] Chang, S.C., Wang, X.Y. and Chow, C.Y., "New Developments in the Method of Space-Time Conservation Element and Solution Element–Applications to Two-Dimensional Time-Marching Problems," NASA TM 106758, December, 1994.

[3] Wang, X.Y., Chow, C.Y. and Chang, S.C., "Application of the Space-Time Conservation Element and Solution Element Method to Shock-Tube problem," NASA TM 106806, December, 1994. Also submitted for publication in the Journal of Computational Physics.

[4] Chang, S.C., Wang, X.Y., Chow, C.Y. and Himansu, A., "The Method of Space-Time Conservation Element and Solution Element–Development of a New Implicit Solver," to appear in the *Proceedings of the Ninth International Conference on Numerical Methods in Laminar and Turbulent Flow*, July 10–14, 1995, Atlanta, Georgia. Also published as NASA TM 106897.

[5] Chang, S.C. and To, W.M., "A New Numerical Framework for Solving Conservation Laws–The Method of Space-Time Conservation Element and Solution Element," NASA TM 104495, August, 1991.

[6] Chang, S.C., "On An Origin of Numerical Diffusion: Violation of Invariance under Space-Time Inversion," *Proceedings of 23rd Conference on Modeling and Simulation*, April 30–May 1, 1992, Pittsburgh, PA, USA, William G. Vogt and Marlin H. Mickle eds., Part 5, pp. 2727-2738. Also published as NASA TM 105776.

[7] Chang, S.C. and To, W.M., "A Brief Description of a New Numerical Framework for Solving Conservation Laws–The Method of Space-Time Conservation Element and Solution Element," *Proceedings of the Thirteenth International Conference on Numerical Methods in Fluid Dynamics*, Rome, Italy, 1992, M. Napolitano and F. Sabetta, eds., Lecture Notes in Physics 414, Springer-Verlag, pp. 396-400. Also published as NASA TM 105757.

[8] Scott, J.R. and Chang, S.C., "A New Flux Conserving Newton's Method Scheme for the Two-Dimensional, Steady Navier-Stokes Equations," to appear in the International Journal of Computational Fluid Dynamics.

[9] Chang, S.C., "New Developments in the Method of Space-Time Conservation Element and Solution Element–Applications to the Euler and Navier-Stokes Equations," NASA TM 106226, August, 1993.

[10] Scott, J.R., "A New Flux-Conserving Numerical Scheme for the Steady, Incompressible Navier-Stokes Equations," submitted for publication in the International Journal of Computational Fluid Dynamics.

[11] Wang, X.Y., Chow, C.Y. and Chang, S.C., "Application of the Space-Time Conservation Element and Solution Element Method to Two-Dimensional Advection-Diffusion Problems," to be published as a NASA Technical Memorandum.

[12] Scott, J.R. and Chang, S.C., "The Space-Time Solution Element Method–A New Numerical Approach for the Navier-Stokes Equations," AIAA paper 95-0763-CP, presented at the 33rd AIAA

Aerospace Science Meeting, Reno, Nevada, January 9-12, 1955.

[13] Loh, C.Y., Chang, S.C., Scott, J.R., and Yu, S.T., "Application of the Method of Space-Time Conservation Element and Solution Element to Aeroacoustics Problems," to be presented at 6th International Symposium of CFD, Lake Tahoe, California, September 1995.

[14] Yee, H.C., Warming, R.F. and Harten, A., "Implicit Total Variation Diminishing (TVD) Schemes for Steady-State Calculations," AIAA paper 83-1902.

[15] Anderson, D.A., Tannehill, J.C. and Pletcher, R.H., *Computational Fluid Mechanics and Heat Transfer* (Hemisphere, 1984).

[16] Lapidus, L. and Pinder, G.F., *Numerical Solution of Partial Differential Equations in Sciences and Engineering*, John Wiley & Sons, Inc., 1982.

[17] Thomas, J.P. and Roe P.L., "Development of Non-Dissipative Numerical Schemes for Computational Aeroacoustics," AIAA paper 93-3382-CP, presented at the 11th AIAA Computational Fluid Dynamics Conference, Orlando, Florida, July 6–9, 1993.

[18] Roe, P.L., "Linear Bicharacteristic schemes without dissipation," ICASE Report No. 94-65, July 1994.

[19] Courant, R. and Hilbert, D., *Methods of Mathematical Physics*, Vol. II (Interscience, 1962).

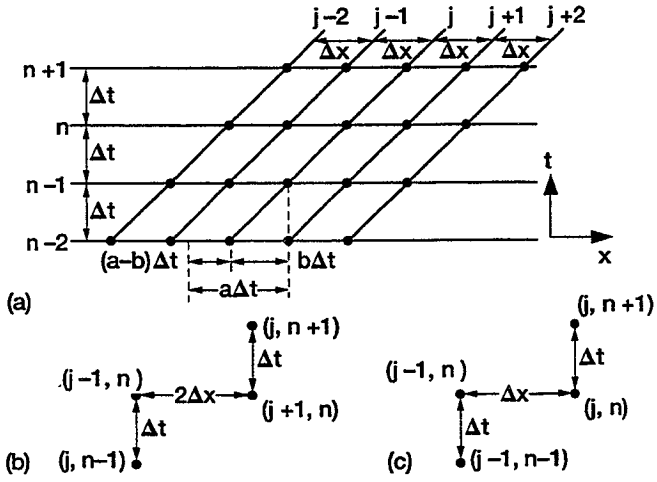

Figure 2.—The leapfrog scheme using a moving mesh and the upwind leapfrog scheme.

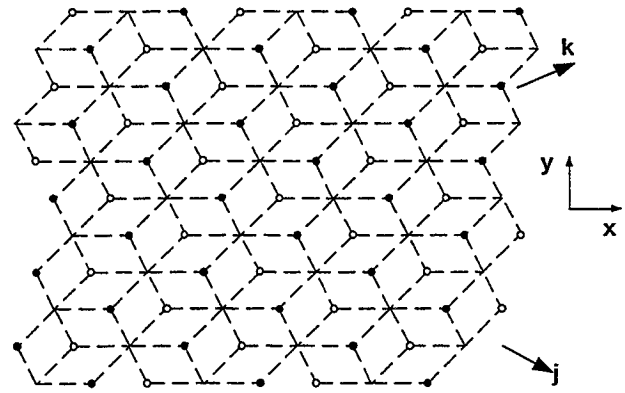

Figure 3.—The relative spatial positions of the mesh points $\in\Omega_1$ and the mesh points $\in\Omega_2$ (dash lines are spatial boundaries of the conservation elements depicted in figs 7(a) and 7(b)).

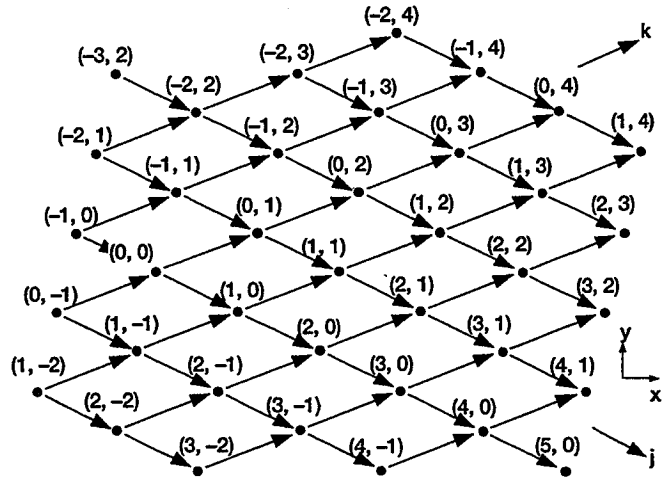

Figure 4.—The spatial mesh indices (j, k) of the mesh points $\in\Omega_1$ (n = ±1/2, ±3/2, ±5/2, ···).

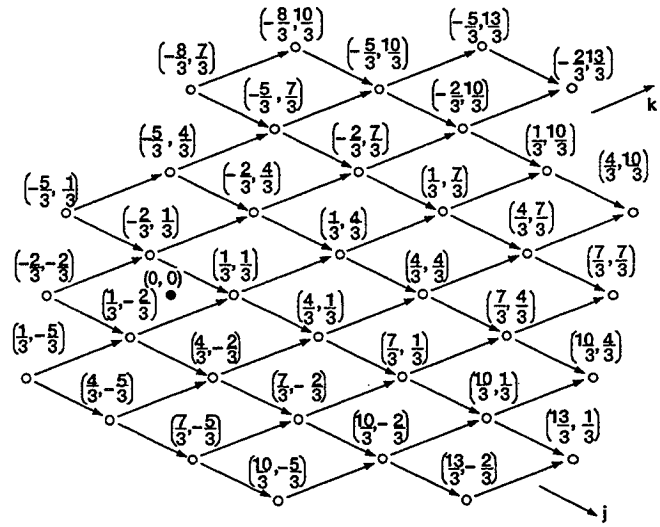

Figure 5.—The spatial mesh indices (j, k) of the mesh points $\in\Omega_2$ (n = 0, ±1, ±2, ···).

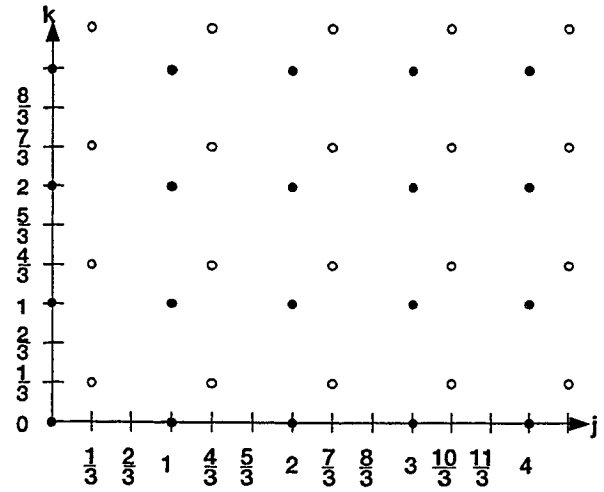

Figure 6.—The spatial mesh positions of the mesh points marked by • and those marked by○ .

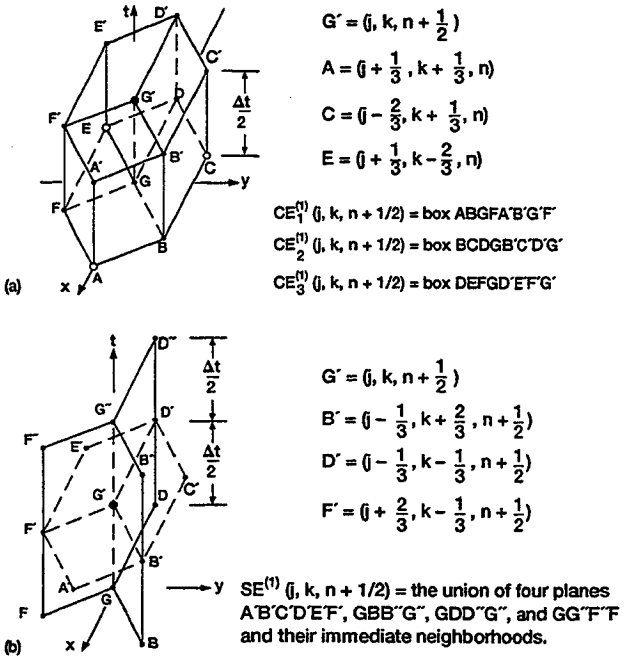

Figure 7.—(a) Conservation elements $CE_\ell^{(1)}$ (j, k, n + 1/2), ℓ = 1, 2, 3, and j, k, n = 0, ±1, ±2, ···. (b) Solution elements $SE^{(1)}$ (j, k, n + 1/2), j, k, n = 0, ±1, ±2, ···).

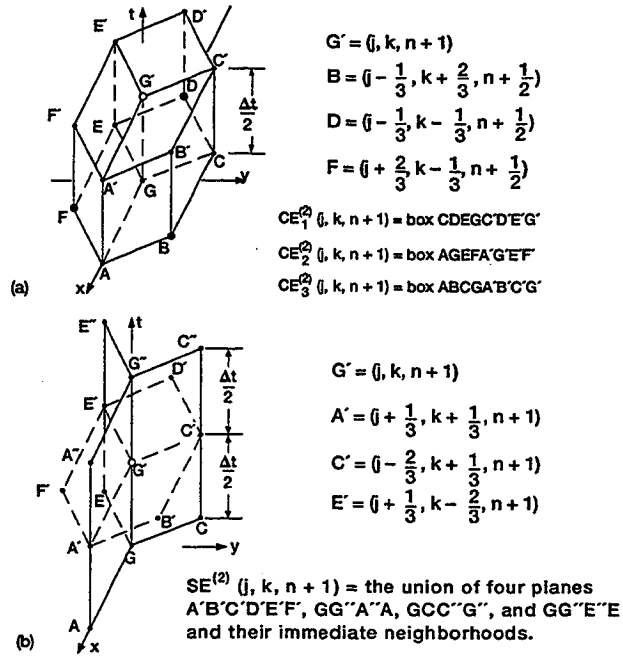

Figure 8.—(a) Conservation elements $CE_\ell^{(2)}$ (j, k, n + 1), ℓ = 1, 2, 3, j, k, = 1/3, 1/3 ±1, 1/3 ±2, ···, and n = 0, ±1, ±2, ···.
(b) Solution elements $SE^{(2)}$ (j, k, n + 1), j, k = 1/3, 1/3 ±1, 1/3 ±2, ···, and n = 0, ±1, ±2, ···).

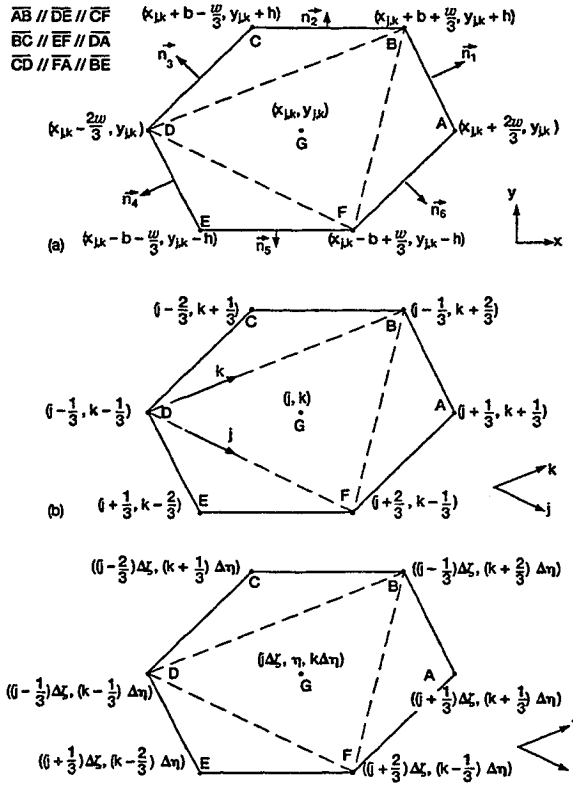

Figure 9.—Geometry of the hexagon ABCDEF. (a) Relative positions of the vertices in terms of (x, y). (b) Relative positions of the vertices in terms of (j, k). (c) Relative positions of the vertices in terms of (ζ, η).

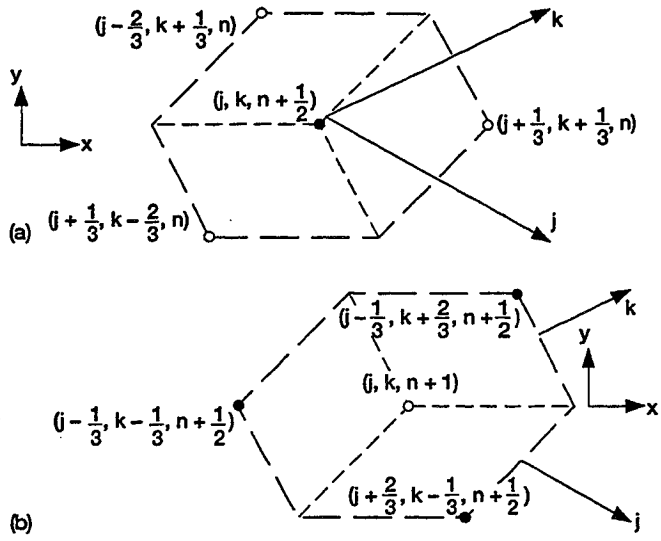

Figure 10.—(a) The mesh points (j, k, n + 1/2), (j + 1/3, k + 1/3, n), (j − 2/3, k + 1/3, n) and (j + 1/3, k − 2/3, n) with (j, k, n + 1/2) $\in \Omega_1$. (b) The mesh points (j, k, n + 1), (j − 1/3, k − 1/3, n +1/2), (j + 2/3, k − 1/3, n + 1/2), and (j − 1/3, k + 2/3, n + 1/2) with (j, k, n + 1) $\in \Omega_2$.

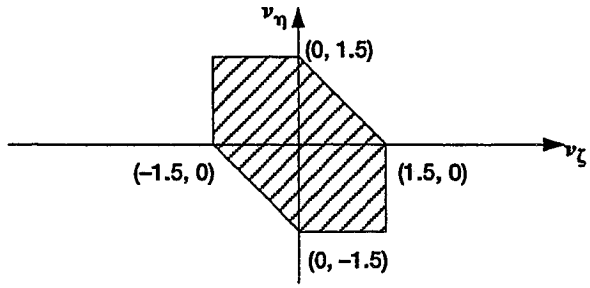

Figure 11.—The stability domain of the a scheme.

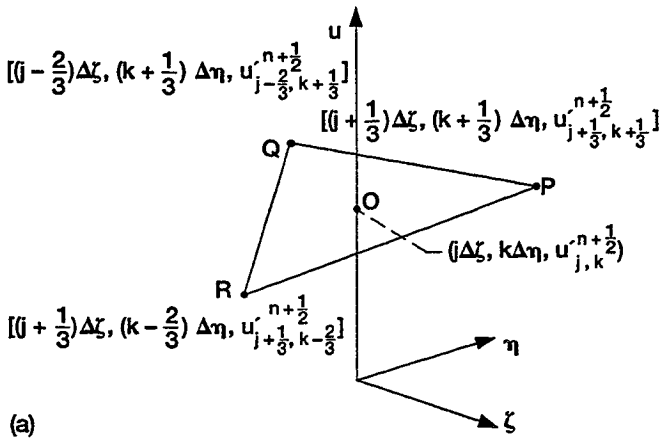

Figure 12.—The ζ-η-u space. (a) (j, k, n + 1/2) $\in \Omega_1$. (b) (j, k, n + 1) $\in \Omega_2$.

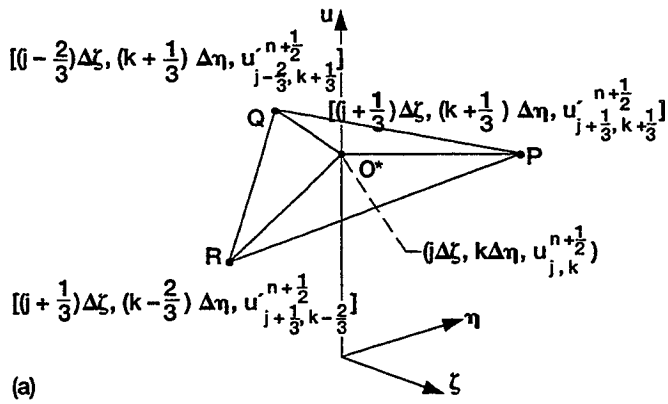

Figure 13.—The weighted-average a-ϵ scheme. (a) (j, k, n + 1/2) $\in \Omega_1$. (b) (j, k, n + 1) $\in \Omega_2$.

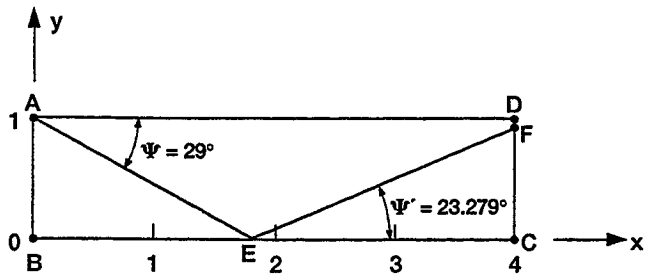

Figure 14.—The computation domain and the shock locations of a steady-state shock reflection problem.

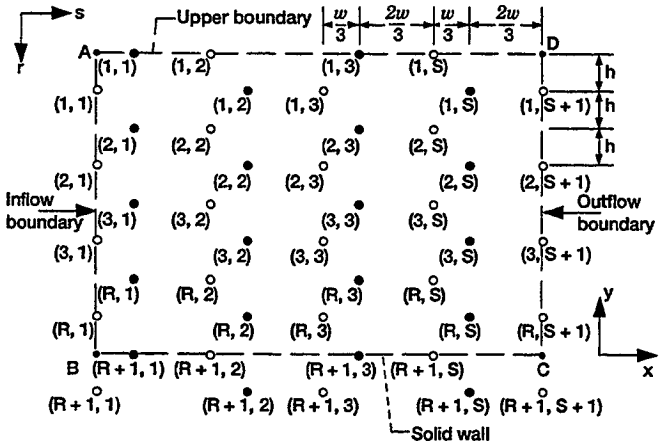

Figure 15.—The spatial locations and the new mesh indices (r, s) of mesh points (R = S = 4).

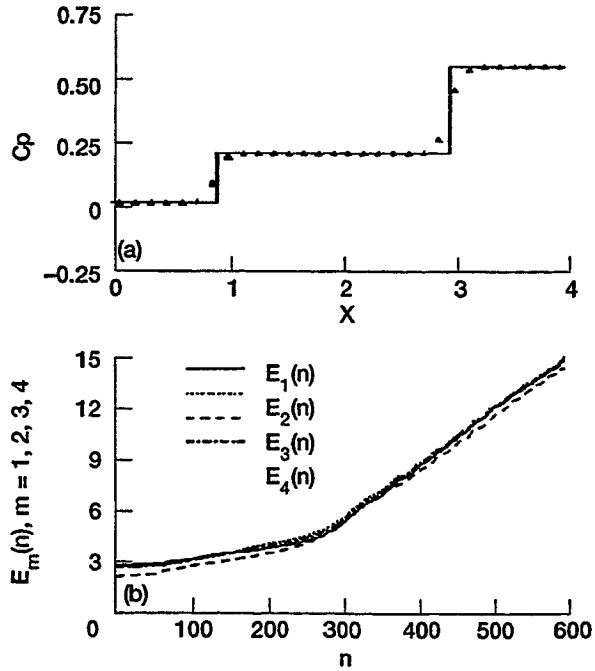

Figure 16.—Numerical results and convergence histories for problem #1. (a) Pressure coefficients at the mid-section of the computation domain (y = 0.5 in Fig. 14). (b) Convergence histories for u_m, m = 1, 2, 3, 4.

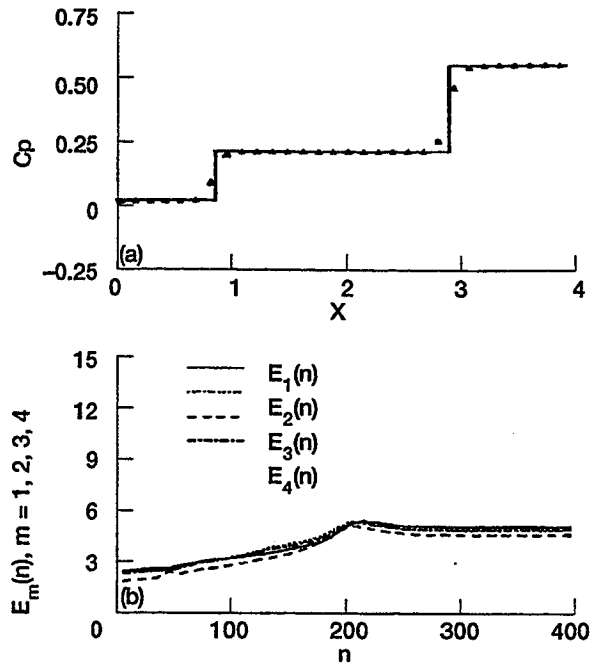

Figure 17.—Numerical results and convergence histories for problem #2. (a) Pressure coefficients at the mid-section of the computation domain (y = 0.5 in Fig. 14). (b) Convergence histories for u_m, m = 1, 2, 3, 4.

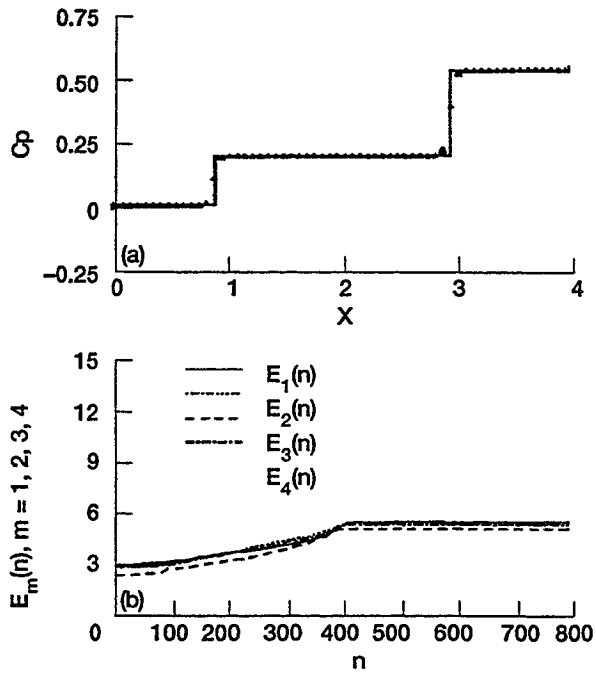

Figure 18.—Numerical results and convergence histories for problem #3. (a) Pressure coefficients at the mid-section of the computation domain (y = 0.5 in Fig. 14). (b) Convergence histories for u_m, m = 1, 2, 3, 4.

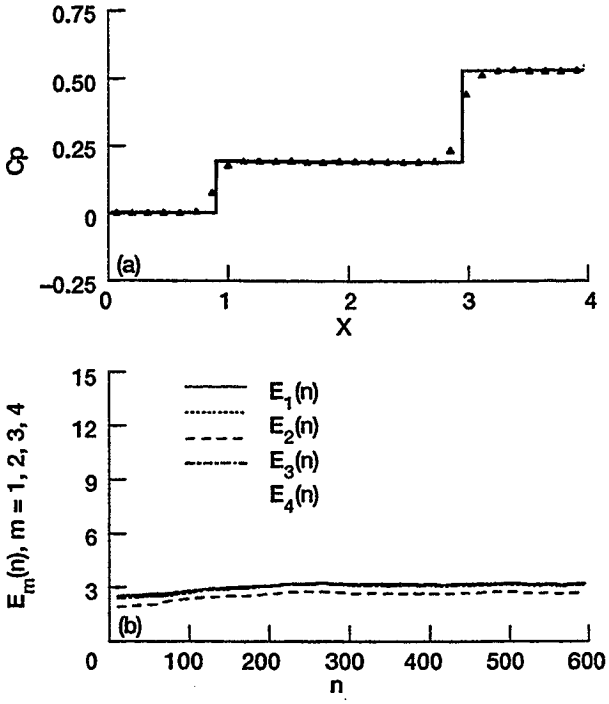

Figure 19.—Numerical results and convergence histories for problem #4. (a) Pressure coefficients at the mid-section of the computation domain (y = 0.5 in Fig. 14). (b) Convergence histories for u_m, m = 1, 2, 3, 4.

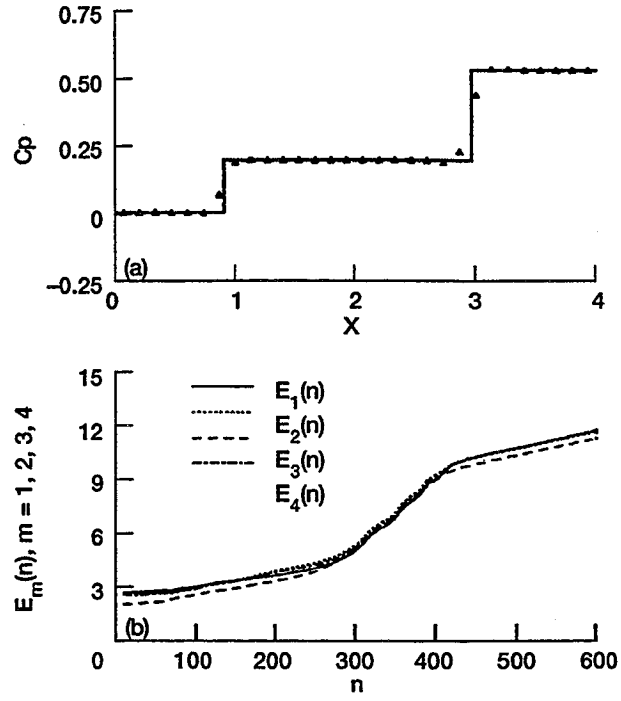

Figure 21.—Numerical results and convergence histories for problem #6. (a) Pressure coefficients at the mid-section of the computation domain (y = 0.5 in Fig. 14). (b) Convergence histories for u_m, m = 1, 2, 3, 4.

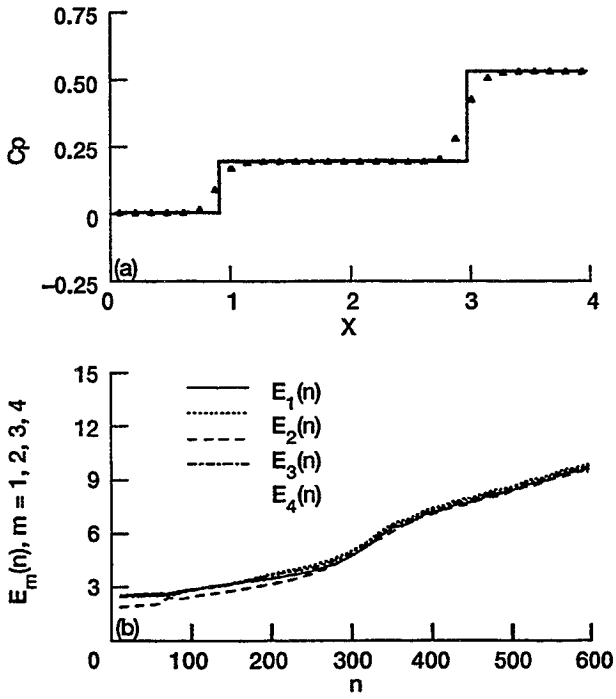

Figure 20.—Numerical results and convergence histories for problem #5. (a) Pressure coefficients at the mid-section of the computation domain (y = 0.5 in Fig. 14). (b) Convergence histories for u_m, m = 1, 2, 3, 4.

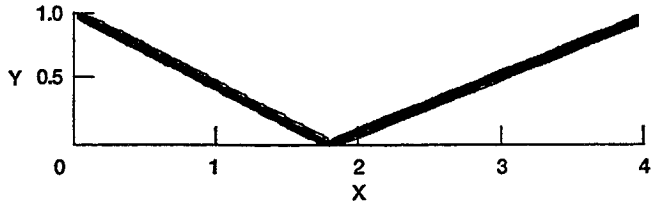

Figure 22.—Pressure contours for problem #3.

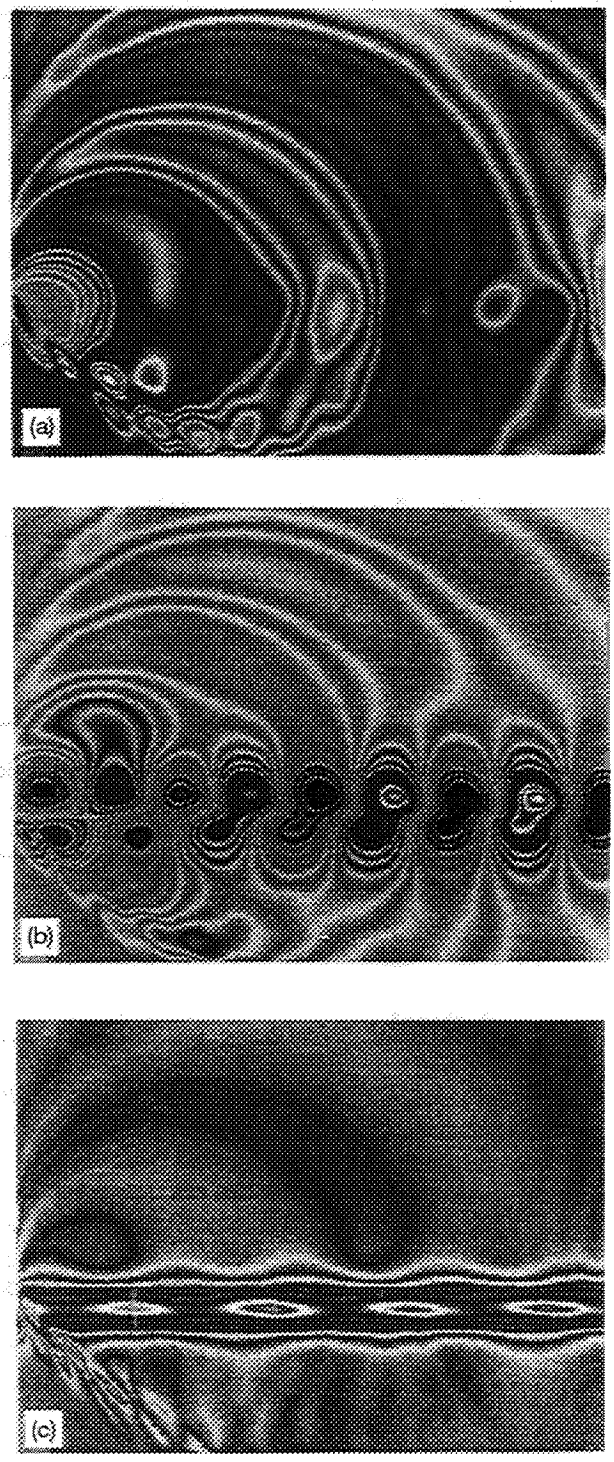

Figure 23.—Aeroacoustic computation of a free shear layer. (The fast stream lies in the bottom 1/3 domain while the slower stream lies in the top 2/3 domain. A small sinusoidal time-dependent perturbation is applied at the shear layer separating two streams.) (a) Pressure contours. (b) v-velocity contours. (c) Vorticity contours.

Table 1.—Definitions of test problems numbers 1 to 6 and the corresponding values of T, v_{ems}, v_{em}, and n_c

	ε	α	R	S	Δt	n_t	T	v_{ems}	v_{em}	n_c
1	0.5	2	20	60	0.01	600	6	0.585	0.6204	152.32
2	.5	2	20	60	.015	400	6	.8775	.9305	101.55
3	.5	2	40	120	.0075	800	6	.8775	.9302	203.09
4	.2	2	20	60	.01	600	6	.585	.6303	152.32
5	.8	2	20	60	.01	600	6	.585	.6212	152.32
6	.5	1	20	60	.01	600	6	.585	.6206	152.32

REPORT DOCUMENTATION PAGE

Form Approved
OMB No. 0704-0188

1. AGENCY USE ONLY (*Leave blank*)	2. REPORT DATE	3. REPORT TYPE AND DATES COVERED
	May 1995	Technical Memorandum

4. TITLE AND SUBTITLE

The Method of Space-Time Conservation Element and Solution Element-Applications to One-Dimensional and Two-Dimensional Time-Marching Flow Problems

5. FUNDING NUMBERS

WU–505–62–52

6. AUTHOR(S)

Sin-Chung Chang, Xiao-Yen Wang, and Chuen-Yen Chow

7. PERFORMING ORGANIZATION NAME(S) AND ADDRESS(ES)

National Aeronautics and Space Administration
Lewis Research Center
Cleveland, Ohio 44135–3191

8. PERFORMING ORGANIZATION REPORT NUMBER

E–9623

9. SPONSORING/MONITORING AGENCY NAME(S) AND ADDRESS(ES)

National Aeronautics and Space Administration
Washington, D.C. 20546–0001

10. SPONSORING/MONITORING AGENCY REPORT NUMBER

NASA TM–106915
AIAA–95–1754

11. SUPPLEMENTARY NOTES

Prepared for the 12th Computational Fluid Dynamics Conference sponsored by the American Institute of Aeronautics and Astronautics, San Diego, California, June 19–22, 1995. Sin-Chung Chang, NASA Lewis Research Center; Xiao-Yen Wang and Chuen-Yen Chow, University of Colorado, Boulder, Colorado 80302. Responsible person, Sin-Chung Chang, organization code 2660, (216) 433–5874.

12a. DISTRIBUTION/AVAILABILITY STATEMENT

Unclassified - Unlimited
Subject Category 64

This publication is available from the NASA Center for Aerospace Information, (301) 621–0390.

12b. DISTRIBUTION CODE

13. ABSTRACT (*Maximum 200 words*)

A nontraditional numerical method for solving conservation laws is being developed. The new method is designed from a physicist's perspective, i.e., its development is based more on physics than numerics. Even though it uses only the simplest approximation techniques, a 2D time-marching Euler solver developed recently using the new method is capable of generating nearly perfect solutions for a 2D shock reflection problem used by Helen Yee and others. Moreover, a recent application of this solver to computational aeroacoustics (CAA) problems reveals that: (i) accuracy of its results is comparable to that of a 6th order compact difference scheme even though nominally the current solver is only of 2nd-order accuracy; (ii) generally, the non-reflecting boundary condition can be implemented in a simple way without involving characteristic variables; and (iii) most importantly, the current solver is capable of handling both continuous and discontinuous flows very well and thus provides a unique numerical tool for solving those flow problems where the interactions between sound waves and shocks are important, such as the noise field around a supersonic over- or under-expansion jet.

14. SUBJECT TERMS	15. NUMBER OF PAGES
Space-time; Conservation element; Solution element; Two-dimensional; Time-marching	37
	16. PRICE CODE: A03

17. SECURITY CLASSIFICATION OF REPORT	18. SECURITY CLASSIFICATION OF THIS PAGE	19. SECURITY CLASSIFICATION OF ABSTRACT	20. LIMITATION OF ABSTRACT
Unclassified	Unclassified	Unclassified	